SENESCENCE AND IMMORTALITY GENES AS MARKERS OF HEPATOCELLULAR CARCINOGENESIS

A THESIS

SUBMITTED TO THE DEPARTMENT OF MOLECULAR BIOLOGY

AND GENETICS

AND THE INSTITUTE OF ENGINEERING AND SCIENCES

OF BILKENT UNIVERSITY

IN PARTIAL FULFILLMENT OF THE REQUIREMENTS

FOR THE DEGREE OF

DOCTOR OF PHILOSOPHY

By

Ayça Arslan Ergül

August 2009

I certify that I have read this thesis and that, in my opinion, it is fully adequate, in scope and in quality, as a thesis for the degree of Doctor of Philosophy.

_____

Prof. Dr. Mehmet Öztürk (Supervisor)

I certify that I have read this thesis and that, in my opinion, it is fully adequate, in scope and in quality, as a thesis for the degree of Doctor of Philosophy.

_____

Asst. Prof. Dr. Özlen Konu

I certify that I have read this thesis and that, in my opinion, it is fully adequate, in scope and in quality, as a thesis for the degree of Doctor of Philosophy.

_____

Asst. Prof. Dr. Cengiz Yakıcıer

I certify that I have read this thesis and that, in my opinion, it is fully adequate, in scope and in quality, as a thesis for the degree of Doctor of Philosophy.

_____

Prof. Dr. Funda Yılmaz-Barbet

I certify that I have read this thesis and that, in my opinion, it is fully adequate, in scope and in quality, as a thesis for the degree of Doctor of Philosophy.

_____

Assoc. Prof. Dr. Esra Erdal

Approved for the Institute of Engineering and Science

_____

Prof. Dr. Mehmet Baray

Director of Institute of Engineering and Science

ABSTRACT

SENESCENCE AND IMMORTALITY GENES AS MARKERS OF HEPATOCELLULAR CARCINOGENESIS

Ayça Arslan Ergül
Ph.D. in Molecular Biology and Genetics
Supervisor: Prof. Dr. Mehmet Öztürk
August 2009

Cellular senescence is a tumor-suppression mechanism, and immortalization facilitates neoplastic transformation. Both mechanisms may be highly relevant to hepatocellular carcinoma (HCC) development. We worked on two major aspects of cellular senescence and immortality in HCC. First, we analyzed the role of ZEB2 (Smad-interacting protein SIP1, ZFXH1B) gene for a senescence-related role in HCC. Then, we extended our work on the identification and analysis of a senescence and immortality gene network (SIGN) in relation to hepatocellular carcinogenesis. ZEB2 is a transcriptional repressor of E-cadherin, and induces epithelial-mesenchymal transition (EMT), a key process involved in tumor metastasis and progression. However, ZEB2 is also a repressor of telomerase reverse transcriptase (TERT) gene, which encodes a key enzyme required for telomere maintenance and tumor cell immortality. We performed in-vivo, in-silico and in-vitro studies to explore potential implications of ZEB2 in hepatocellular carcinoma (HCC). Tissue expression of ZEB2 transcripts displayed stepwise decreases in HCC lesions, as compared to liver cirrhosis. This inverse correlation suggested that sustained ZEB2 expression is not compatible with HCC progression. Next,

we studied in vitro effects of ZEB2 knockdown and overexpression in HCC cells. Huh7 clones stably transfected with a specific ZEB2-shRNA expression vector displayed increased colony formation and increased proliferation. Conversely, Hep3B cells stably transfected with ZEB2 expression vector displayed permanent cell cycle arrest associated with increased senescence-associated β-galactosidase activity. ZEB2-induced senescence arrest was correlated with the repression of TERT expression and concomitant upregulation of cyclin-dependent kinase inhibitor $p21^{Cip1}$. Transient expression of ZEB2 did not induce $p21^{Cip1}$ expression, suggesting an indirect mechanism. Finally, ZEB2 overexpression was not compatible with in vitro survival of cancer cells, as ZEB2-overexpressing Hep3B and A431 clones depleted progressively during in vitro culture and expansion. These observations suggest that the ZEB2 gene, aside from its role in EMT, also plays a negative role in HCC cell growth and survival.

In the other study, we integrated gene expression data from senescence programmed and immortal HCC cells with the data from cirrhosis and HCC tissues to generate a SIGN signature. The SIGN signature accurately classified normal liver, cirrhosis, dysplasia and HCC lesions, and indicated that senescence-to-immortality conversion first occured during dysplasia-to-early HCC transition. Senescence-to-immortality conversion contributed also to tumor progression. This conversion was accompanied by hepatic dedifferentiation and increased expression of cell proliferation, chromosome modification and DNA damage response genes. Thus, HCC immortalization is closely associated with the acquisition of stem/progenitor-like features. Finally, we identified a large set of upregulated DNA damage checkpoint and DNA repair genes that showed significant associations with tumor initiation and progression. These genes may serve as potential targets for HCC prevention and therapy.

Keywords: Senescence, Liver Cancer, Gene Expression Profiling, Biological Pathways, ZEB2, $p21^{Cip1}$, TERT

ÖZET

HEPATOSELÜLER KARSİNOGENEZ BELİRTECİ OLARAK YAŞLANMA VE ÖLÜMSÜZLÜK GENLERİ

Ayça Arslan Ergül
Moleküler Biyoloji ve Genetik Bölümü Doktora
Tez Yöneticisi: Prof. Dr. Mehmet Öztürk
Ağustos 2009

Hücre yaşlanması tümör baskılayıcı bir mekanizmadır ve ölümsüzlük, neoplastik dönüşümü kolaylaştırır. Her iki mekanizma da hepatoselüler karsinom (HCC) gelişimi ile yakından ilişkilidir. Biz, HCC'de hücre yaşlanması ve ölümsüzlügünü iki açıdan çalıştık. Önce, ZEB2 (Smad ile etkileşen protein SIP1, ZFHX1B) geninin HCC'deki yaşlanma ile ilişkili rolünü inceledik. Sonra, çalışmamızı, hepatoselüler kanser ile ilişkili yaşlanma ve ölümsüzlük gen ağı (SIGN)'nın belirlenmesi ve analizi yönünde genişlettik. ZEB2, E-kaderin'i baskılar ve tümör metastazında ve gelişiminde anahtar rol oynayan, epitel-mezenkimal geçiş (EMT)'yi, indükler. Öte yandan ZEB2, telomer muhafazası ve tümör hücre ölümsüzlügü için gerekli enzim, telomeraz ters transkriptaz (TERT)'i baskılar. Biz, ZEB2'nin hepatoselüler kanserdeki potansiyel anlamını keşfetmek için, in-vivo, in-vitro ve in-silico çalıştık. ZEB2 transkriptlerinin doku ifadeleri, HCC lezyonlarında, karaciğer sirozuna kıyasla dereceli olarak azalma gösterdi. Bu ters bağıntı, ZEB2 ifadesinin, HCC'nin ilerlemesiyle uyumlu olmadığını akla getirdi. Sonra, HCC hücrelerinde ZEB2'nin azaltılması ve artırılmasının in vitro etkilerini çalıştık. Özgün bir ZEB2-shRNA ifade vektörü ile kararlı şekilde transfekte edilen Huh7 klonları, koloni oluşumunda ve çoğalmada artış gösterdiler. Karşıt şekilde, ZEB2 ifade

vektörü ile transfekte edilen Hep3B hücrelerinin, yaşlanma ilişkili β-galaktozidaz aktivitesi ile, kalıcı hücre döngüsü hapsine girdiklerini gördük. ZEB2 ile indüklenen yaşlanma hapsi, TERT ifadesinin baskılanması ve eşlik eden siklin-bağımlı kinaz engelleyici $p21^{Cip1}$'in ifadesindeki artış ile bağıntılı idi. ZEB2'nin geçici ifadesi, $p21^{Cip1}$ ifadesindeki artışı indüklemedi. Son olarak, ZEB2'yi aşırı ifade eden Hep3B ve A431 klonlarının, in vitro kültürde dereceli olarak azalması ile ZEB2 aşırı ifadesinin, kanser hücrelerinin in vitro yaşamı ile uyumlu olmadığı sonucuna varıldı. Bu gözlemler, ZEB2 geninin, EMT'deki rolünün dışında, HCC hücre büyümesi ve yaşamasında negatif rol oynadığını düşündürdü.

Diğer çalışmamızda SIGN imzasını oluşturmak için, yaşlanmaya programlanmış ve ölümsüz HCC hücrelerinden gelen gen ifade datasını, siroz ve HCC dokularından gelen data ile birleştirdik. SIGN imzası normal karaciğer, siroz, displazi ve HCC lezyonlarını doğrulukla sınıflandırdı ve yaşlanmadan ölümsüzlüğe dönüşümün, ilk olarak displaziden erken HCC'ye geçişte gerçekleştiğini belirledi. Bu dönüşüm, tümör ilerlemesine de katkıda bulunur. Yaşlanmadan ölümsüzlüğe dönüşüme, hepatik geri başkalaşım ile ve hücre çoğalması, kromozom değişimi ve DNA hasar yanıtı genlerindeki ifade artışı eşlik etti. Bu nedenle, HCC ölümsüzlüğü, kök hücre/öncü hücre benzeri özellikler ile yakından ilişkilidir. Son olarak, DNA hasar kontrol noktası ve DNA tamir genlerindeki artış ile, tümör başlangıcı ve ilerlemesi arasında ilişki bulduk. Bu genler, HCC'nin engellenmesinde ve terapisinde potansiyel hedefler olabilirler.

Anahtar Kelimeler: Yaşlanma, Karaciğer kanseri, Gen ifade analizi, Biyolojik yolaklar, ZEB2, $p21^{Cip1}$, TERT

ACKNOWLEDGMENTS

I would like to thank my supervisor, Prof. Mehmet Öztürk, for sharing his knowledge with me. I have enrolled to Molecular Biology and Genetics Department after inspired by him and I am proud to be a member of his group. I believe Prof. Öztürk has contributed to science in Turkey to a great extend, and I am grateful to him for all his guidance.

I would like to thank my MS supervisor, Prof. Hakan Bozkaya, for his endless support during years. I have learnt the liver from him, and also by Prof. Bozkaya, I understood the reality of HCC as a disease by observing him as a doctor.

I thank Assist. Prof. Özlen Konu, for guiding me through bioinformatics and for her patience, energy and for being there all the time I needed. I thank Assoc. Prof. Rengül Çetin Atalay and Assoc. Prof. Işık Yuluğ for teaching me, and for their close concern. Its always a pleasure to work with Assist. Prof. Uygar Tazebay and I thank all faculty members of MBG.

I thank Prof. Levent Gürel, for his support, guidance, and for all the things I have learnt from him over the years. I also thank Defne, Aylin, and Assist. Prof. Meltem Gürel for being our family in Ankara.

My group mates, Dr. Nuri Öztürk, Dr. Hani Al-Otaibi, Şerif Şentürk, Mine Mumcuoğlu, Sevgi Bağışlar, Haluk Yüzügüllü, Pelin Gülay, Nilgün Taşdemir, and Özge Yüzügüllü. I have learnt from you, we have shared so much, we worked all-together, and most of all, we have made the MO Group. Thank you for all.

Our lab is always the most cheerful environment, I would like to thank all my collegues from MBG Family, that I cannot list in here. But to the most cheering mates, Ceren Sucularlı, Tolga Acun, and Dr. Bâlâ Gür-Dedeoğlu, thank you for five years full of laugh.

Contents

List of Figures

List of Tables

To My Özgür and My Family...
Özgür'üme ve Aileme...

Chapter 1

INTRODUCTION

1.1 Hepatocellular carcinoma

Hepatocellular carcinoma (HCC) is the fifth most-common cancer worldwide, with more than 600,000 new cases reported and an equal number of deaths each year [1]. HCC develops on a chronic liver disease and cirrhosis background for the majority (70% to 90%) of the cases. Major risk factors of HCC can be listed as hepatitis B, hepatitis C, alcoholic liver disease, and nonalcoholic steatohepatitis. HCC incidence is increasing in Europe and North America, mostly due to hepatitis C virus (HCV) infection [2, 3].

In spite of diverse risk factors, there are common mechanisms affected (Figure 1.1). Hepatitis B and aflatoxin B1, a mutagen, both affect the genome. p53 inactivation is observed in HCV-, HBV and aflatoxin-B1 induced HCC. Also in HBV-, HCV-, and alcohol-induced HCC, inflammation, necrosis, and regeneration are common processes [4].

Although not precisely identified, HCC generally follows a progression as described in Figure 1.2. It takes 20-30 years to develop a chronic liver disease after infection with hepatitis viruses. In some of the patients cirrhosis and HCC arise

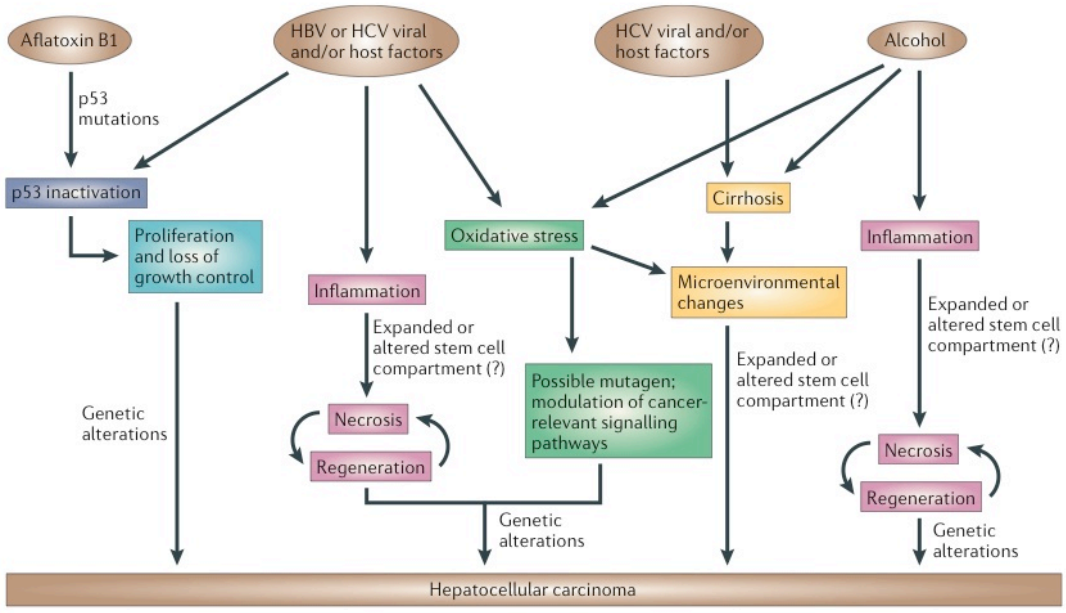

Figure 1.1: Major risk factors and mechanisms responsible from hepatocellular carcinoma. HBV, hepatitis B virus; HCV, hepatitis C virus. Adapted from Farazi and DePinho, 2006 [4].

in sites of chronic hepatitis. HCC can be classified into well differentiated, moderately differentiated, and poorly differentiated tumors, the latter being the most malignant type [4, 5].

Treatment options of this cancer are limited, thus, it is necessary to identify novel genes involved in HCC to implement new diagnostic and treatment options. However, the molecular pathogenesis of HCC largely remains unsolved [2, 4, 5, 6, 7]. Only a few genetic alterations, namely those affecting p53, β-catenin and $p16^{INK4a}$, have been implicated at moderate frequencies in these cancers [6].

The only consistent and highly frequent change in HCC is the reactivation of telomerase activity, which has been detected in more than 80% of cases [2, 8, 9, 10, 11]. Telomerase activity in HCC is linked to the reactivation of telomerase reverse transcriptase (TERT) expression [11].

TERT catalyses the addition of telomere sequences to the chromosome ends

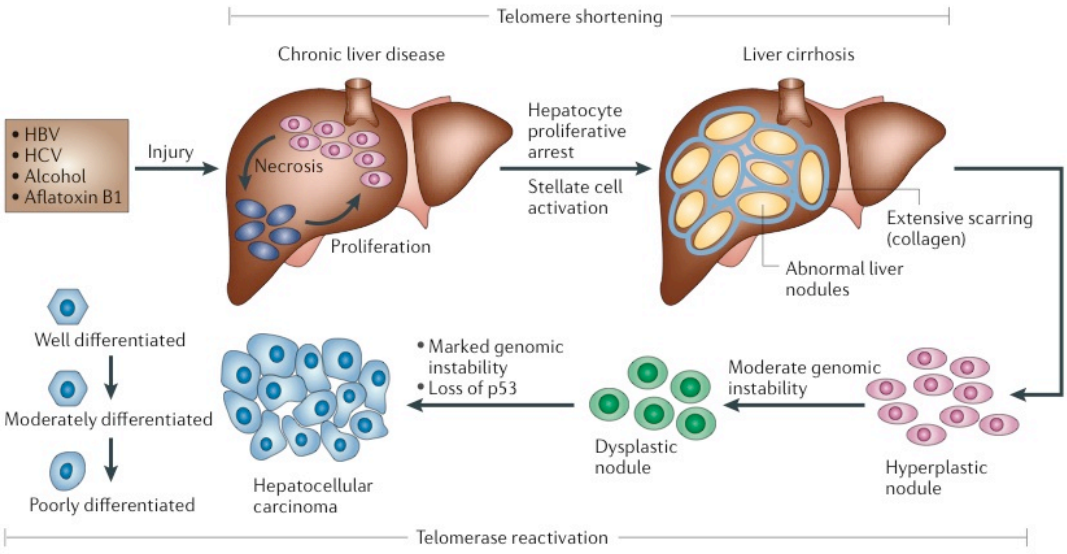

Figure 1.2: Histopatological progression of HCC. HBV, HCV, alcohol, and aflatoxin are the major risk factors leading to HCC by inducing cycles of necrosis and proliferation. After chronic liver disease or damage, collagen is accumulated and causes fibrosis. Deposition of fibrotic tissue and abnormal liver nodules are characteristics of cirrhosis. Nodules then become hyperplastic and finally dysplastic which eventually progress to HCC. Genomic instability is observed in nodules and characterize HCC most prominently with the loss or mutation of p53. Adapted from Farazi and DePinho, 2006 [4].

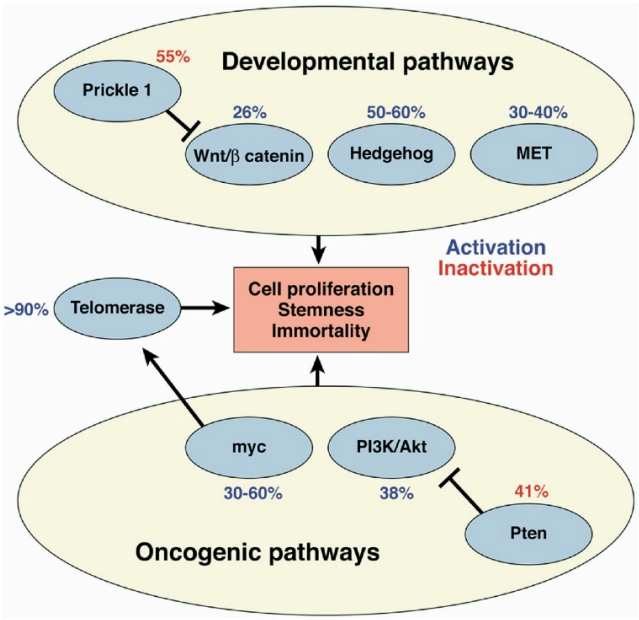

Figure 1.3: Major pathways that are activated in HCC are shown. These pathways, the Akt, the myc, the β-catenin, the hedgehog, and the met pathways are activated in 20-60% in HCCs. Telomerase activation is the most frequent event in HCC. Adapted from El-Serag and Rudolph, 2007 [2]

.

to maintain chromosomal integrity during subsequent cell divisions [12]. Apparently, HCC development requires consistent telomerase activity, as telomerase deficiency in mice causes a significant decline in the occurrence of high-grade liver malignancies [13]. It is currently unclear how TERT expression is repressed in normal hepatocytes, but released in HCC cells. The integration of HBV DNA sequences into the TERT gene provides evidence for a virus-induced deregulation of TERT expression [13], but this appears to occur rarely, as only four cases have been reported so far [14, 15]. HBV X and PreS2 proteins may upregulate TERT expression [16, 17] but HBV X was also shown to repress the TERT promoter [18].

1.2 Senescence

Replicative immortality is a common acquired feature of all cancers. Somatic cells have a limited number of cell divisions due to end replication problem at the ends of the chromosomes, namely telomeric sequences. Replicative senescence is the inevitable consequence of this problem which is also a strong barrier in preventing cancer cell immortality. Senescent phenotype is charaterized by growth arrest and apoptosis resistance, also altered gene expressions accompany these phenotypic changes. A pre-senescent cell can turn into a senescent cell in diverse ways. Dysfunctional damage as well as non-telomeric DNA damage, strong mitogenic signals and also chromatin perturbations may cause this shift [19].

Most human somatic cells are telomerase deficient. Telomerase reverse transcriptase (TERT) enzyme is repressed in somatic cells during differentiation and this leads to progressive erosion of telomeric DNA in each round of cell division. This form of senescence is called replicative or telomere-dependent senescence (Figure 1.4).

Human chromosome telomere ends are composed of TTAGGG repeats (5-20

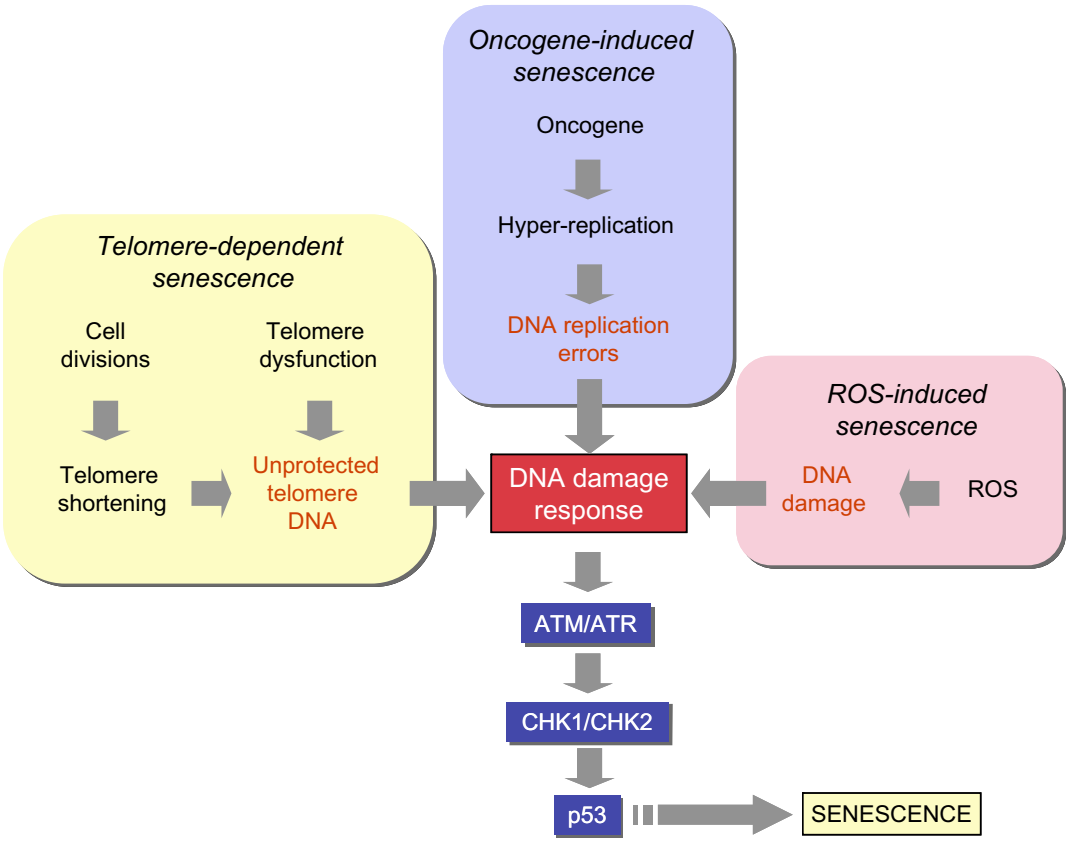

Figure 1.4: Different pathways that lead to senescence. DNA damage and p53 activation play a central role in all pathways [20].

kb) in a DNA-protein complex formed by six telomere-specific proteins, called "shelterin" [21] . Telomeres get shorten with every cell division because cellular DNA polymerases are unable to copy the ends of linear DNA. By this perspective, telomeres are often referred as the "cell cycle counter" for the cell [22] . The loss of telomeres were thought to be the signal for senescence induction. Now we know that disruption of telomeric structure induces senescence and shortened telomeres contribute to this process [23]. Chromosomal end-to-end fusions through DNA repair pathways is induced by loss of telomere protection. Also dysfunctional telomeres recruit DNA damage machinery by inducing a double-stranded DNA break response [24].

Oncogene-induced senescence had been identified as a response to expression of Ras oncogene in normal fibroblasts [25]. The expression of oncogenic Ras in primary human or rodent cells results in permanent G1 arrest. The arrest was accompanied by accumulation of p53 and $p16^{INK4a}$, and was phenotypically identical to senescence. In addition to Ras, other oncogenes including Raf, Mos, Mek, Myc and Cyclin E also induce senescence [26]. On the other hand, the loss of PTEN tumor suppressor gene also leads to senescence [27]. Oncogene-induced senescence is also primarily a DNA damage response (Figure 1.4).

Reactive oxygen species (ROS)-induced senescence is the other telomere-independent senescence pathway. Mitochondria are the major intracellular sources of ROS which are mainly generated at the respiratory chain. ROS have been identified as critical mediators of both telomere-dependent and oncogene-induced senescence. Telomere-dependent senescence arrest is accelerated in cells grown under high O_2 conditions. In the opposite, cells have a longer lifespan when grown under low O_2 conditions [28].

DNA damage is one of the common steps in generation of senescence arrest in all pathways of senescence (Figure 1.4). Senescence arrest which is mediated by p53 starts with activation of upstream checkpoint kinases, such as ATM or ATR,

in response to DNA damage in the form of double-strand breaks. These kinases then phosphorylate CHK1 and CHK2 that in turn phosphorylate p53. With the phosphorylation, MDM2 protein is displaced and p53 is activated. p53 activating pathway is critical in both telomere-dependent and oncogene-induced senescence [29, 30].

Other mechanisms of senescence include INK4 locus encoding two inhibitors of cyclin-dependent kinases. $p16^{INK4a}$ and $p15^{INK4b}$, and ARF a p53 regulatory protein [31]. $p16^{INK4a}$ and $p15^{INK4b}$ connect some senescent initiating signals to the retinoblastoma (Rb) pathway, independent of p53 activation. Cells that escape senescence often display inactivation of $p16^{INK4a}$, $p15^{INK4b}$ and ARF either by homozygous deletion or by shutting-down gene expression.

$p21^{Cip1}$ is one of the main targets of p53 for the induction of cell cycle arrest following DNA damage [32]. Pathways that generate DNA damage response and p53 activation use $p21^{Cip1}$ as a major mediator of cellular senescence to control pRb protein [33]. Exceptionally, $p21^{Cip1}$ can be activated by p53-independent pathways to induce senescence [34].

Senescent cells cannot enter into S phase and initiate DNA synthesis, hence accumulate at G1 phase of the cell cycle. Retinoblastoma protein (pRb), binds to and inhibits E2F factors which are required for the transition of proliferating cells from G1 to S phase. Cyclin-dependent kinases (CDKs), specifically CDK4/6 and CDK2 phosphorylate pRb, cause it to be released from E2F [31]. The senescence arrest is mediated by inhibition of pRb phosphorylation by CDK4 and CDK2. CDKIs inhibit actions of CDKS and are the major proteins that are involved in the control of senescence arrest. Well-known CDKIs, $p16^{INK4a}$ and $p15^{INK4b}$) inhibit CDK4/CDK6, and $p21^{Cip1}$ inhibits CDK2 (Figure 1.5).

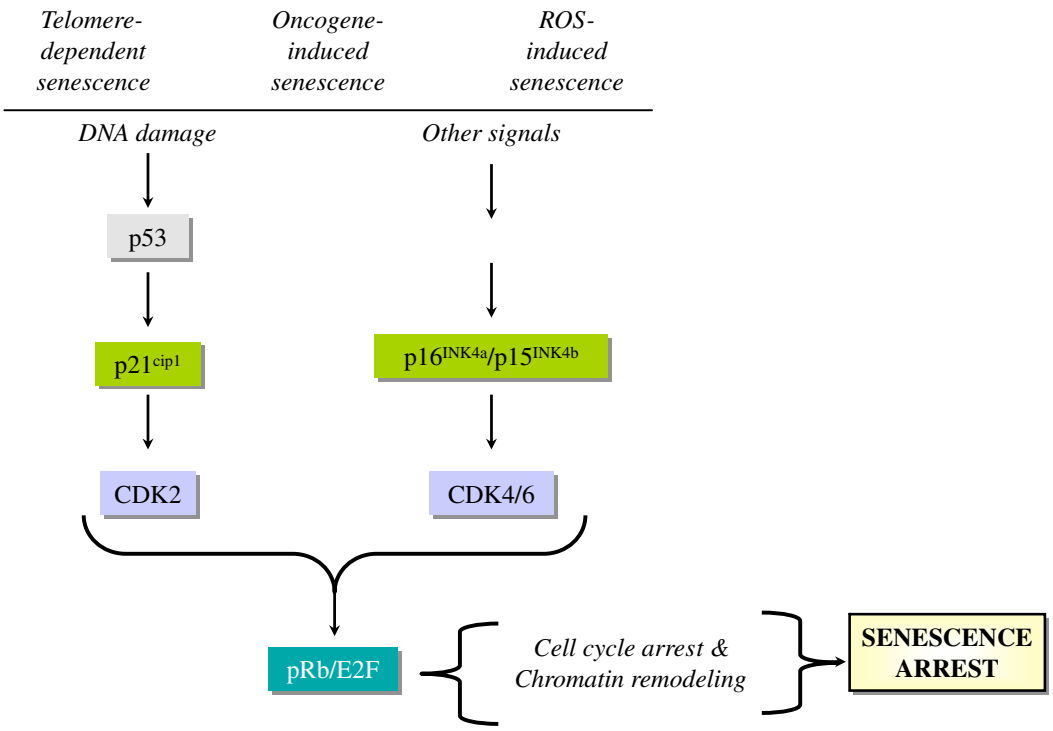

Figure 1.5: Senescence pathways whether induced by oncogenes or ROS, or through telomere shortening, all converge at the level of activation of CDKIs ($p16^{INK4a}$, $p15^{INK4b}$) and $p21^{Cip1}$. CDKIs keep the Rb protein in the active form. The Rb protein prevents the expression of growth-promoting genes for cell cycle exit [20].

1.3 Senescence in HCC

Cellular senescence appears to play a major role in liver diseases [2]. Adult hepatocytes, like other somatic cells, are programmed for senescence, a mechanism that blocks excessive cell proliferation by a telomere-dependent mechanism [19, 33, 20]. In contrast to in vivo conditions, mature hepatocytes are resistant to cell proliferation in cell culture. Fetal hepatocytes which have better proliferation capacity in culture, were shown to enter replicative senescence [35]. This is accompanied by progressive shortening of telomeres down to ∼6 kbp, as these cells like adult hepatocytes lack telomerase activity.

Chronic liver diseases are associated with progressive telomere shortening leading to the cellular senescence that is observed frequently in cirrhosis, but also in some HCCs [10, 36, 37, 38, 39]. Wiemann et al. showed that replicative senescence (as tested by SABG assay) displayed a gradual increase from 10% in normal liver, to 84% in cirrhosis. Telomere lengths were shorter in cirrhosis when compared to noncirrhotic tissues. Also it was shown that telomere shortening was hepatocyte-specific and not observed in lymphocytes and stellate cells [39].

Experimental animal models also provide strong evidence for a critical role of cellular senescence in HCC [40, 41].However, the role of cellular senescence and immortality in human HCC remains elusive.

HCC is characterized by mutational inactivation of p53. By epigenetic mechanisms like promoter methylation, well-known CDKIs, $p16^{INK4a}$, $p15^{INK4b}$, and $p21^{Cip1}$ are often inactivated in this cancer. In the cirrhosis phase, some cells bypass senescence barrier and start to proliferate. More than 80% of HCCs display telomerase activity, so those cells are able to continue proliferating. Inactivation of major CDKIs also play a critical role in HCC development by conferring premalignant and malignant cells to proliferate indefinitely (Figure 1.6).

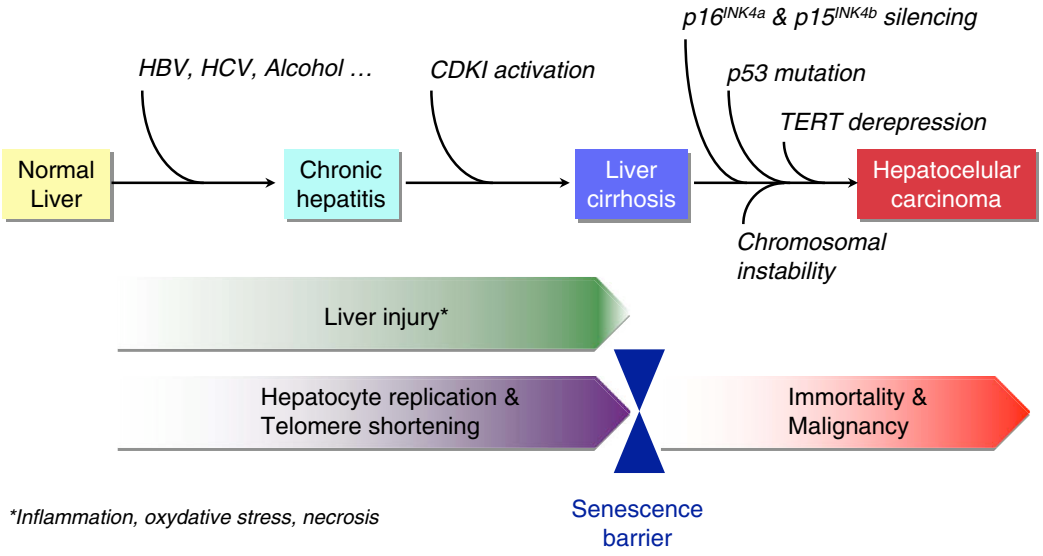

Figure 1.6: Role of cellular senescence and immortalization in hepatocellular carcinogenesis. HBV, HCV and alcohol are the major causes of HCC, and all lead to hepatitis. Chronic hepatitis is followed by liver cirrhosis for a subset of cases. CDKI activation leads to senescence during cirrhosis. Cells which lack telomerase activity cease to proliferate at this stage. Yet some cells can overcome the senescence barrier by $p16^{INK4a}$, $p15^{INK4b}$ silencing and via p53 mutations. TERT derepression enable cells to proliferate by preventing telomere lengths from shortening.

1.3.1 Reprogramming of replicative senescence in HCC

Our group have reported the replicative senescence induction in hepatocellular carcinoma-derived cells [42]. In that study, hepatocellular carcinoma cells were shown to engage in replicative senescence program independent from p53 and pRb pathways. Yet, this phenomenon was characterized with hTERT repression, telomere shortening, and senescence arrest. Immortal, presenescence and senescence programmed clones were obtained from the same parental cell, Huh7. This spontaneous generation of senescence programmed clones were unique in their life span. Although immortal clones had the same replication potential even after 150 population doublings, senescence programmed clones had lost their ability to replicate after 80 population doublings. This finding were of great importance since it demonstrated the reversal of immortality phenotype in a cancerous cell line. What we observed in cancerous cells was replicative senescence, but not a stress-induced premature senescence-like arrest. Senescent clones displayed telomerase repression, progressive telomere shortening, and permanent growth arrest with senescence-associated morphological changes and positive SABG staining.

The replicative senescence arrest that we observed in these cells was not dependent on p53, $p16^{INK4a}$, $p14^{ARF}$, or $p21^{Cip1}$ gene. Huh7 cells express a mutant p53 protein, and they are deficient in $p16^{INK4a}$ expression [42]. The lack of induction of these genes indicates that there are additional genes involved in senescence arrest in these tumor derived cells.

1.4 SIP1/ZEB2/ZFHX1B gene and its relationship with HCC and senescence

In the study by Ozturk et al. [42], we analyzed the expression of genes that have been implicated in hTERT regulation. HCC cells have telomerase reactivation,

and this is also a marker for Huh7 cells. Yet in C3 clones. which were derived from Huh7 cells, TERT gene was repressed. This led us to search for genes that can repress TERT expression. In Lin and Elledge paper [43], negative regulators of TERT were identified (Figure 1.7).

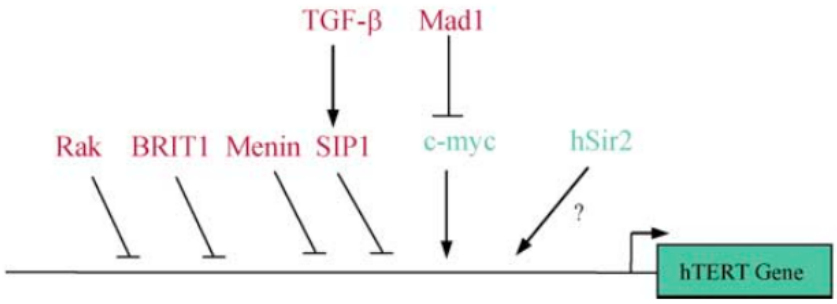

Figure 1.7: Regulators of TERT promoter. Repressive proteins are shown in red and activating proteins in green. [43]

We analyzed seven candidate genes, only one of them, ZEB2, was found to be differentially expressed between senescent and immortal clones. ZEB2 was not expressed in immortal C1 clone, but in senescent C3 clone. Expression of ZEB2 was inversely related with TERT expression. When ZEB2 is depleted through shRNA in C3 cells, these cells rescued from senescence, started to proliferate again as measured by BrdU assay, and also TERT is up-regulated (Figure 1.8).

TERT expression is controlled by a dozen transcriptional regulators, including ZEB2 acting as a repressor [44, 43]. The ZEB2 gene, also called SMAD interacting protein-1 or ZFHX1B, is better known for its role in epithelial-mesenchymal transition (EMT) as a repressor of E-cadherin [45]. Based on this EMT-promoting activity, ZEB2 is considered to positively contribute to tumor progression. Conversely, the same gene could play an anti-tumor role as a repressor of the TERT gene, encoding a key enzyme required for telomere maintenance and tumor cell immortality[43, 42]. Moreover, ZEB2 could inhibit cell proliferation directly by attenuation of cyclin-D expression [46].

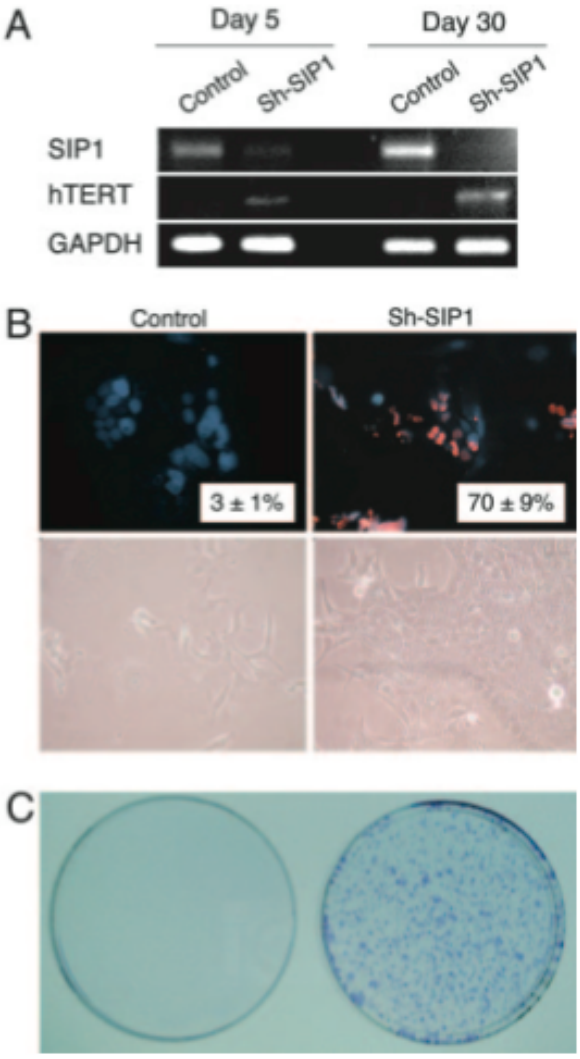

Figure 1.8: ShRNA mediated down-regulation of endogeneous ZEB2 transcripts in senescent cells. A) In senescent C3 cells, shRNA mediated down-regulation leads to the up-regulation of TERT. The increase in TERT expression is significant even at day 5, and as evidenced by the increase in day 30, it is not temporary. B) BrdU incorporation assay and cell photos of C3 cells are given. ShRNA downregulation of ZEB2 causes cells to start proliferating. C) Colony formation ability of senescent cells are recovered. C3 cells on the left, C3 cells with Sh-ZEB2 are on the right. [42]

The role of ZEB2 in HCC is poorly known. It has been reported to repress E-cadherin expression in HCC cells, leading to increased cell invasiveness [47].

ZEB2 is a member of two-handed zincfinger/homeodomain proteins. In target promoters, it binds to 5'-CACCT sequences [48]. ZEB2 acts as a repressor and two zinc finger clusters are required and must be intact for its activity [49].

ZEB2 is essential for embryonic neural and neural crest development [50] and its mutations cause severe defects in mouse [51] and in humans, namely Hirschsprung disease [52] and Mowat-Wilson disease [53].

E-cadherin down regulation is known to be the critical molecular feature of epithelial-mesenchymal transition [54]. ZEB2 induces EMT by down regulating E-cadherin transcription via direct binding of ZEB2 to E2 boxes at E-cadherin promoter [45, 55] and repressing genes of epithelial cell-cell junctions [56]. Also ZEB2 is mentioned in breast tumor cell migration since it is induced in vimentin positive migratory cells [57]. Other studies have shown that in breast carcinomas and effusions [58] and HCC cell lines [47], suppression of E-cadherin by Snail and ZEB2 is correlated with cancer invasions. These data implicate ZEB2 as a promoter of invasion in malignant epithelial tumors. ZEB2 was identified in yeast-two-hybrid studies as a protein binding to the MH2 domain of Smad1. It was then discovered to bind to activated, receptor regulated Smads [48]. Smad proteins are intracellular mediators of TGF-β signaling [59]. ZEB2 is a transcriptional target of TGF-β pathway and has been implicated in repression of hTERT downstream of a TGF-β signal [43].

1.5 DNA damage repair

DNA damage alter cellular dynamics including biochemical pathways, cellular growth and pathways related to cell cycle. Four pathways are activated in response to DNA damage. These are DNA repair, transcriptional response, DNA

damage checkpoints, and apoptosis 1.9. DNA repair pathways enable the reversal of the damage. This may be the removal of the incorrect base or structure and restoration of the original double helix structure. Damage can be of different kind, but mostly it prevents the DNA replication or causes mistakes in the DNA sequence. It is vital to prevent further DNA replication and this is maintained by DNA damage checkpoints. This type of response prevents cell cycle from continuing so that the damage is not transmitted to daughter cells. Transcriptional response is the changes in transcription according to the needs of the cell after checkpoint activation. If the damage is harmful to the cell and if it disrupts the genomic stability of the cell, then apoptosis is induced [60].

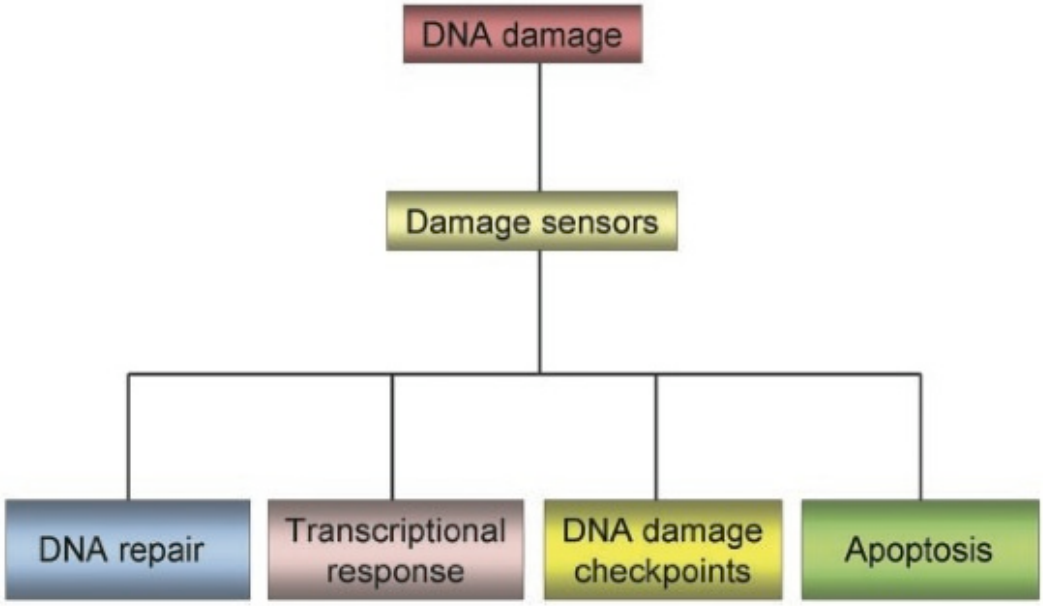

Figure 1.9: DNA damage response reactions in mammalian cells. These four pathways function independently or by a common protein in response to DNA damage. [60]

DNA repair mechanisms include direct repair, base excision repair (BER), nucleotide excision repair (NER), double-strand break repair, and cross-link repair. Direct repair utilizes two protein machineries; photolyase and methylguanine

DNA methyltransferase. In BER, a DNA glycosylase recognizes oxidized/reduced bases, alkylated bases, deaminated bases or base mismatches. If there is a bulky DNA lesion, then NER is the repair system. These lesions may be formed by protein addition to DNA, exposure to radiation or by chemicals. Double-strand breaks are formed upon exposure to reactive oxygen species, ionizing radiation or after V(D)J recombinations. Homologous recombination and single-strand annealing are two ways of repairing double-strand breaks. Cross-link repair is utilized when an interstrand DNA cross-link is formed. Chemotherapeutic drugs and bifunctional DNA-damaging agents induce formation of these structures.

Hepatitis B and hepatitis C viruses induce the release of free radicals, which cause inflammation. Free radicals contribute to DNA damage. The p53 pathway is the major player in response to this oxidative stress [61].

1.6 Gene expression profiling

Gene expression profiling utilizes the state-of-the-art technology, microarrays, to reveal all of the expressed genes in a given sample, at a given time point. Each tumor or tissue is unique in its expression profile. By obtaining a small sample from different tumor or tissue even from the same tissue at different time points, it is possible to learn what set of genes are actively transcribed. By gene expression profiling, it is possible to classify tumors into homogenous subtypes that are characterized by distinct molecular pathways that maintain the malignant phenotype, discover genes associated with other prognosis and/or pathological features of the tumors, and to provide potentially new therapeutic targets and monitor response to therapy. In year 2002, a study had published pioneering the subject [62]. By profiling tumors of young patients, they had identified a signature of poor prognosis consisting of 70 genes. Then, 295 patients with primary breast carcinomas were classified as having a gene-expression signature associated with

either a poor prognosis or a good prognosis [62]. Segal and collegues, defined module-level analysis of a cancer compendium from multiple studies to obtain a global view of shared and unique molecular modules in human cancer [63]. Cancer module map showed that activation and repression of some modules (e.g. cell cycle) was shared across multiple cancer types and could be related to general tumorigenic processes. In 2004, 406 survival genes were listed to uncover some of the molecular pathways responsible for the differences in subclasses of HCC [64]. These genes enabled the prediction of two distinctive subclasses that are highly associated with the survival of the patients. In this study, it is also found that while dysregulation in proliferation and survival pathways are common to all cancers, there are other pathways that may be specific for certain types of cancers. Many other studies have followed these works. Ultimate aim for most of these work is to find the signature genes that can discriminate the tumor associated processes.

Microarrays have developed in the last decade, and still in its progression. There are several platforms for microarray experiments and Affymetrix GeneChip Arrays are one of the most frequently utilized systems. GeneChip Human Genome U133 plus 2 Arrays enables to analyze whole genome expression on a single chip. It analyzes the relative expression level of more than 47,000 transcripts corresponding to 38,500 well characterized genes. The probe sets were designed from sequences in GenBank, dbEST and RefSeq databases. GeneChip arrays are manufactured via photolithography and combinatorial chemistry [1].

Bioinformatics tools are utilized to analyze microarrays data. In the most conventional way, a microarray data is normalized to equilibrate the signal intensities among experiments, so the variation is reduced. Robust multichip average (RMA) is a widely used normalization method. It has three steps: background adjustment, quantile normalization, and summarization. Quantile normalization

[1] http://www.affymetrix.com/

makes the distribution of probe intensities for each array in a set of arrays the same [65].

Clustering utilizes statistical algorithms to group genes depending on the similarity in gene expression patterns. Cluster analyzes have to be visualized by other tools, which eventually produce a graphical picture, in which every data is represented on a color scale depending on downregulation or upregulation of individual genes [66].

Chapter 2

OBJECTIVES AND RATIONALE

Hepatocellular carcinoma (HCC) is one of the most frequent cancers in the world and causing high number of deaths each year. Current therapies are far from adequate. Development of new therapeutic strategies depends on better understanding the molecular pathogenesis of HCC. Few genes are found to play role in transforming a normal hepatocyte to a cancerous one. It is necessary to identify novel genes involved in HCC to implement new diagnostic and treatment options. Replicative immortality is a common acquired feature of all cancers. Somatic cells have a limited number of cell divisions due to end replication problem at the ends of the chromosomes, namely telom- eric sequences. Replicative senescence is the inevitable consequence of this problem which is also a strong barrier in preventing cancer cell immortality.

In this study, we worked on two major aspects of cellular senescence and immortality in HCC. First, we analyzed the role of ZEB2 (Smad-interacting protein SIP1, ZFXH1) gene for a senescence-related role in HCC. ZEB2 gene is actually involved in epithelial-mesenchymal transition, but it also represses telomerase reverse transcriptase enzyme by directly binding to the promoter of TERT gene.

We observed that when we down-regulate ZEB2 via shRNA in senescent cells, these cells start to proliferate again and retain their immortal properties. We worked on Hep3B cells that overexpress ZEB2 gene, and observed high percentage of senescent cells among them. BrdU assays also conrmed the low proliferation rate. Further we found that these Hep3B-ZEB2 cells have relatively high expression of p21. We repeated the experiments on another system, tet-regulated overexpression of ZEB2 in A431 cells which we obtained from our collaborators. Also in liver tumors, we checked the ex- pression of ZEB2 and found that ZEB2 is downregulated in liver tumors. We now are able to say that ZEB2 has anti-growth effects in HCC. Then, we extended our work on the identication and analysis of a senescence and immortality gene network (SIGN) in relation to hepatocellular carcinogenesis. We worked on the microarray analysis of liver tumors, obtained from HCC patients with a cirrhosis background. We obtained a list of signature genes that can discriminate tumor from cirrhosis. We were able to compare the gene signatures coming from senescent-immortal clones with the genes coming from cirrhosis-tumor tissues. By this way, we tried to identify the genes that are responsible from the tumorigenesis process in the liver. We also utilized another in-vivo data set to test our signicant genes. We are now able to discriminate the different stages of HCC.

Chapter 3

MATERIALS AND METHODS

3.1 MATERIALS

3.1.1 Cell Culture Solutions

PBS, 10X NaCl, 80 g; KCl, 2 g; KH_2PO_4, 2.4 g, Na_2HPO_4, 14.4 g; dissolved in 1 L of ddH_2O. pH of the 10X buffer should be around 6.8, when diluted to 1X, pH should be 7.2–7.4.

DMEM-10 medium To 500 ml Dulbecco's modified Eagle's medium (Biochrom) supplemented with 3.7 g/L $NaHCO_3$, 1 g/L D-Glucose and stable glutamine, add 50 ml fetal calf serum (passed through 0.2 μm filter), 5 ml penicillin/streptomycin solution, 5 ml non-essential aminoacids, store at 4°C, warm to 37°C prior to use.

RPMI-10 medium To 500 ml RPMI medium (Gibco), add 50 ml fetal calf serum (passed through 0.2 μm filter), 5 ml penicillin/streptomycin solution, 5 ml non-essential aminoacids, store at 4°C, warm to 37°C prior to use.

3.1.2 Microbiology Solutions

LB medium Tryptone, 10 g; yeast extract, 5 g; NaCl, 5 g; add 1 L ddH_2O and autoclave immediately after preparation.

Agar medium Add 10% (w/v) bacto agar to LB medium, autoclave, pour onto plates and wait at room temperature until agar solidifies.

3.1.3 Western Blot Solutions

Protein lysis buffer Tris 1M, pH 8.0, 50 μL; NaCl, 2M, 125 μL; 25X proteinase inhibitor coctail, 40 μL; NP40, 10 μL; filtered ddH_2O, 775 μL.

RIPA lysis buffer Tris 1M, pH 8.0, 50 μL; NaCl, 2M, 300 μL; 25X proteinase inhibitor coctail, 40 μL; NP40, 10 μL; 10% SDS, 10 μL; filtered ddH_2O, 775 μL.

10% (w/v) SDS Wear mask, SDS is irritative to respiratory tract. Dissolve 10 g lauryl sulfate in 90 ml ddH_2O with stirring, then bring to 100 ml final volume.

Transfer Buffer, 1X Glycine, 2.25 g; Tris base, 5.81 g; SDS (from 10% SDS solution), 3.7 ml; methanol, 200 ml; to final volume of 1 L with ddH_2O. Transfer buffer should be prepared freshly for each experiment.

Running Buffer, 5X Tris base, 15.1 g; glycine, 95 g; SDS (from 10% SDS solution), 50 ml; bring to 1 L with ddH_2O. Store at 4°C and do not adjust pH. pH should be around 8.3 for the 1X solution. When diluted to 1X, water should be added first in order to prevent excess bubbling.

Wet transfer buffer, 1X Tris base, 6 g; glycine, 28.8 g; SDS (from 10% SDS solution), 1 ml; methanol, 200 ml; bring to 1 L with ddH_2O.

TBS, 10X Trisma base, 12.19 g; NaCl, 87 g; bring to 1 L with ddH_2O, adjust to pH 8.0 with 1N HCl.

Gel staining solution Coomassie brilliant blue G.250, 100 mg; absolute ethanol, 50 ml; phosphoric acid (85%), 100 ml; bring to final volume of 1 L with ddH_2O. Filter the solution through Whatman paper, store at 4°C.

Gel de-stain solution In ddH_2O, add 20% methanol and 7% acetic acid.

30% acrylamide Wear mask, dissolve 146 g acrylamide and 4 g N'-N'-bis-methylene acrylamide in 500 ml ddH_2O. Filter for 20 min, store at dark and 4°C.

APS, 10% (w/v) Dissolve 0.1 g ammonium persulfate in 1 ml ddH_2O.

Gel loading buffer, 2X ddH_2O, 3.55 ml; 0.5 M Tris HCl, pH 6.8, 1.25 ml; glycerol, 2.5 ml; 10% (w/v) SDS, 2 ml; 0.5% (w/v) Bromophenol blue, 0.2 ml. Store at room temperature. Add 5% β-mercaptoethanol to buffer prior to use.

1.5 M Tris-HCl, pH 8.8 Tris base, 27.23 g; ddH_2O, 80 ml. Adjust pH with 6N HCl. Bring total volume to 150 ml with ddH_2O. Store at 4°C.

0.5 M Tris-HCl, pH 6.8 Tris base, 6 g; ddH_2O, 60 ml. Adjust pH with 6N HCl. Bring total volume to 100 ml with ddH_2O. Store at 4°C.

Gel formulations (10 ml) Mix 30% acrylamide, tris buffer and SDS according to the gel percentage as described in the Table 3.1. For resolving gel, 1.5 M Tris-HCl, pH 8.8; for stacking gel, 0.5 M Tris-HCl, pH 6.8 Immediately prior to pouring the gel, add 50 μL 10% APS and 5 μL TEMED for the resolving gel; add 50 μL 10% APS and 10 μL TEMED for the stacking gel; swirl gently to initiate polymerization.

Blocking solution Milk powder, 2.5 g; TBS, 50 ml; Tween-20, 250 μL.

Table 3.1: SDS-PAGE Gel Formulations

Percent gel	**ddH_2O** (ml)	**30% acrylamide** (ml)	**Tris buffer** (ml)	**10% SDS** (ml)
5%	5.7	1.7	2.5	0.1
8%	4.7	2.7	2.5	0.1
10%	4.1	3.3	2.5	0.1
12%	3.4	4.0	2.5	0.1
15%	2.4	5.0	2.5	0.1

Stripping solution 10% (w/v) SDS, 10 ml; 1 M Tris-HCl, pH 6.8, 3.125 ml; β-mercaptoethanol, 357 μL; to final volume of 50 ml with ddH_2O.

3.1.4 Agarose gel solutions

Etidium bromide Wear mask and gloves, dissolve 0.2 g in 20 ml ddH_2O. Store at dark and 4°C.

TAE, 50X Tris base, 242 g; Tritiplex III (EDTA), 37.2 g; glacial acetic acid, 57.1 ml; bring to 1 L with ddH_2O, stir over night to dissolve.

Agarose gel, 2% Weigh 2 g of agarose powder and add to 100 ml TAE buffer. Boil and cool down, add 1 μg/μL etidium bromide, swirl and pour onto gel casting apparatus.

3.1.5 SABG solutions

SABG buffer Mix 200 mM citric acid, 600 μL; Na-P buffer, 600 μL; 100 mM K ferrocyanide, 150 μL; 100 mM K ferricyanide, 150 μL; 2 M NaCl, 225 μL; 100 mM MgCl2, 60 μL; 40 mg/ml X-gal solution, 75 μL; ddH_2O, 1140 μL. Adjust pH to 6.0 with NaH_2PO_4. Pass through 0.2 μm cellulose acetate filter, keep away from light and prepare freshly just before the experiment.

NaH_2PO_4, 1M dissolve 4.8 g sodium phosphate in 40 ml ddH_2O, store at 4°C.

Na_2HPO_4, 1M dissolve 7.12 g di-sodium hydrogen phosphate di-hydrate in 40 ml ddH_2O, heat to 40°C in a water bath to prevent precipitation, store at 4°C.

X-gal, 40 mg/ml dissolve 0.2 g in 5 ml dimethyl formamide, store at -20°C, in dark.

K ferricyanide, 100 mM Dissolve 0.658 g potassium ferricyanide in 20 ml ddH_2O, store at 4°C, in dark.

K ferrocyanide, 100 mM Dissolve 0.844 g potassium ferrocyanide in 20 ml ddH_2O, store at 4°C, in dark.

$MgCl_2$, 100 mM Dissolve 0.406 g magnesium chloride in 20 ml ddH_2O, store at 4°C.

NaCl, 2M Dissolve 2.34 g natrium chloride in 20 ml ddH_2O.

Citric acid, 200 mM Dissolve 2.85 g trisodium citrate in 40 ml ddH_2O, adjust pH to 6.0 with HCl.

Na-P buffer Mix 10.20 ml Na_2HPO_4, 1M and 29.80 ml NaH_2PO_4, 1M, adjust pH to 6.0 with NaH_2PO_4, 1M.

3% formaldehyde Mix 3 ml of 37% formaldehyde and 36 ml ddH_2O. Prepare freshly before the experiment.

3.1.6 Microarray reagents

All reagents used for the microarray experiments were purchased from Affymetrix. GeneChip Human Genome U133 Plus 2 (HG-U133 Plus 2.0, Affymetrix, P/N 900467), One-Cycle cDNA synthesis kit (Affymetrix, P/N 900431), IVT labeling kit (Affymetrix, P/N 900449), Poly-A exogenous positive controls (Affymetrix, P/N 900443) were utilized.

3.2 METHODS

3.2.1 Tissues

Surgically resected tissues were snap frozen in liquid nitrogen and stored at -80°C. The use of human material for research has been pre-approved by Ankara University Ethical Committee. For the tumor samples, tissues were resected inside the tumor. For the nontumor samples, tissues were resected from the adjacent tissue surrounding the tumor. The use of human material for research has been pre-approved by the Ankara University and Dokuz Eylul University Ethical Committees, and the written consent was obtained for each patient. Histology slides were prepared for all samples and scored by an experienced pathologist. Histology slides were prepared for all samples and analyzed by an experimented pathologist Dr. Önder Bozdoĝan.

3.2.2 Cell lines

HCC cell lines, Hep3B and Huh7, HepG2, Hep40, Hep3B, PLC/PRF/5, Snu182, Snu387, Snu398, Snu423, Snu449, Snu475, Focus, Mahlavu, and SKHep1, squamous epidermoid cell line A431 cells were used. HCC cell lines were grown in DMEM-10 or RPMI-10 (for Snu cell lines only) media. Hep3B clones that stably express ZEB2, Hep3B-S1, -S3, and -S4 were cultivated in DMEM-10 medium. For time intervals, medium was supplemented with 200 μg/ml geneticin 418 (neomycin) for the maintanence of stable expression of ZEB2. Huh7 clones, C1, C3, g12, and g11 that harbor empty pcDNA3 vector were cultivated like Hep3B clones. For all Huh7 and Hep3B, for each subculturing, passage numbers were recorded.

A431 cells were stably transfected with dox-on plasmid system that expresses ZEB2 with the addition of doxycycline. Culture medium for A431/ZEB2 cells was supplemented with 60 μg/ml hygromycin B (Roche) and 0.5 μg/ml puromycin

(Sigma). For ZEB2 induction, cells were plated at low density (1500-2500 cells/well in 6-well plates). Plating day was designated as day -2. At day 0, culture medium was replaced with fresh culture medium supplemented with 2 μg/ml Dox (Doxycycline, Sigma). Medium was changed every 3 days with the fresh medium supplemented with Dox. A431/ZEB2 cells were a gift from Eugene Tulchinsky from Leicester University, details about these clones can be found in Mejlvang et al. [46].

Huh7 and Hep3B clones were generated by Nuri Öztürk, former member of our group, and details were described in Ph.D. thesis of the researcher [67]. For all cells, medium was replaced in every 3 days, and cells were subcultured to new flasks or plates when confluency was over 80%. Cryopreservation was performed as follows: cells were trypsinized and pelleted. Cell pellets were suspended in growth medium supplemented with 8% DMSO and placed in a cryotube. Tubes were placed immediately to -20°C for 1 hour, then -80°C overnight, and then stored in liquid nitrogen for long term storage.

3.2.3 RNA isolation

Immortal, presenescent and senescent cells (described above) were plated in triplicate and subjected to RNA extraction. Frozen tissue samples were cut into 20 μm thick slices, and scraped into microtubes for RNA extraction. Two 6 μm slices were also cut for pathological examination of tissues to be used for RNA extraction. Both cells and tissues were homogenized using a 0.8 mm needle before processing the sample. Total RNA isolation kit (Promega, Madison, USA) and NucleoSpin RNA II Kit (MN Macherey-Nagel) were used for RNA extraction for the cell lines and for the tissues, respectively. DNAse digestion was performed according to the kit protocol. RNA concentrations were determined by NanoDrop spectrophotometer (NanoDrop, USA). All but two tissue RNA samples were analyzed using Agilent Bioanalyzer, and two with integrity number < 4.0

were discarded from the study. Two tissue samples without Agilent data have been evaluated according to the quality of microarray data (Table 4.3). Cell line RNA quality was evaluated by the ratio of 18S to 28S RNAs by Agilent Bioanalyzer; all samples passed this quality control test (data not shown).

3.2.4 cDNA preparations

cDNAs were synthesized from DNase I-treated RNA using RevertAid First Strand cDNA synthesis kit (MBI Fermentas). 1-4 μg of RNA was used for cDNA synthesis. RNAs were first heated to 70°C for 5 min, together with oligo dT primer, then incubated at 37°C for 5 min, in a mixture containing buffer, dNTP and RNase inhibitor, and finally incubated at 42°C for 1 h followed by 70°C for 10 min for the synthesis of first strand cDNA by using reverse transcriptase enzyme. All reagents were supplied by the kit.

3.2.5 Semi-quantitative RT-PCR

cDNAs were used as templates for PCR. Primers were designed using Primer3 program[1]. The main criteria was to skip an intron to prevent amplifications from genomic DNA. All primers were designed to amplify transcripts spanning two adjacent exons with an intronic sequence in the genome. The primer list is given in Table 3.2. PCR amplifications were performed in 25 μL of volume. 1X PCR buffer supplemented with $(NH_4)_2SO_4$, 1.5 mM $MgCl_2$, 200 μM dNTP, 10 pmoles of each primer, and 1 U of Taq DNA polymerase were mixed in the presence of ddH_2O. All PCR reagents were purchased from Fermentas. Thermal cycler conditions were as follows: an initial denaturation of 94°C for 5 min, followed by cycles of 94°C, 30 sec; annealing temperature, 30 sec; 72°C, 30 sec. A final extension of 72°C, 10 min was performed. Number of cycles were differed for each primer set (Table 3.2). TC-512, Techne or TechGene, Techne thermal

[1]http://fokker.wi.mit.edu/primer3/input.htm

Table 3.2: Primer List

Gene	**Sequence (5' to 3')**	**Annealing temperature**
hTERT–F	CGGAAGAGTGTCTGGAGCAA	58°C
hTERT–R	GGATGAAGCGGAGTCTGGA	58°C
hZEB2–F	ATGGCTGTGTCACTGCGCTGA	60°C
hZEB2–R	GGAAGACAAGCTTCATATTGC	60°C
mZEB2–F	GGCTTACCTGCAGAGCATC	60°C
mZEB2–R	CCTCTGAACTGTCGTCCATC	60°C
E-Cadherin–F	TCCCATCAGCTGCCCAGAAA	60°C
E-Cadherin–R	TGACTCCTGTGTTCCTGTTA	60°C
β-Actin–F	GAAATGGTGCGTGACATTAAG	60°C
β-Actin–R	CTAGAAGCATTTGCGGTGGA	60°C
GAPDH–F	GGCTGAGAACGGGAAGCTTGTCAT	60°C
GAPDH–R	CAGCCTTCTCCATGGTGGTGAAGA	60°C

cyclers were used for PCR reactions. GAPDH was used as an internal control for PCR reactions.

PCR products were analyzed on a 2% (w/v) agarose gel prepared with TAE buffer and stained with 1 μg/ml ethidium bromide and visualized under UV transillumination using Gel-Doc 2000, Bio-Rad or ChemiCapt, Vilber Lourmat visualization systems.

3.2.6 Quantitative real-time RT-PCR

The iCycler iQ PCR machine (Bio-Rad) was used. Reactions were performed in 20 μL volume consisting 2X Master Mix (Finnzymes), primers and ddH_2O. Reaction conditions were as follows: 94°C, 5 min for initial denaturation; 45 cycles of the loop 95°C, 30 sec; 60°C, 30 sec; 72°C, 30 sec. Data collection is enabled after this reaction. All reactions were followed by melting curve analysis: 94°C, 30 sec for initial denaturation, 60°C, 30 sec; 80 cycles starting with 60°C, 15 sec and then increase set point temperature after cycle 2 by 0.5°C. Melt curve data collection and analysis enabled after this reaction. 45 cycles of amplification enabled

Table 3.3: Antibodies used in western blot (WB), immunofluorescence (IF), and immunoperoxidase (IP) experiments and corresponding dilutions.

Anti-:	**Link:**	**Company:**	**Catalog no:**	**Dilution:**
BrdU	—	Dako	M0744	1:500 (IF)
p21	—	Calbiochem	OP64	1:100 (IP, WB)
c-Myc	—	SantaCruz	sc-40	1:150 (IF, IP)
p16	—	SantaCruz	sc-468	1:200 (IP)
p15	—	SantaCruz	sc-612	1:200 (IP)
E-Cadherin	—	SantaCruz	sc-7870	1:500 (WB)
ZEB2	—	SantaCruz	sc-18392	1:500 (IF)
Calnexin	—	Sigma	C4731	1:10000 (WB)
Rabbit	FITC	Dako	F0054	1:150 (IF)
Mouse	FITC	Dako	F0479	1:150 (IF)
Rabbit	HRP	Sigma	A6154	1:5000 (WB)
Mouse	HRP	Sigma	A0168	1:5000 (WB)

almost all products to be saturated. Melting curve analysis was done as a quality control to verify the amplification of the single gene product. Expression levels were calculated using the following formula: $2^{-[(\mathrm{Ct(Gene\ of\ interest)}-\mathrm{Ct}(\beta-\mathrm{actin})]}$. β-actin was used as an internal control for real-time PCR experiments. All experiments were done in triplicate and Ct values >35 or <11 were excluded from data analysis.

3.2.7 Antibodies

Antibodies used and the corresponding dilution factors are given in the Table 3.3.

3.2.8 Western Blotting

Western blotting experiments were started with total protein lysates from cells. Cells were trypsinized or scraped from flasks or plates respectively. Cell pellets were suspended in RIPA lysis buffer or protein lysis buffer, 30 min incubation on ice was followed by centrifugation at 13000 rpm, 20 min at 4°C. Supernatants were transferred into a new tube, stored at -20°C and 2 μL of each sample were

taken for Bradford assay. For the Bradford assay, a BSA curve was drawn with 0, 1, 2, 4, 8, 16, 32 μL of BSA (1 mg/ml) and Bradford solution (Sigma, B6916). A formula was obtained and used for calculation of concentration of the protein samples. Protein samples were mixed with Bradford reagent, equilibrated at room temperature for 10 min, and then measured at 590 nm wavelength by using spectrophotometer (Beckman, DU640). Defined amounts of protein was mixed with loading buffer and run on a SDS-Page gel at constant voltage at room temperature, together with protein markers (Fermentas, SM0671, SM0441) under denaturing conditions. Bio-Rad Mini-Protean Tetra Cell apparatus was used for electrophoresis and wet transfer. For semi-dry transfer, Bio-Rad Transblot Semidry apparatus was used. After electrophoresis, proteins were transferred to PVDF membranes (Roche), either by semi-dry or wet transfer. Semi-dry transfer was held at room temperature, at a constant voltage of 12 V, 20-30 min. Wet transfer was held at 4°C, at a constant voltage of 80 V, 90 min. Gels were then stained with gel staining solution to validate the efficiency of transfer. Membranes were immediately soaked in blocking buffer for 1 h. Primary antibody incubations were performed in blocking buffer at room temperature,1 h or at 4°C, overnight. 30 min of 6X washing with Tween-20 supplemented TBS was followed by secondary antibody incubation at room temperature for 45-50 min. Washing step was repeated and HRP substrate was added for 5 min (ECL-plus, Amersham). Developer ensured the transfer of bands from PVDF to X-ray films (Kodak), by using a hyperprocessor (Amersham). To validate equal loading, immunoblotting steps were repeated for calnexin antibody. Before calnexin incubation, membranes were either passed through stripping solution or blocking solution depending on the molecular weights of the target proteins.

3.2.9 Immunofluorescence

Cells were seeded on coverslips in 6-well plates. On the day of experiment cells were taken out from cell culture facility, washed twice with PBS, then fixed with methanol for 5 min. Removal of excess methanol through washing steps was followed by 1 h incubation with PBS supplemented with 1% BSA. Incubation with primary and secondary antibody was performed in PBS-BSA, 1h at room temperature. After each antibody incubation, cells were washed with PBS supplemented with 0.1% Tween-20 for 5 min intervals, 3 times. DAPI (Roche) was applied as a counterstain with a dilution of 1:10000, for 5 min. 10 min of ddH_2O removed the precipitates and cleared background signals. Coverslips were covered onto glass slides with mounting medium (Dako), images were taken with Zeiss microscope attached with an AxioCam.

3.2.10 Immunoperoxidase

Cells that were seeded onto coverslips one or two days before the experiment, were fixed with 4% formaldehyde for 10 min, washed with ddH_2O and PBS for 3 min. Cells were permeabilized in PBS supplemented with 0.5% saponin and 0.5% TritonX for 3 times at 5 min intervals, washed with PBS for 3 min, and then incubated at 37°C for 1 h in the presence of 10% FCS, 0.3% TritonX in PBS. Primary antibody incubations were performed in 2% FCS, 0.3% TritonX in PBS, overnight at 4°C and 1 h at room temperature. Secondary antibody (DakoCytomation Envision+Dual link) was performed in the same solution with primary antibody, 1h at room temperature. After each antibody incubation, cells were washed with PBS supplemented with 2% FCS and 0.3% TritonX for 5 min intervals, 3 times. DAB detection solution (Dako) was applied onto coverslips and waited till the color change is obvious (15 sec–3 min). Counterstaining was done with hematoxylene and coverslips were attached to glass slides with glycerol.

3.2.11 Senescence-associated beta-galactosidase (SABG) assays

SABG activity was detected using a described protocol [68]. Briefly, cells were seeded onto plates for a confluency of 50-80% confluency on the day of experiment. Tissues were cut as 6 μm slices onto glass plates and stored in -80°C for a maximum of 1 day. Cells or tissues were washed with PBS twice, fixed with 4% formaldehyde at room temperature. SABG buffer was applied onto cells, plates were covered with aluminum folio, placed in a CO_2 free incubator set at 37°C, for 16-18 hours. After incubation, counterstaining was done with nuclear fast red for 3 min. Images were taken by using Zeiss microscope. SABG-positive and -negative cells were identified and counted manually by three independent observers under inverted light microscope.

3.2.12 Long term BrdU labeling assay

For long term BrdU labeling assay, cells were replaced with a fresh medium with 1 μg/ml BrdU 24 hours before the experiment. On the day of experiment, cells reached at a confluency of 50-80%. After 24 hours, cells were fixed with cold ethanol for 15 min, washed with PBS 2-3 times, then 2N HCl was applied for 20 min. Excess HCl was removed by 15 min of washing with PBS. After incubation with PBS supplemented with 0.1% Tween-20 and 3% BSA for 1 h, primary and secondary antibodies were applied in the same solution. Washing steps were performed after antibody incubations, counterstaining was done with DAPI. Coverslips were covered onto glass slides with mounting medium (Dako), images were taken with Zeiss microscope attached with an AxioCam.

3.2.13 Statistical Analysis

For the comparison of 2 groups, Student t-test was used. A p value of less than 0.01 was considered to be significant.

3.2.14 Microarray experiments

Microarray experiments were performed on Affymetrix platform. GeneChip Human Genome U133 Plus 2 (HG-U133 Plus 2.0, Affymetrix, P/N 900467) arrays were utilized. Protocols that were supplied by the manufacturer were strictly followed [69].

Sample preparation Isolated total RNA was evaporated (when necessary) to reach a concentration of more than 1 μg/μL. 8-10 μg of RNA was converted to double-stranded cDNA by using One-Cycle cDNA synthesis kit (Affymetrix, P/N 900431). To provide exogenous positive controls, a set of poly-A RNA controls are added to the RNA samples. These poly-A controls are synthesized from B. subtillis genes. Poly A control stock was diluted with Poly-A control dilution buffer according to the dilution scheme. RNA concentrations at the beginning of the experiment and cRNA concentrations before fragmentation were measured by ND-1000 spectrophotometer (NanoDrop) and also Agilent 2100 Bioanalyzer (Agilent Technologies). Bioanalyzer also utilized to determine the integrity of RNA and for fragmentation efficiency. For these purposes, RNA Nano LabChip (Agilent Technologies) was used to obtain RNA integrity numbers (RIN), digital RNA gels, and 18S/28S values.

First Strand cDNA synthesis 8-10 μg of sample RNA and diluted poly-A controls were added to a microfuge tube, and 2 μg of T7-Oligo(dT) primer (50 μg) was also added. Volume was completed to 12 μg with RNase-free water. In a thermal cycler, the mixture was incubated at 70°C for 10 min, then it was

cooled to 4°C for at least 2 min. In another tube, First-Strand Master Mix was prepared by adding 4 μL of 5X 1st Strand Reaction Mix, 2 μL of 0.1M DTT, 1 μL of 10 mM dNTP, to a total volume of 7 μL. After a brief centrifuge, 7 μL of First-Strand Master Mix was added to each RNA/T7-Oligo(dT) Primer Mix. After a brief centrifuge, tubes were placed in 42°C for 2 min. Finally 2 μL of SuperScript II was added to the mixture, and tubes were placed immediately into 42°C to be incubated for 1 hour. Tubes were cooled down to 4°C before continuing to the next step.

Second Strand cDNA synthesis Second-Strand Master Mix were prepared according to the recipe given in Table 3.4. 130 μL of Second-Strand Master Mix to each first-strand synthesis sample. This mixture was incubated at 16°C for 2 hours, then 2 μL of T4 DNA Polymerase was added to each sample and incubated for 5 min at 16°C. To finalize the reaction, 10 μL of 0.5M EDTA was added to the tubes.

Table 3.4: Preparation of Second-Strand Master Mix

Component	**Volume**
RNase-free water	91 μL
5X 2nd Strand Reaction Mix	30 μL
10mM dNTP	3 μL
E. coli DNA ligase	1 μL
E. coli DNA Polymerase I	4 μL
RNase H	1 μL
Total volume	130 μL

Cleanup of Double-Stranded cDNA Double-stranded cDNA synthesis reaction was immediately followed by cleanup protocol. 600 μL of cDNA Binding Buffer was added to the mixture, vortexed by 3 seconds, the mixture then applied to cDNA Cleanup Spin Column, and centrifuged. 750 μL of cDNA Wash

Buffer which contains alcohol was used to wash the column, which is then dried by centrifugation. Finally cDNA was recovered by 14 μL of cDNA Elution Buffer.

Synthesis of Biotin-Labeled cRNA The double-stranded cDNA served as a template in in vitro transcription (IVT) reaction to obtain biotinylated and amplified cRNA. IVT labeling kit (Affymetrix, P/N 900449) was used. Biotin labeling reaction was started with 6 or 12 μL of cDNA, depending on the starting RNA. Then the mixture was prepared according to the Table 3.5.

Table 3.5: Preparation of IVT Reaction Mix

Component	**Volume**
Template cDNA	6 or 12 μL
RNase-free Water	to a final volume of 40 μL
10X IVT Labeling Buffer	4 μL
IVT Labeling NTP Mix	12 μL
IVT Labeling Enzyme Mix	4 μL
Total Volume	40 μL

After mixing the reagents, mixture was incubated at 37°C in a thermal cycler for 16 hours.

Cleanup and quantification of Biotin Labeled cRNA 60 μL of RNase-free water was added to the IVT reaction and mixed. Then 350 μL of IVT cRNA Binding Buffer and 250 μL of 96% ethanol were added to the mixture, by vortexing in between. Sample was applied to IVT cRNA Cleanup Spin Column, centrifuged, washed with IVT cRNA Wash Buffer. Another washing was performed with 80% ethanol, and membrane dried by centrifugation. Finally first 11 then 10 μL of RNase-free water was used to elute the cRNA. Purified cRNA was quantified by using NanoDrop Spectrophotometer, then calculated for the total amount of labeled RNA. Labeled RNA was calculated with the following formula:

adjusted cRNA yield = RNAm - (total RNAi)

RNAm = amount of cRNA measured after IVT (μg)

total RNAi = starting amount of total RNA (μg)

y = fraction of cDNA reaction used in IVT

Fragmenting the cRNA Fragmenting the cRNA is required before hybridization, cRNA is fragmented to 35 to 200 base fragments by metal induced hydrolysis. 20 μg of labeled cRNA was fragmented with 8 μL of 5X Fragmentation Buffer in a final volume of 40 μL supplied by RNase-free water. Reactions took place at 95°C for 35 minutes. Tubes were placed on ice immediately. Fragmentation efficiency were monitored by Agilent Systems.

Target Hybridizations 15 μg of fragmented RNA was hybridized to GeneChips. Poly-A exogenous positive controls (Affymetrix, P/N 900443) and probe sets for non-eukaryotic transcripts (Affymetrix, P/N 900454), which serve as controls for hybridization, washing, and staining procedures were added in the hybridization cocktails. Hybridization cocktail was prepared according to the Table 3.6.

Table 3.6: Hybridization Cocktail

Component	**Volume**
Framented and Labeled cRNA	15 μg
Control Oligonucleotide B2 (3 nM)	5 μL
20X Eukaryotic Hybridization Controls (bioB, bioC, bioD, cre)	15 μL
2X Hybridization Mix	150 μL
DMSO	30 μL
Nuclease Free Water	to a final volume of 300 μL
Total volume	300 μL

Hybridization cocktail was heated to 99°C for 5 minutes in a heat block. A probe array was equilibrated to room temperature, and then wetted with 200 μL

of Pre-Hybridization Mix. The probe array filled with Pre-Hybridization Mix was incubated to 45°C for 10 minutes in hybridization oven. Hybridization cocktail was moved to 45°C heat block for 5 minutes. After centrifuging at high speed, pre-hybridization mix was removed and probe arrays were filled with 250 μL of hybridization cocktail. Probe arrays were placed in hybridization oven, rotated at 60°C, at 45 rpm. Hybridization took place in GeneChip Hybridization Oven 640 (Affymetrix) for 17 hours. Suggested incubation time was 16 hours, but due to the low efficiency of RNAs extracted from tissues, this duration was prolonged to 17 hours.

Fluidics and Scanning Immediately following hybridization, the GeneChip arrays were washed and stained with streptavidin phycoerythrin conjugate using an automated protocol (FS450_0001) on a GeneChip Fluidics Station 450 (Affymetrix), followed by scanning on a GeneArray Scanner (Affymetrix). First fluidics station was primed using the "Prime_450" module, then the experiment descriptions were recorded to the GCOS software. Wash Buffer A and Wash Buffer B were placed in the appropriate positions in the fluidics station, probe arrays then placed in the sockets. 600 μL of each of Stain Cocktail 1 and 2 and 800 μL of Array Holding Buffer were also placed in microfuge tubes. Washing protocol followed by the fluidics station is given in Table 3.7. Probe arrays were immediately scanned.

Data Storage GeneChip Operating Software (GCOS, Affymetrix) was used to collect and store the data. Image data (*.dat file), cell intensity data (*.cel file), and expression cell intensity data (*.chp) files were created and stored. Also from all experiments a report file (*.rpt) was created and array quality measures (presence %, actin and gapdh hybridization values) were extracted.

Table 3.7: Fluidics Protocol

Post Hyb Wash #1	10 cycles of 2 mixes/cycle with Wash Buffer A at 30°C
Post Hyb Wash #2	6 cycles of 15 mixes/cycle with Wash Buffer B at 50°C
1st Stain	Stain the probe array for 5 minutes with Stain Cocktail 1 at 35°C
Post Stain Wash	10 cycles of 4 mixes/cycle with Wash Buffer A at 30°C
2nd Stain	Stain the probe array for 5 minutes with Stain Cocktail 2 at 35°C
3rd Stain	Stain the probe array for 5 minutes with Stain Cocktail 3 at 35°C
Final Wash	15 cycles of 4 mixes/cycle with Wash Buffer A at 35°C
Array Holding Buffer	Fill the probe array with Array Holding Buffer

3.2.15 Data processing and quality control

GeneChip Operating Software (GCOS, Affymetrix) was used to collect and store the data. CEL files were uploaded to RMAExpress program to assess the quality of the arrays at the image level[2]. Quality assessment of the Affymetrix datasets was performed using affy PLM[3]. Affy PLM was used to detect artifacts on arrays that could pose potential quality problems and also for assessment of homogeneity of expression signal across arrays. Accordingly, NUSE and RLE plots were drawn by using PLM as the summarization method; outliers with high deviation from the average probe intensity value were identified and excluded from further analyses. CDF files were required for RmaExpress to process CEL files. CDF file *"hgu133plus2AnnoData.zip"* was downloaded[4].

[2]http://rmaexpress.bmbolstad.com
[3]http://www.bioconductor.org/packages/2.4/bioc/html/affyPLM.html
[4]http://www.affymetrix.com

3.2.16 Data Import.

BRB Array Tools[5] developed by Dr. Richard Simon and BRB-ArrayTools Development Team were used extensively for exploratory and statistical analysis of the arrays. CEL files were imported into BRB-Array Tools. During import, "justRMA" normalization was applied without any filtering criteria.

3.2.17 Class Comparison.

In order to find a subset of genes that can discriminate tumor samples from cirrhosis samples, class comparison tool from BRB Array Tools was utilized. At a significance level of 0.05, random variance model was used.

3.2.18 Hierarchical Clustering

For all cluster analyses, Cluster 3.0 program[6] was used. First data was adjusted by centering genes and arrays separately based on mean values, then average linkage was applied to genes and arrays using correlation (uncentered) similarity metric. Cluster files were visualized by Java Treeview[7].

3.2.19 Intersection lists

Common probe-sets between the two significant gene lists were found by CROPPER[8] and custom perl-codes developed in Bilkent University.

3.2.20 Scatterplots

To find the genes changing in the same direction between HCC and immortal samples and between cirrhosis and senescent samples, scatterplots were drawn in

[5]http://linus.nci.nih.gov/BRB-ArrayTools.html
[6]http://bonsai.ims.u-tokyo.ac.jp/ mdehoon/software/cluster/
[7]http://jtreeview.sourceforge.net
[8]http://katiska.uku.fi/jmpaanan/cgi-bin/cropper/multi.pl"

BRB Array Tools by using 1.5 fold change.

3.2.21 Pathways Analysis

DAVID[9] [70] was used to identify the pathways associated with different gene lists by using Functional Annotation Clustering. As the cutoff for significance; we selected biological groups with >1.3 enrichment score, >5 FDR, and >0.05 Benjamini Hochberg multiple test corrected values.

3.2.22 Clinical Dataset Analysis

Wurmbach data [71] was downloaded[10]. 75 CEL files were uploaded into BRB-ArrayTools by using "justRMA" normalization method without any filters. Five classes set from Wurmbach data were as follows: control (n=10), cirrhosis (n=13), dysplasia (n=17), early HCC (n=18), and advanced HCC (n=17).

3.2.23 Prediction analysis

We performed binary tree classifier for utilizing gene expression profile to predict the class of future samples using BRB array tools. The individual binary classifiers were based on the Support Vector Machines incorporating genes that were differentially expressed among genes at the 0.001 significance level as assessed by the random variance t-test.

3.2.24 Creation of immortality- and senescence-associated gene lists

Class comparison tool was applied to Wurmbach [71] and Boyault [72] datasets, independently at an alpha level < 0.001 and/or < 0.01. For the former, pairwise

[9]http://david.abcc.ncifcrf.gov/
[10]http://www.ncbi. nlm.nih.gov/pro-jects/geo" (GSE 6764)

comparisons based on a progressive staging were performed: normal vs. cirrhosis, cirrhosis vs. dysplasia, dysplasia vs. early HCC, early HCC vs. advanced HCC. For Boyault data [72], class comparison lists between specified pairs were determined, then filtered to reduce the probeset information into genes. For each gene with multiple probesets, the probeset with the highest discriminating p-value was chosen. These genes were then assessed for their expression modulation in Huh7 clones immortality/senescence dataset. The genes whose expression was upregulated in immortal clones were called immortality-associated genes, whereas those with increased expression in senescent clones were considered as senescence-associated genes. A custom PERL routine by Raşit Öztürk was used to identify the proportion of immortality and senescence genes in each class comparison gene list. Briefly, genes are classified according to their fold change values (up if >1 or down if <1) of the two classes to be compared (e.g., Class I: control vs. Class II: cirrhosis). In the second filtering step, fold change between immortal versus senescence groups was assessed such that a probeset was considered upregulated or downregulated if the fold change value between immortal and senescent classes was equal to or bigger than 1.5 or equal to or less than 0.66, respectively. The numbers of upregulated and downregulated probesets were counted and these counts were used to perform a two-tailed Fishers exact test to assess whether the divergence between the numbers of immortality versus senescence genes within a list was significant.

Chapter 4

RESULTS

4.1 Downregulation and the Anti-growth Effect of ZEB2 in Hepatocellular Carcinoma

4.1.1 Extraction of ZEB2 expression from the publicly available microarray datasets

To explore the expression patterns of ZEB2 in different liver disease stages, we first performed in silico analysis of publicly available global expression data. Microarray expression dataset recently generated by Wurmbach et al. [71] was selected for this study, as it is composed of a well-defined set of liver tissues at different stages of HCC development, ranging from a normal liver to very advanced HCC. The reported data was normalized and average probe intensities were calculated for individual samples. We regrouped samples reported by Wurmbach et al. [71] into five categories: normal liver (n=10), cirrhosis (n=12), dysplasia (early and late dysplasia combined; n=17), early HCC (very early and early HCC combined; n=17), and advanced HCC (advanced and very advanced HCC combined; n=15). As shown in Figure 4.1, cirrhosis samples displayed significantly increased ZEB2 expression, when compared to normal liver samples ($p<0.005$).

One-Way ANOVA was performed with significant results (F=12.9; p= 000). Accordingly, pairwise t-tests were performed to see which of the groups were significantly different from others.Thereafter, ZEB2 levels displayed stepwise decreases in dysplasia, early HCC and advanced HCC, respectively. When compared to cirrhosis, this decrease was statistically significant for all three categories (p values 0.0061, 0.0001 and <0.0001 for dysplasia, early HCC and advanced HCC, respectively). A statistical difference was also evident between normal liver and advanced HCC (p<0.001).

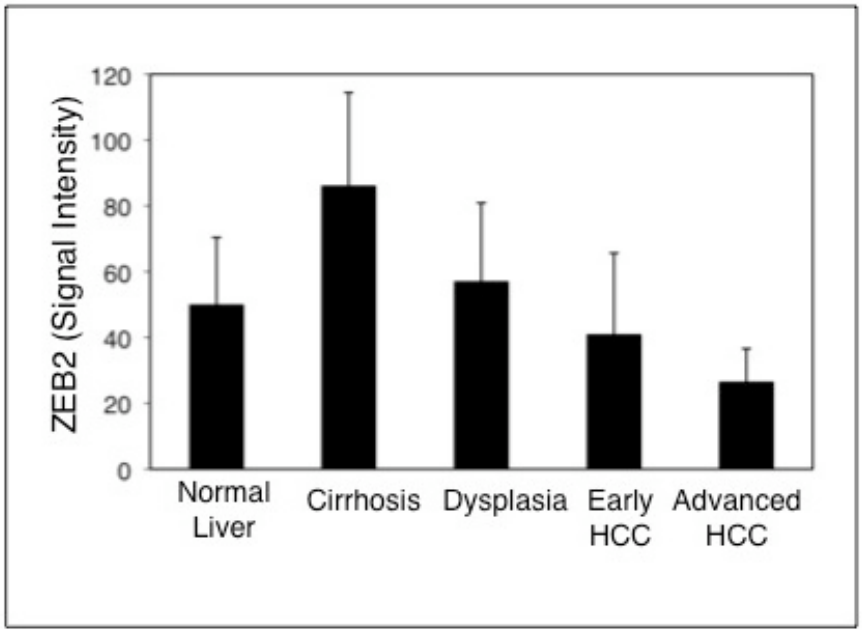

Figure 4.1: ZEB2 expression is induced in cirrhosis, but lost during malignant progression of HCC. In silico reanalysis of ZEB2 expression in normal liver, HCV-induced cirrhosis, dysplasia and HCC. Global expression data reported by Wurmbach et al. [71] was normalized and probe intensities for each disease group were used for comparison.

4.1.2 ZEB2 expression in tumor and nontumor pairs

To confirm in silico observations, we tested ZEB2 expression in seven pairs of tumor and nontumor liver tissues from cirrhotic patients by quantitative PCR

analysis. The expression of ZEB2 in cirrhotic tissues was high but displayed variability between patients (Figure 4.2). In contrast, all paired HCC samples displayed consistently lower levels of ZEB2 expression, as compared to cirrhotic liver samples.

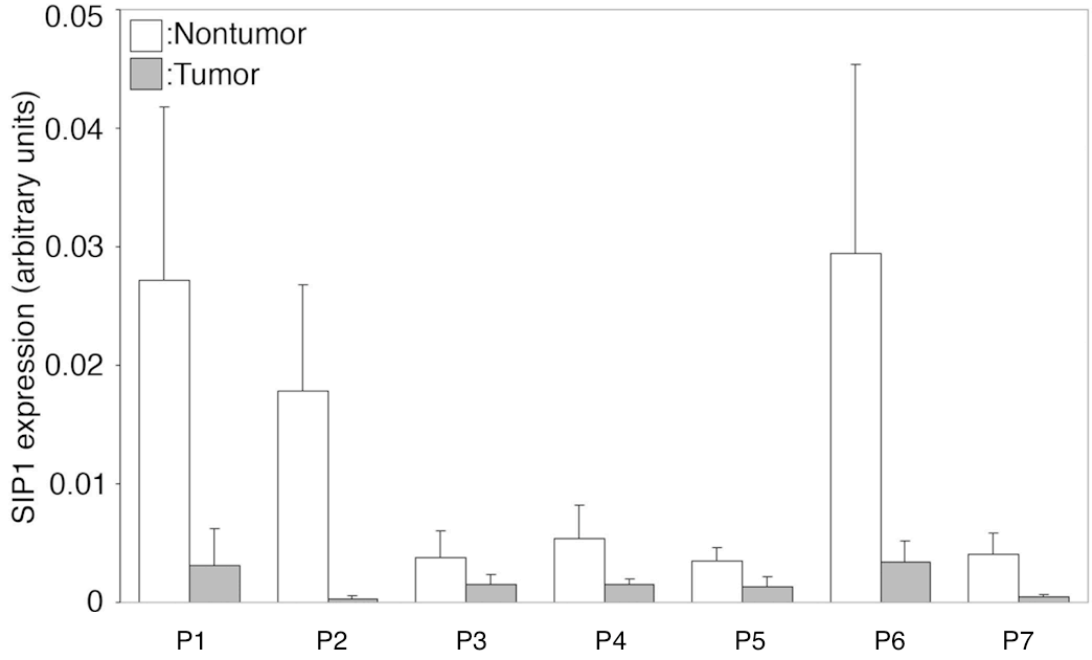

Figure 4.2: Real-time quantitative PCR analysis of ZEB2 expression in seven pairs of HCC and non-tumor liver tissues (all cirrhosis), indicating consistent loss of expression in tumors. Real-time PCR analysis was performed for ZEB2 and β-actin in triplicate, and Ct values were determined. Relative levels of ZEB2 transcripts were calculated using β-actin as reference. Numbers below the x axis indicate patient codes.Tumors, gray bars; cirrhosis; white bars.

Together, in silico and in vivo tumor studies that correlated with each other indicated that ZEB2 expression is downregulated during malignant progression from cirrhosis to HCC.

4.1.3 Senescence-like growth arrest in ZEB2-overexpressing Hep3B clones

Hep3B cells were transfected with Flag-tagged ZEB2 vector, and early passages (passages 6-9) of G418-resistant clones were screened for ZEB2 overexpression by

RT-PCR and three clones (S1, S3 and S4 clones) were selected together with an empty vector-derived C1 clone Figure 4.3.

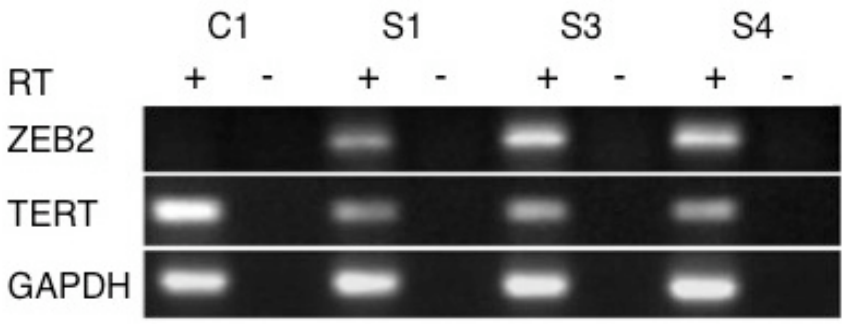

Figure 4.3: ZEB2 represses TERT expression and induces senescence-like growth arrest in HCC-derived Hep3B cells. RT-PCR data showing that ZEB2-expressing clones display repression of telomerase reverse transcriptase (TERT) transcription. RT; reverse transcriptase.

We were not able to show Flag-ZEB2 expression by immunoperoxidase or by immunofluorescence assays using commercially available anti-Flag antibody in any of the clones, probably because of the low level of expression (data not shown). Next, we compared the levels of TERT expression in the same set of clones. We observed a partial repression of TERT transcript levels in all ZEB2-expressing clones, as compared to the C1 clone Figure 4.3. Based on our previously published data on senescence induction associated with TERT repression in Huh7 clones [42], we screened Hep3B-derived clones with senescence markers. The C1 control clone was usually free of senescence-associated β-galactosidase (SABG)-positive cells, except for one or two cells that were occasionally observed (Figure 4.4-top left).

In contrast, SABG-positive and flattened cells were abundant in S1, S3 and S4 clones (4.4, top right and bottom). In order to confirm senescence-like arrest and to quantify the rates of permanently arrested cells in different Hep3B-derived

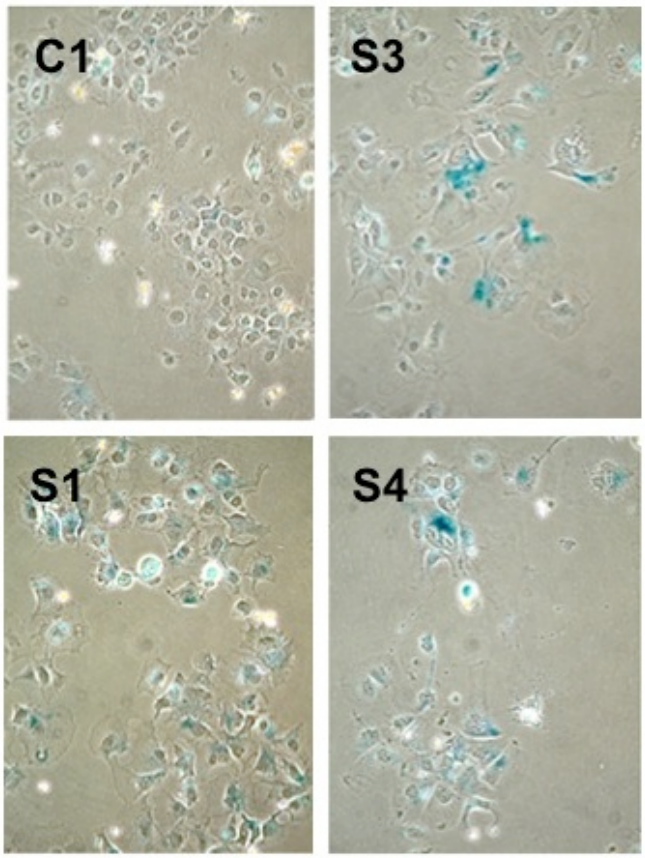

Figure 4.4: ZEB2-expressing clones display positive staining for SABG. Senescent cells (blue) were abundant in ZEB2-expressing S1, S3 and S4 clones, but not in C1 clone. ZEB2-expressing clones (S1, S3 and S4) were generated after transfection of Hep3B cells with Flag-tagged ZEB2 expression vector. C1; negative control clone generated with empty vector.

clones, we calculated the DNA labeling index after long-term (24h) BrdU labeling under mitogenic stimulation, as described previously [42], [73]. Low-density clonogenic conditions were used for this assay. Colonies were derived from different clones and labeled with BrdU for 24h, followed by anti-BrdU fluorescence staining. Cell nuclei were then counterstained with DAPI and observed under a fluorescent microscope. Colonies derived from the C1 control clone displayed permanently arrested (i.e. BrdU-negative) cells at low rates, whereas colonies derived from ZEB2-overexpressing clones usually had higher rates of permanently arrested cells (Figure 4.5).

To test the significance of these findings, BrdU-positive and BrdU-negative cells were counted in randomly selected colonies (n=10) that were derived from each clone. Then, a DNA labelling index (mean±SD) was calculated for each clone tested. This index was 13±10% for C1-derived colonies. In contrast, ZEB2-overexpressing clones displayed permanently arrested cells at significantly higher index rates (Figure 4.6).

The DNA labeling indices were 45±15%, 38±12% and 34±13% for S1, S3 and S4, respectively ($p < 0.001$ for any ZEB2-expressing clone versus C1 clone). These observations provided plausible evidence that ectopic expression of ZEB2 in Hep3B HCC cells results in senescence-like growth arrest in association with the repression of TERT expression in these cells. Senescence arrest in different cell types is commonly mediated by an induced expression of $p15^{INK4b}$, $p16^{INK4a}$ and/or $p21^{Cip1}$ cyclin-kinase inhibitors (reviewed by [20]). Therefore, we compared the expression of these senescence mediators in clones C1 and S4. Both clones were plated in triplicate and subjected to immunoperoxidase staining using appropriate antibodies. There was no detectable expression of $p15^{INK4b}$ in either the C1 or in the S4 clones. $p16^{INK4a}$ expression was positive in both C1 and S4 clones, as reported previously for the parental Hep3B cells [74]. In contrast, we observed a significant difference in the rates of $p21^{Cip1}$-expressing cells (Figure

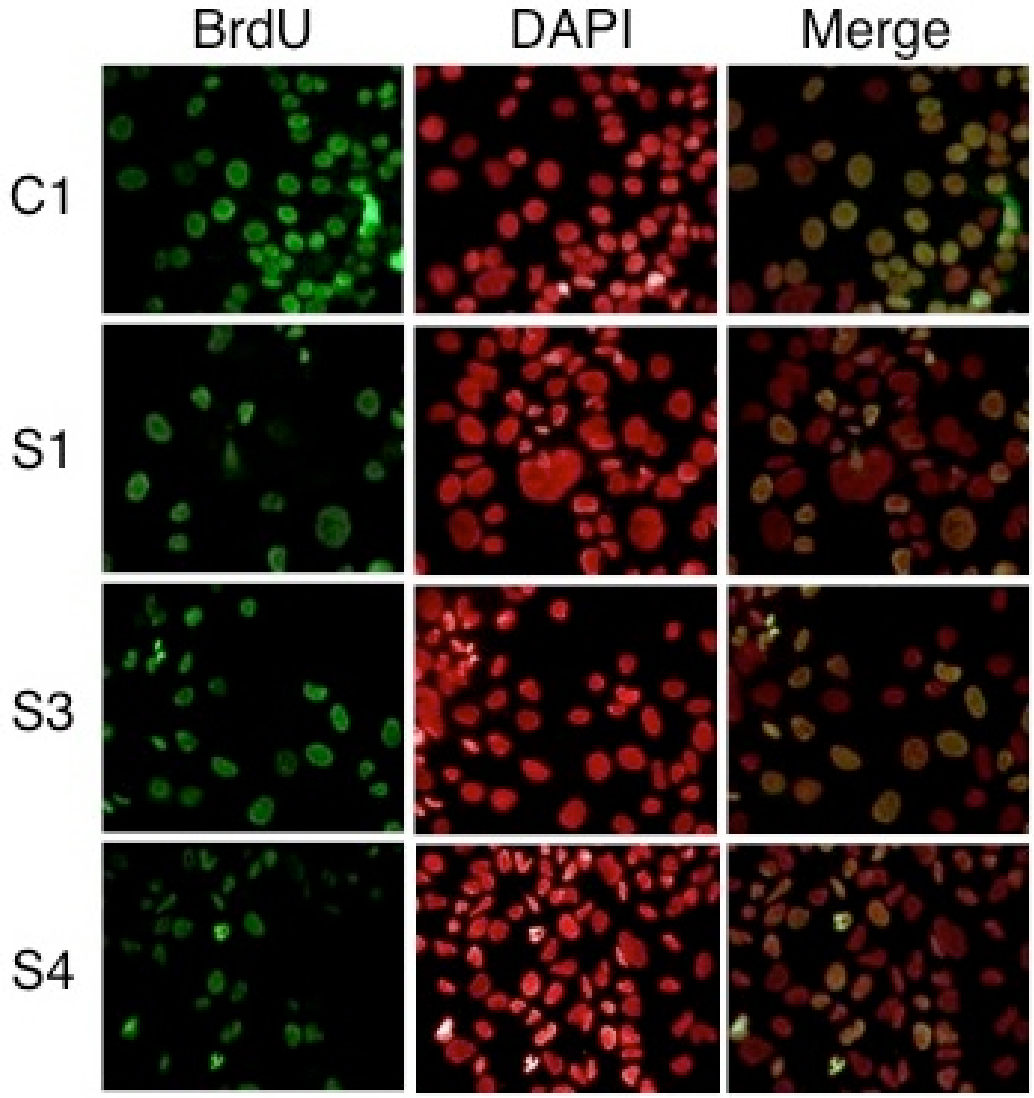

Figure 4.5: ZEB2-expressing S1, S3 and S4 clones generate colonies with high rates of permanently arrested cells, as demonstrated with negative BrdU incorporation into nuclear DNA after 24h BrdU labeling. (a) Double immunostaining using anti-BrdU antibody (green) and DAPI (red). BrdU-positive nuclei, yellow; BrdU-negative nuclei; red in merged pictures. Studies were performed with the following passage numbers: 3B-C1, passages 13-17; 3B-S1 and 3B-S3, passage 9; 3B-S4, passage 6.

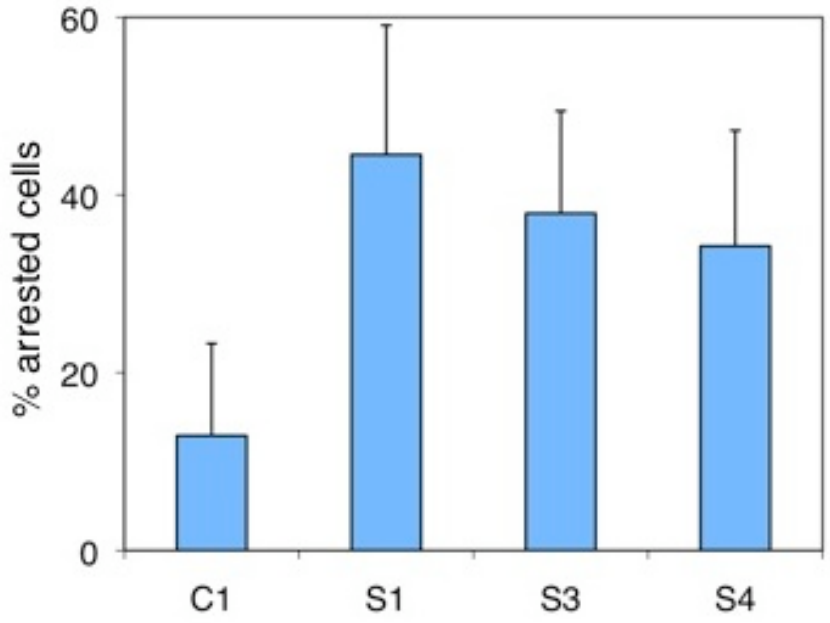

Figure 4.6: Quantitative analysis of permanent growth arrest showing a significant increase of non-proliferating cells in ZEB2-expressing clones. Data represent mean values (bars) with standard deviation (lines) of % BrdU-negative (non-proliferating) cells in randomly selected colonies (n=10 for each clone). C1; control clone.

4.7).

As represented in Figure 4.8, the ZEB2-overexpressing S4 clone displayed cells with nuclear $p21^{Cip1}$ at a rate of 26% (±1%), as compared to C1 cells that showed background staining only (2±1%).

4.1.4 Sustained expression of ZEB2 is not compatible with the expansion of Hep3B cell line

Based on partial responses of Hep3B clones to ZEB2 overexpression (for example, only 25% of cells were positive for $p21^{Cip1}$ expression), we were unsure whether its stable expression was maintained during in vitro expansion. Therefore, we kept S1, S3 and S4 cells in culture until they reached the passages 15-19, and we examined them.

We compared the rates of SABG-positive cells to those of early passages. SABG-positive and SABG-negative cells were counted on randomly selected colonies ($n > 6$ colonies for each passage and each clone tested). Mean values (± s.d.) of SABG index (% SABG-positive) were calculated and illustrated in Figure 4.9. The SABG index values of early passages were 13±3%, 28±14%, 20±5%, and 37±7% for C1, S1, S3 and S4, respectively. Statistical comparison of SABG indexes of early passage ZEB2 expressing clones with that of C1 clone indicated a significant increase in ZEB2 expressing clones (p values: 0.0026, 0.0008, and <0.0001 for S1,S3 and S4, respectively). At late passages, the C1, S1, S3 and S4 clones displayed 8±4%, 9±2.5%, 8±3% and 26±8% SABG-positive cells, respectively. Thus, the senescence rates in late passage of S1 and S3 clones dropped to background levels observed in C1 clone, whereas S4 clone displayed a partial (30%) loss.

We observed a general loss in RT-PCR levels of ectopically expressed ZEB2 transcripts in later passages, as compared to early passages (Figure 4.10). This correlated with the restitution of E-cadherin protein levels that were repressed

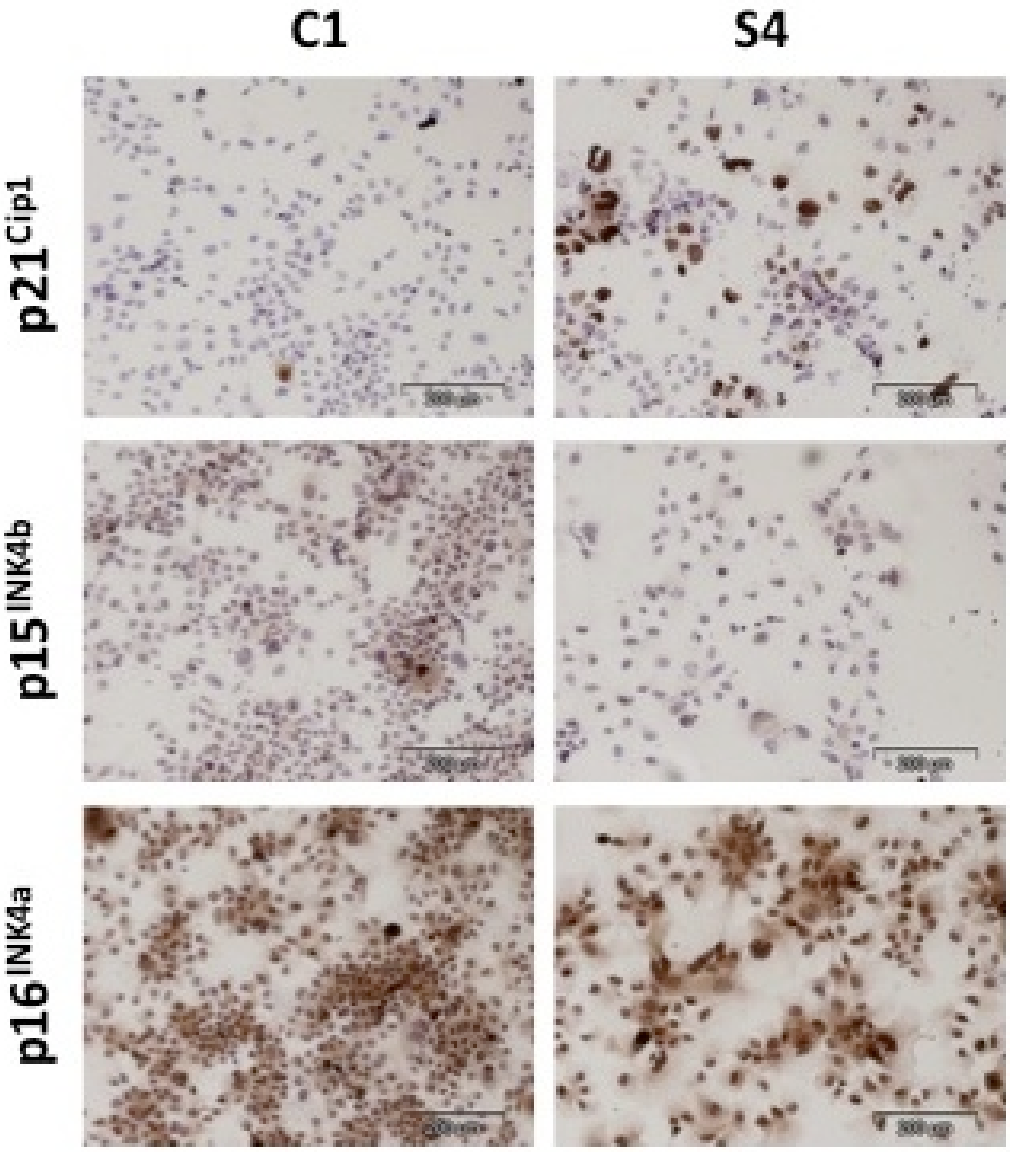

Figure 4.7: $p21^{Cip1}$ expression is induced in a fraction of ZEB2-expressing S4 clones, as compared to C1 control clone. S4 and C1 clones were plated at equal cell density in triplicate and the expression of $p21^{Cip1}$, $p15^{INK4b}$ and $p16^{INK4a}$ were tested by immunocytochemistry using appropriate antibodies. Representative examples of immunostaining patterns were shown here.

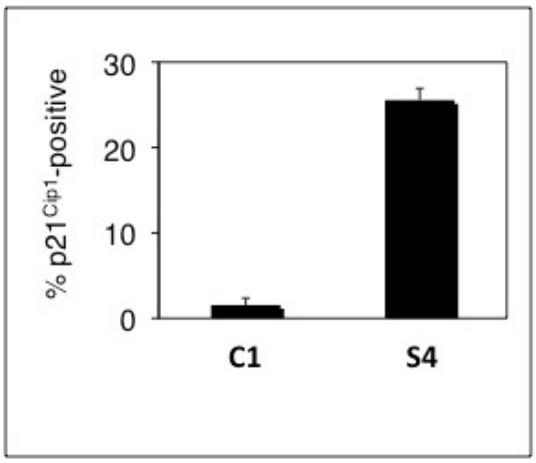

Figure 4.8: $p21^{Cip1}$-positive and total number of cells tested in 4.7 were counted manually (in triplicate), percent $p21^{Cip1}$-positive cells were calculated and plotted as mean (bars) ± s.d. (lines).

in early passages (Figure 4.11). Similarly, telomerase activity, which had been inhibited in early passage cells, was restored to control levels at in late passages (Figure 4.12). Respective p values for the telomerase activity assay are given in Table 4.1. Finally, we did not observe high levels of senescent cells, nor did we observe nuclear $p21^{Cip1}$ expression in late passages.

Taken together, these observations strongly suggested that ZEB2 overexpression was not maintained and its effects were not lost progressively during in vitro expansion of Hep3B cells.

4.1.5 Sustained expression of ZEB2 is not compatible with the expansion of A431 cells

To validate our observations using another cell line, we used A431/ZEB2 clone with Dox-regulated expression of 6xMyc-tagged human ZEB2 [46]. Treatment of this clone with Dox was previously shown to induce rapid accumulation of ZEB2

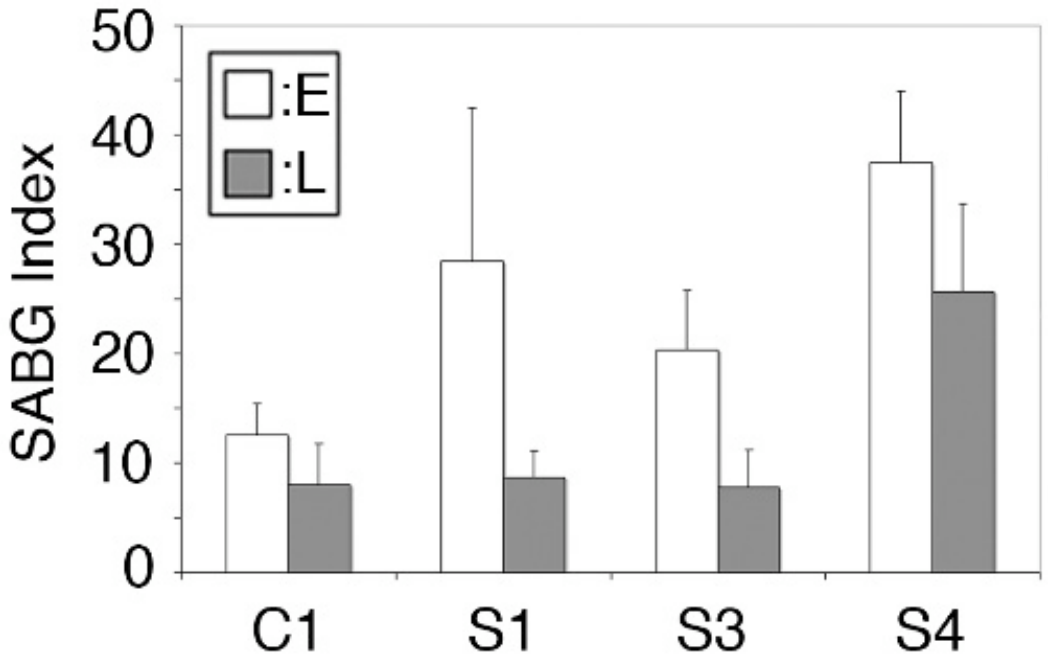

Figure 4.9: ZEB2 effects in Hep3B clones are reversible. Late passages of ZEB2-transfected S1, S3 and S4 cell lines were compared with their early passages. C1; negative control. (A) SABG-positive senescent cells are depleted in late passages. SABG index was determined by manual counting of individual colonies. E: early passages; L: late passages. Early passages: C1, p12; S1, S3, p9; S4, p8. Late Passages: C1, p19; S1, S3, p16; S4, p15.

Table 4.1: p values for the telomerase data in Figure 4.12

C1E vs. Early pas. of each clone	p value
C1E vs S1E	0.0003
C1E vs S3E	0.0001
C1E vs S4E	0.0027
C1L vs. Late pas. of each clone	
C1L vs S1L	0.0011
C1L vs S3L	0.0115
C1L vs S4L	0.0114
Early vs. Late for each clone	
C1E vs C1L	0.0327
S1E vs S1L	0.0007
S3E vs SEL	0.0001
S4E vs S4L	0.0083

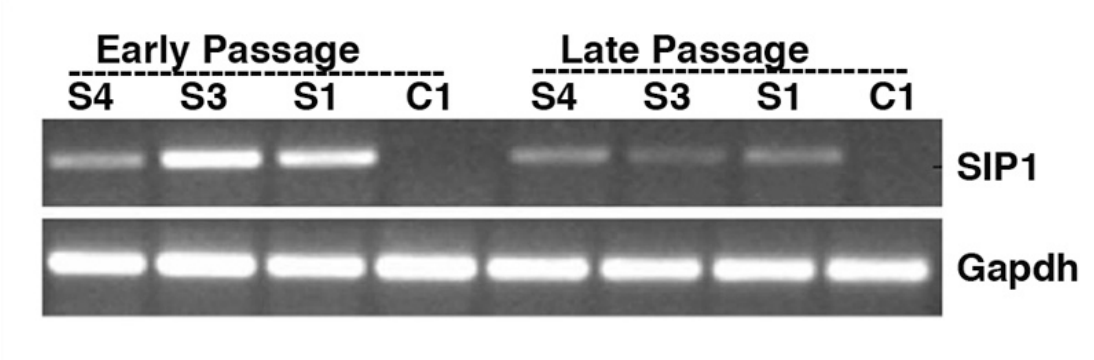

Figure 4.10: In vitro expansion of S1, S3 and S4 clones is not compatible with ZEB2 overexpression. Late passages (passages 15-19) of ZEB2-transfected S1, S3 and S4 cell lines were compared with their early passages (passages 6-9). Down-regulation of ectopic ZEB2 expression in late passages. ZEB2 and GAPDH (control) transcripts were tested by RT-PCR. Early passages: 3B-S4, p7; 3B-S3, p6; 3B-S1, p6; 3B-C1, p10. Late passages: 3B-S4, p20; 3B-S3, p21; 3B-S1, p21; 3B-C1, p25.

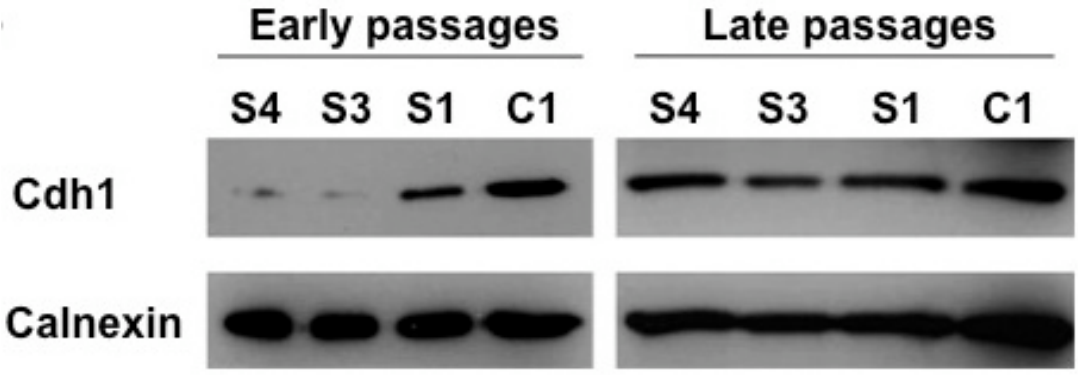

Figure 4.11: Loss of ZEB2-mediated E-cadherin repression in late passages. E-cadherin and calnexin (control) were tested by western blotting. Early passages: 3B-S4, p7; 3B-S3, p6; 3B-S1, p6; 3B-C1, p10. Late passages: 3B-S4, p20; 3B-S3, p21; 3B-S1, p21; 3B-C1, p25.

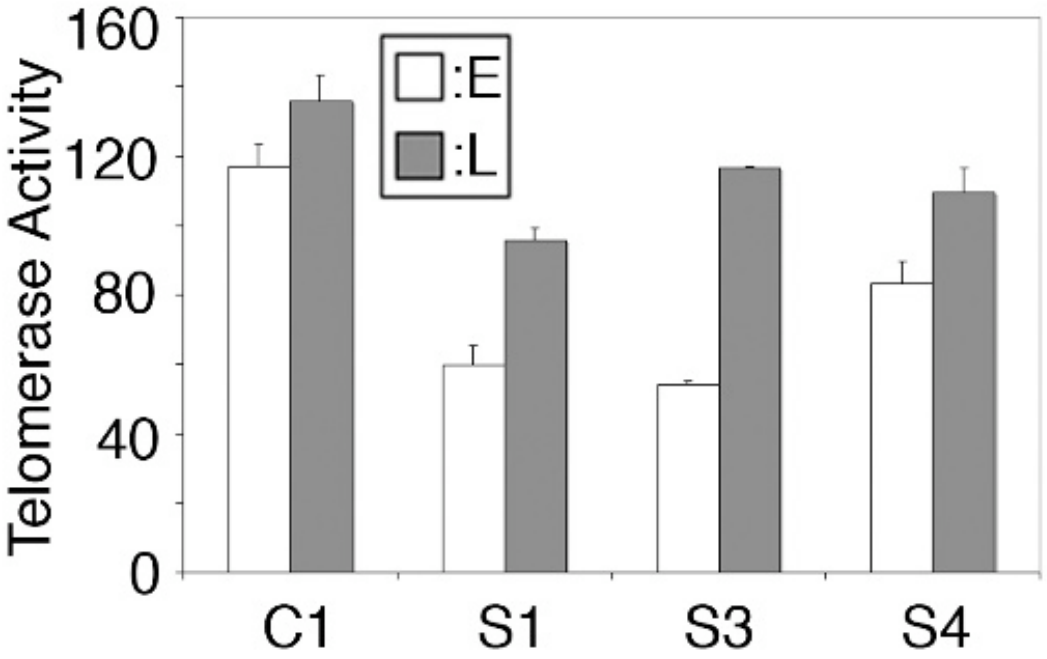

Figure 4.12: ZEB2-expressing clones display decreased telomerase activity at early, but not in late passages. Telomerase activity was presented in reference to positive control in telomerase assay. C1: negative control, E: Early passages, L: Late passages.

protein in 95–98% of cell nuclei, leading to cell scattering and dramatic morphological conversion from an epithelial cell state to a fibroblast-like phenotype (Figure 4.13).

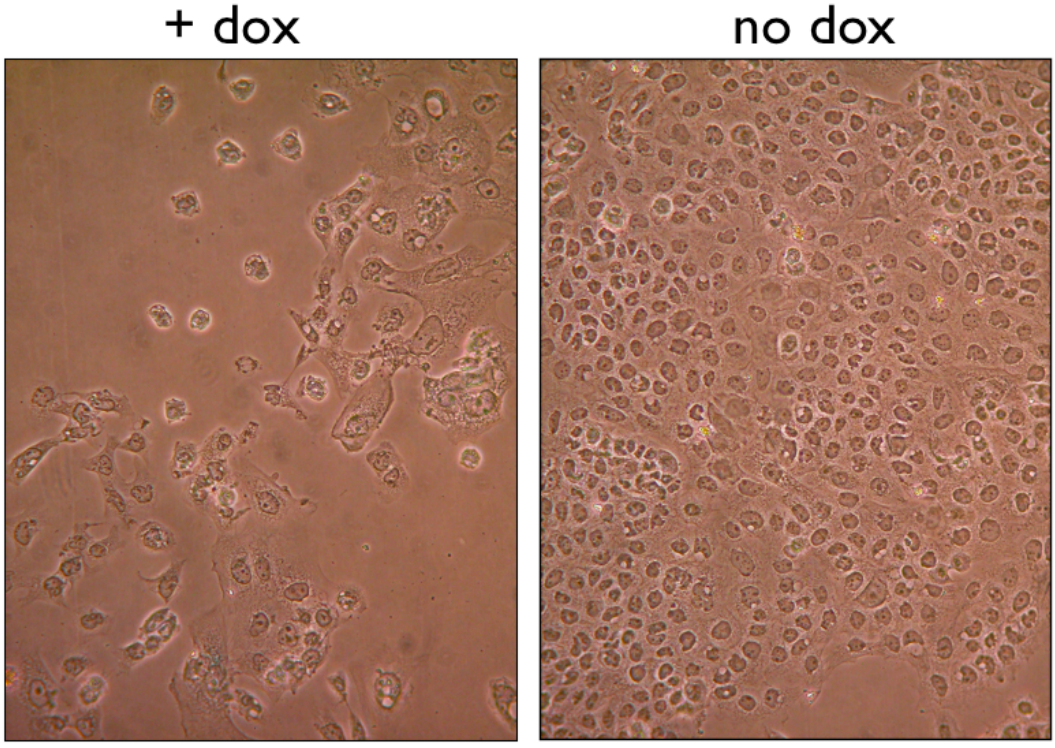

Figure 4.13: A431 cells change their morphology upon ZEB2 induction. ZEB2 induction with the addition of doxycyclin (on the left) induces a morphological shape change leading to cell scattering. Normal morphology of these cells is given on the right.

We analyzed A431/ZEB2 cells under low density clonogenic conditions. As shown in Figure 4.14 and 4.15, after 3 days of Dox treatment, colonies displayed 75±27% nuclear Myc-ZEB2. When cells were left to grow in the presence of Dox, Myc-ZEB2 positive cells in colonies were progressively depleted to 31±19% and 17±13%, at days 6 and 9, respectively. There was no detectable expression in the absence of Dox.

To test time-dependent senescence effects of ZEB2 in A431/ZEB2 cells, we first performed SABG staining assays. A431/ZEB2 cells were completely negative

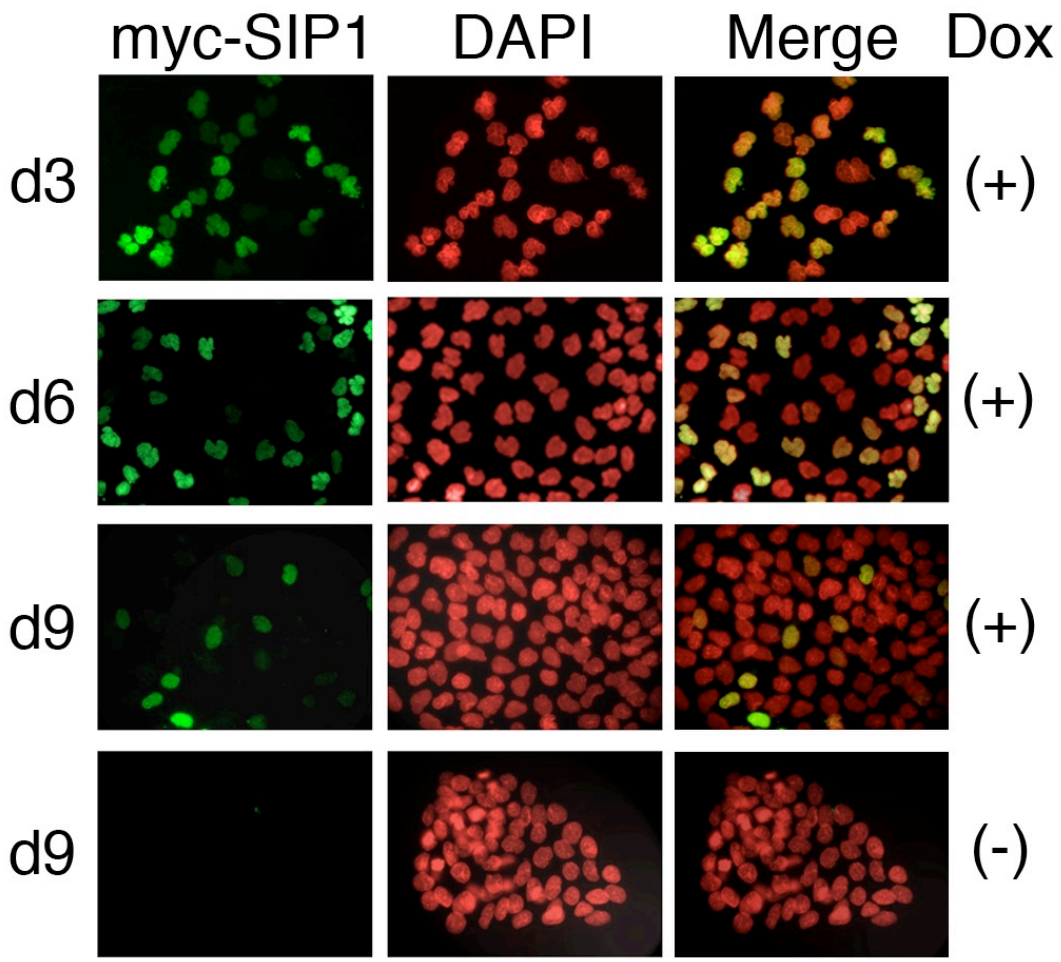

Figure 4.14: Tetracycline-regulated ZEB2 expression in A431/ZEB2 cells induces permanent growth arrest and its forced expression is not compatible with cell expansion. Dox-induced Myc-tagged ZEB2 (Myc-ZEB2) expression in A431/ZEB2 cells is lost progressively in cell culture. ZEB2 immunofluorescence (green) and nuclear DAPI staining (red) were shown. Merged pictures (Merge) identify ZEB2-positive (yellow) and -negative (red) cells. Nearly all Dox-induced cells display positive Myc-ZEB2 staining at day 3, followed by a progressive loss of expression.

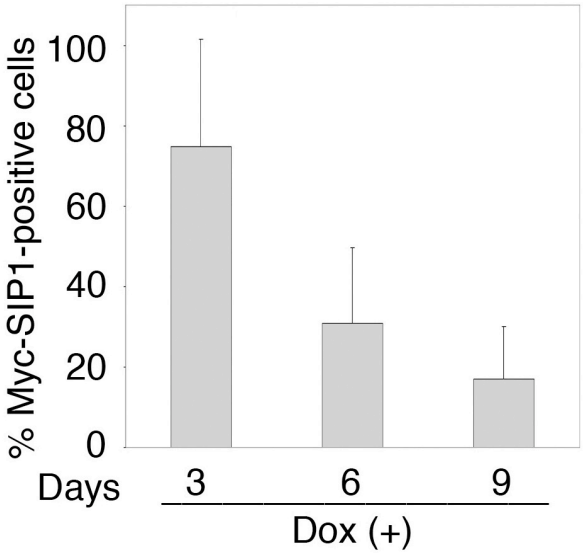

Figure 4.15: Quantitative analysis confirms loss of ZEB2 expression. Cell colonies were counted, and mean (bars) and s.d. (lines) values were calculated. day 3: mean=75, SD=27, n=12; day 6: mean=31, SD=19, n=18; day 9: mean=17, SD=13, n=19.

for SABG in the presence or in the absence of ZEB2 expression (data not shown). Therefore, we used long term BrdU labeling assay as an alternative approach [46, 73]. As shown in Figures 4.16 and 4.17, cells at terminal growth arrest (i.e. negative for BrdU staining after 24h mitogenic stimulation) were detected at low rates in uninduced A431/ZEB2 cells (3±3%, 7±7% and 9±7% at days 3, 6, and 9, respectively). The induction of ZEB2 expression raised the ratios of terminally arrested cells to 14±7%, 34±18% and 22±10% at days 3, 6 and 9, respectively. This increase of growth-arrested cells by ZEB2 expression was statistically significant ($p < 0.0001$, at all time points tested). When the rates of Myc-ZEB2 positive cells (Figure 4.16) are compared with that of BrdU negative cells (Figure 4.17), it is easily noticeable that ZEB2 expression causes a delayed growth arrest. Myc-ZEB2 expression was maximum at day 3, whereas the rate of growth arrested cells reached a peak at day 6. Myc-ZEB2 levels decreased gradually at days 6 and 9, and this was accompanied with a decrease of BrdU negative cells at day 9.

Thus, as we observed with Hep3B cells, ZEB2 also induces growth arrest in A431 cells, but both cell lines are able to escape this restriction by progressively down-regulating ZEB2 expression. If this is indeed the case, if maintained in the presence of Dox for a long time, the whole surviving cell population of A431/ZEB2 clone should become Myc-ZEB2-negative. We tested this possibility by using an experimental protocol that is described in Figure 4.18. A431/ZEB2 cells were passaged in medium supplemented with hygromycin and puromycin, in absence (set II) or in the presence of Dox (set I) until day 23. At day 23, medium supplemented with Dox was added in both sets, and cells were subjected to Myc-ZEB2 staining at day 25. As shown in Figure 4.19, long term growth of cells in the presence of Dox to keep ZEB2 expression induced (set I) resulted in the loss of Myc-SIP expression, as only a few weakly positive cells remained in the pool (Figure 4.19 top). This was in sharp contrast with set I where nearly all

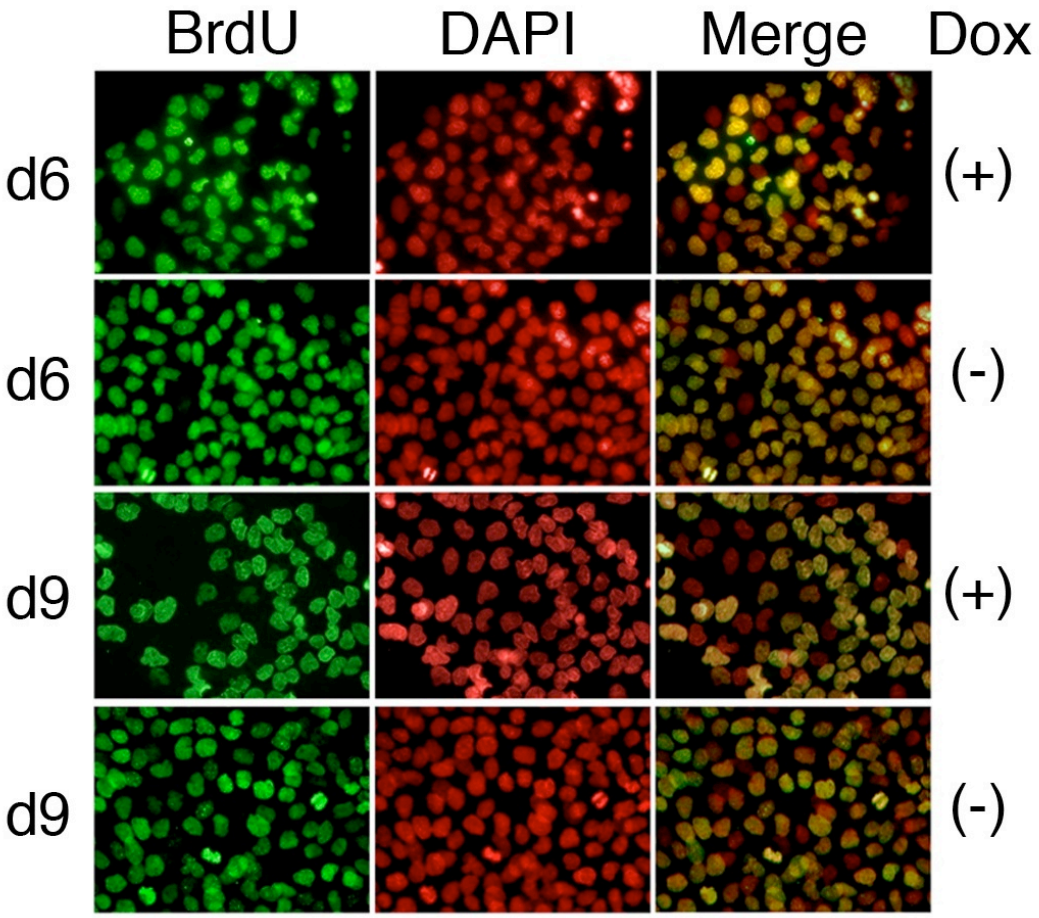

Figure 4.16: ZEB2-induction (Dox+) results in increased rates of permanently growth arrested cells. Cells were incubated in fresh BrdU-supplemented medium for 24h prior to BrdU (green) and DAPI (red) staining. The figure shows representative illustrations (days 6 and 9), in the presence (+) or absence (-) of Dox treatment.

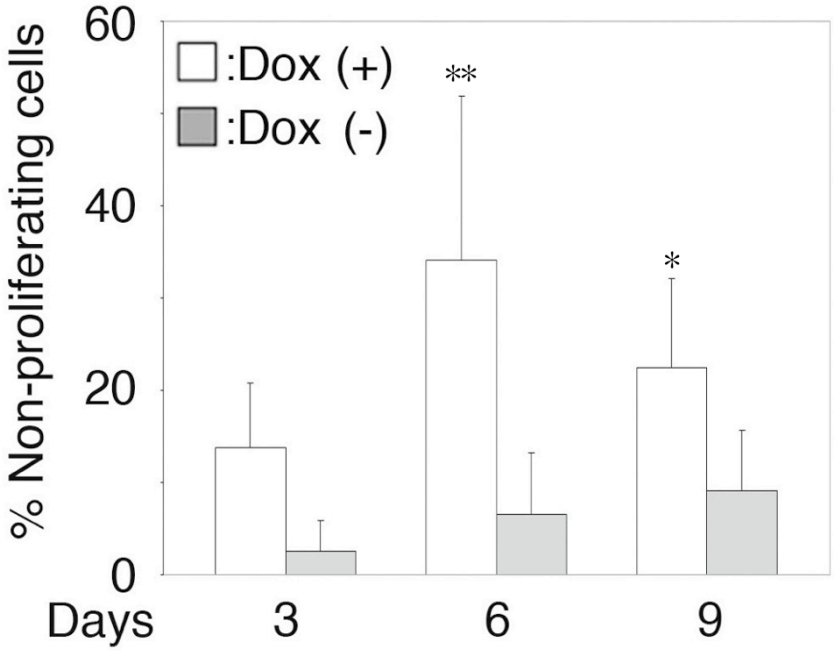

Figure 4.17: Quantitative analysis of BrdU-negative non proliferating cells. Dox-induced cells (gray bars) display a delayed increase at day 6, followed by a drop at day 9. * denotes that the observed changes in ratios between days were statistically significant. day3: mean=14, SD=7, n=24; **: $p<0.0001$, day6: mean=34, SD=18, n=32;. *: $p<0.0014$, day9: mean=23, SD=10, n=18. For the non-induced state: day 3: mean=3, SD=3, n=24; day 6: mean=7, SD=7, n=14; day 9: mean=9, SD=7, n=16

cells were strongly positive for Myc-ZEB2 (Figure 4.19 bottom). This experiment was repeated with another lot of A431/ZEB2 cells with 13 days of Dox induction, followed by 2 days of release. Again, virtually all ZEB2-positive cells were deleted (data not shown).

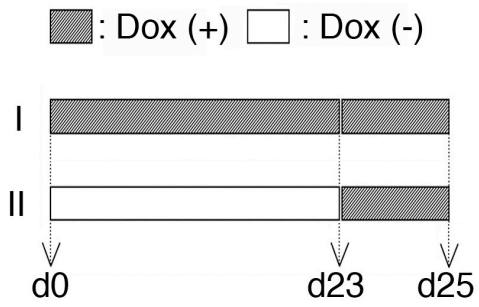

Figure 4.18: Loss of ZEB2 expressing cells over long term culture under induced conditions. Schematic representation of cell culture conditions where cells were subcultivated in the presence (set I) or in the absence (set II) of Dox for 23 days, followed by Dox induction for 2 days.

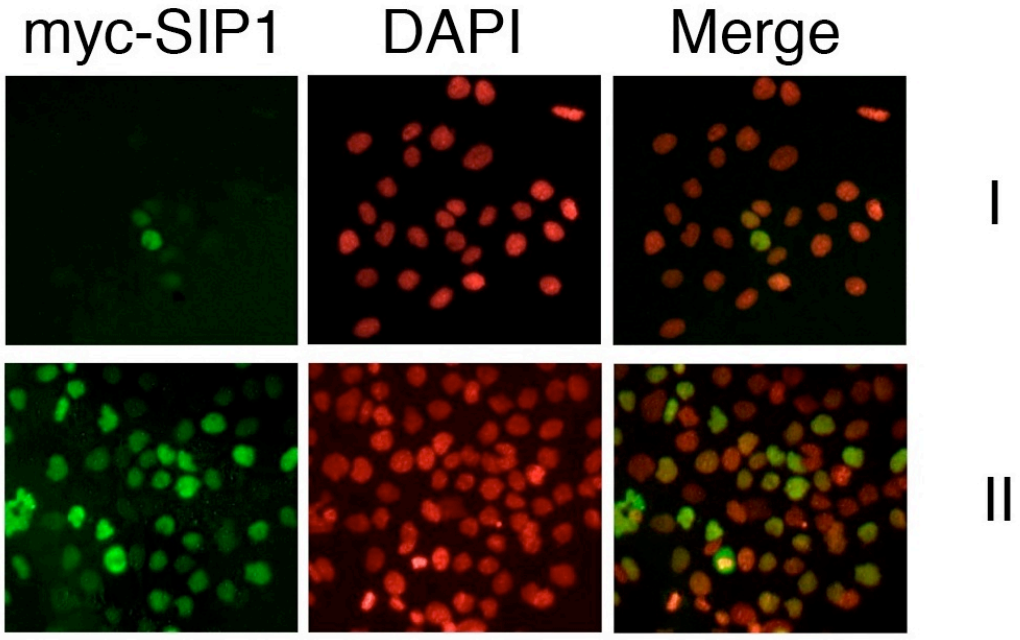

Figure 4.19: Cells exposed to continuous Dox treatment (set I) have lost Myc-ZEB2 expression almost completely, as opposed to strongly positive non-induced cells (set II).

4.2 A Major Role for Senescence and Immortality Gene Network in Hepatocellular Carcinoma

4.2.1 Microarray experiments with HCC and cirrhosis samples

Microarray experiments require high quality RNA with high concentration. Agilent 2100 Bioanalyzer (Agilent Technologies) is a microcapillary electrophoretic technique that seperates RNA in an automated fashion. It calculates an RNA integrity number (RIN) which is based on a 1-10 scale, 10 representing the highest quality [75]. System also produces an electropherogram, showing the marker as the first appearing peak, and then small rRNA fragments are plotted. Ratio of 28S to 18S rRNA fragments is a common way of analyzing RNA, usually through conventional RNA agarose gel electrophoresis. Agilent system calculates 28S/18S rRNA ratios via this electropherogram and also produces a virtual gel photo. Interpretation of electropherogram is given in Figure 4.20

Agilent Analyses For the microarray experiments RNA was isolated from 64 samples. All of them (except two) were analyzed by Agilent system but a portion of the RNAs were analyzed with an earlier version of the system. Electropherograms and virtual gel photos of the samples analyzed in the newer and earlier version of the Agilent system are given in Appendix. Two samples were not tested since no RNA left after the microarray experiment.

RIN values obtained from Agilent are summarized in the Table 4.2.1. MRC5 cell line was used as a positive control. RNA was isolated from early and late clones and RIN values were obtained from Agilent System. A perfect RIN value,

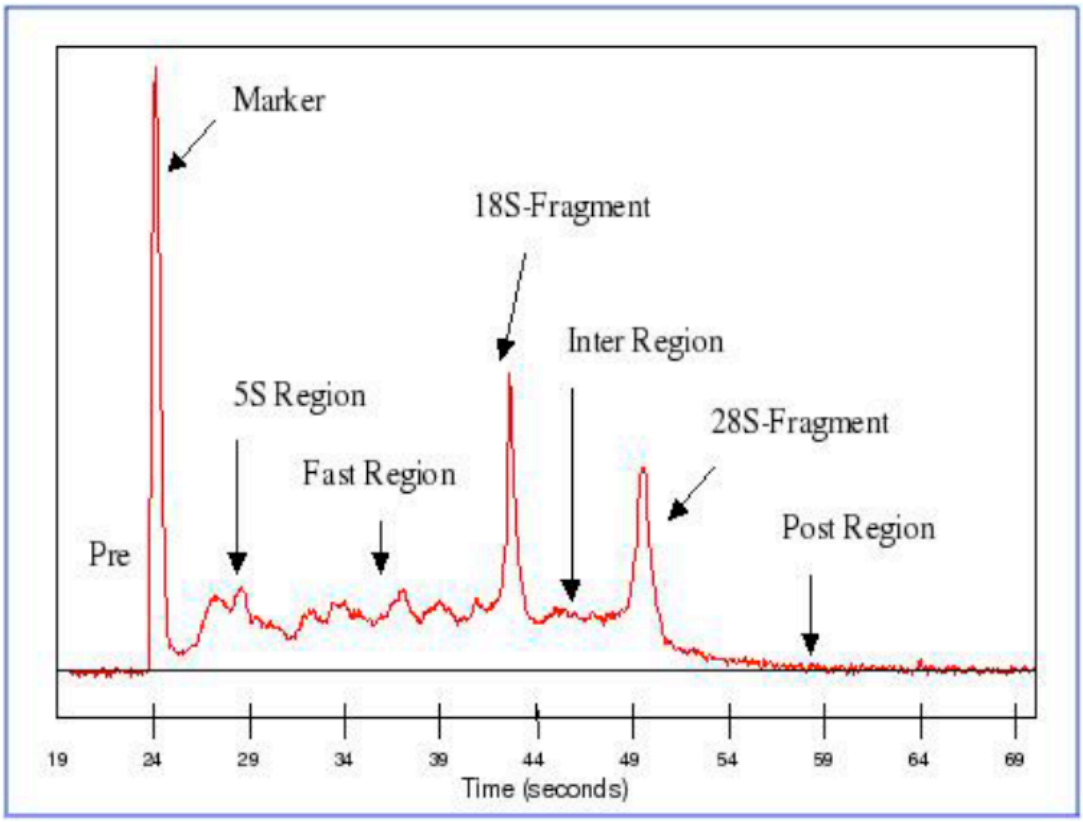

Figure 4.20: Each electropherogram is divided into nine segments: a pre-region, a marker region, a 5S region, a fast region, an 18S region, an inter region, a 28S region, a precursor region and a post region. Marker is shown as the first appearing peak. The 5S-region covers the small rRNA fragments (5S and 5.8S rRNA and tRNA). The 18S region and 28S region cover the 18S rRNA peak and 28S rRNA peak, respectively. Figure adapted from Ref. [75]

10, was obtained from early passage MRC5 and also from the late passage cells, RIN values were 8.5. Overall RIN values were ranged between 1.1 and 10. RNAs with RIN values lower than 4 were not included in the final analysis. These RNAs if included in the microarray experiments also gave lower presence and absence values. FC-NT and BG-T, although they have RIN values higher than 4, were not included in the analysis regarding to other quality measurements. MC-T and MC-NT were excluded from the analysis because with the pathology examinations, they were identified as cholangiocarcinoma which is a different pathology than HCC. Ses-NT, RE-NT, KaK-NT, HG-NT, HK-NT, MST-NT, MAS-NT, OU-NT, and RU-NT were not included in the microarray experiments despite their high RIN values, they are saved for future analysis. Agilent Bioanalyzer plots of the samples that were not included in the analysis due to low RNA quality and plots of the samples that were saved for future analysis are given in Appendix.

Data processing and quality control CEL files were uploaded to RMA-Express program to assess the quality of the arrays at the image level. NUSE (Normalized Unscaled Standard Error) and RLE (Relative Log Expression) plots were drawn using affyPLM package Figures 4.21 and 4.22. AffyPLM is a tool to detect artifacts on arrays that could pose potential quality problems and also for assessment of homogeneity of expression signal across arrays. Outliers with high deviation from the average probe intensity value were identified and excluded from further analyses. Accordingly, from 46 samples that have been included in NUSE and RLE plots, 39 have passed the criteria NUSE < 1.05, RLE < 0.1. .

MA-plots Evaluation of the individual array qualities were done using MA-plots which gives the relation between the intensity levels and distribution of the ratios. It compares log 2 transformed intensities to the avarage of all the other samples. MA-plots for each array is compared to the calculated median of all arrays. Perfect correlation is given as blue line and LOESS are given as red line.

	Tissue	Hospital	Agilent RIN values	Included in the analysis
1	FC-T	Ankara	2.7	No
2	FC-NT	Ankara	5.5	No
3	BG-T	Ankara	4.2	No
4	BG-NT	Ankara	5.4	Yes
5	IA-T	Ankara	3	No
6	IA-NT	Ankara	4.2	Yes
7	YA-T	Ankara	7.0	Yes
8	YA-NT	Ankara	6.8	Yes
9	MA-T	Ankara	8.3	Yes
10	MA-NT	Ankara	2.3	No
11	ET-T	Ankara	8.5	Yes
12	ET-NT	Ankara	7.6	Yes
13	VA-T	Izmir	6.6	Yes
14	VA-NT	Izmir	NA	Yes
15	SB-T	Izmir	NA	Yes
16	SB-NT	Izmir	6.7	Yes
17	MC-T	Izmir	6.9	No
18	MC-NT	Izmir	8.8	No
19	FM-T	Izmir	7.6	Yes
20	FM-NT	Izmir	4.0	Yes
21	ASF-T	Ankara	8.4	Yes
22	ASF-NT	Ankara	4.3	Yes
23	EK-T	Ankara	7.4	Yes
24	EK-NT	Ankara	2.2	Yes
25	AM-T	Ankara	7.8	Yes
26	AM-NT	Ankara	6.7	Yes
27	GS-T	Ankara	2.6	No
28	GS-NT	Ankara	1.9	No
29	281207-T	Izmir	8.0	Yes
30	281207-NT	Izmir	7.1	Yes
31	SA-T	Ankara	8.8	Yes
32	SA-NT	Ankara	4.3	Yes
33	HY-T	Ankara	6.4	Yes
34	HY-NT	Ankara	8.2	Yes
35	SO-NT	Ankara	7.8	Yes
36	CO-T	Ankara	3.9	No
37	AO-T	Izmir	8.1	Yes
38	TA-T	Izmir	8.8	Yes
39	TA-NT	Izmir	8.8	Yes
40	FiC-T	Izmir	7.8	Yes

Table 4.2: Agilent Values of the RNAs isolated from HCC and cirrhosis tissues

	Tissue	**Hospital**	**Agilent RIN values**	**Included in the analysis**
41	HU-NT	Izmir	8.3	Yes
42	IP-T	Ankara	7.8	Yes
43	MB-NT	Izmir	8.5	Yes
44	HaU-NT	Izmir	8.9	Yes
45	OC-NT	Izmir	8.2	Yes
46	RH-NT	Izmir	7.3	Yes
47	IT-NT	Izmir	8.4	Yes
48	SeS-NT	Izmir	8.8	Yes
49	RE-NT	Izmir	8.2	No
50	KaK-NT	Izmir	9.1	No
51	HG-NT	Izmir	8.0	No
52	HK-NT	Izmir	7.4	No
53	MST-NT	Izmir	6.5	No
54	MAS-NT	Izmir	6.6	No
55	OU-NT	Izmir	8.8	No
56	RU-NT	Izmir	5.9	No
57	MB-T	Izmir	NA	No
58	KK-T	Ankara	3.7	No
59	KK-NT	Ankara	1.1	No
60	SS-T	Ankara	1.2	No
61	SS-NT	Ankara	NA	No
62	SO-T	Ankara	1.0	No
63	MRC5-E	Cell Line	10.0	No
64	MRC5-L	Cell Line	8.5	No

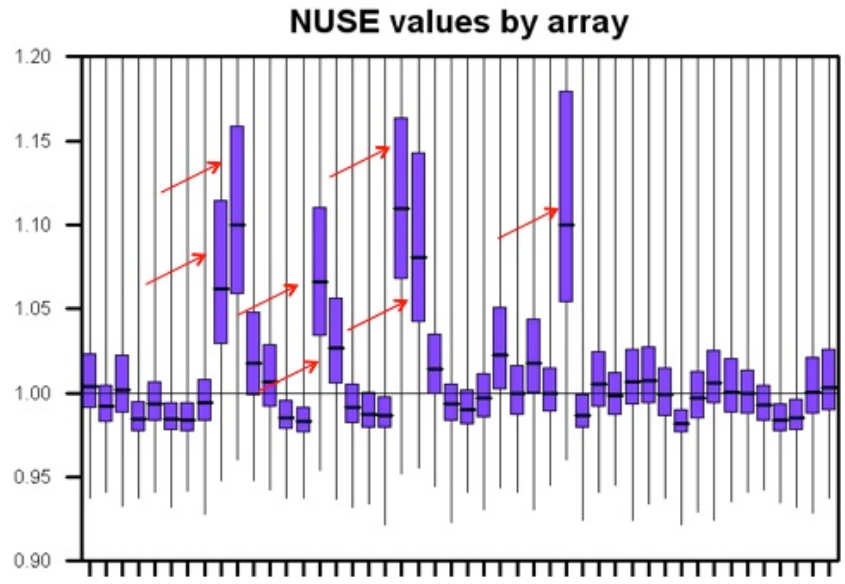

Figure 4.21: NUSE values plotted for 46 arrays. Each bar represents an individual array. Mean value is shown with a black line. NUSE values are on the y axis. Red arrows indicate outlier samples that were not included in the analyses.

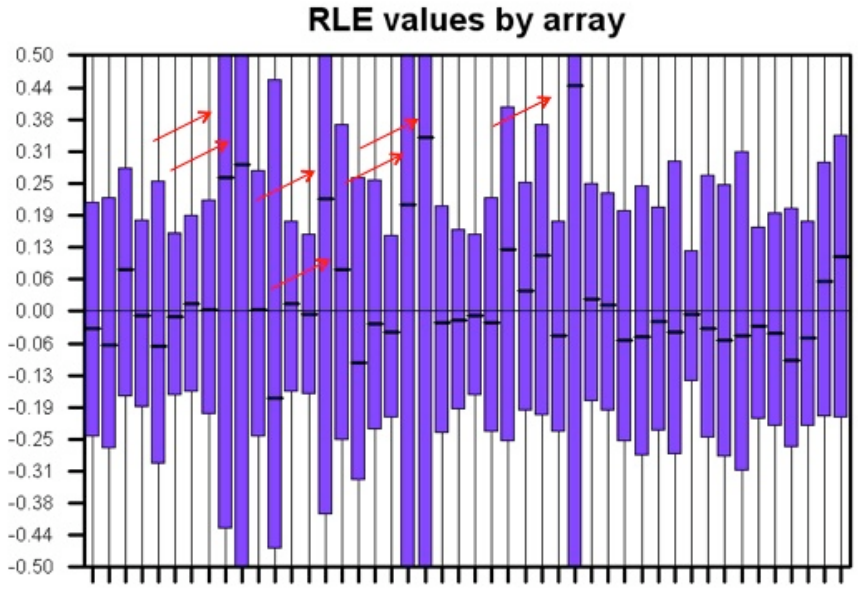

Figure 4.22: RLE values plotted for 46 arrays. Each bar represents an individual array. Mean value is shown with a black line. RLE values are on the y axis. Red arrows indicate outlier samples that were not included in the analyses.

Representative MA-plots can be found in Appendix. MA-plots were drawn in **R** with the code given below:

```
> source ("http://bioconductor.org/bioclite.R")
> bioclite ("affy")
> library (affy)
> library (affyPLM)
> mydata1 <-ReadAffy()
> pdf (file=‘‘MAplot1.pdf’’)
> MAplot (mydata1, plot.method=‘‘smoothscatter’’,
ylim=c(-3,3), nrpoints=256)
> dev.off()
```

Clinical data of the samples Clinical data including origin of the samples -which hospital the samples were collected from-, sample ID, patient code, age, gender, etiology, tumor size, and diagnosis are given in Table 4.3. Tumor samples were all HCC and nontumor samples were diagnosed with cirrhosis in most of the cases. Tumor sizes differed with diameters ranged from 2.5 to 26 cm. Etiologies were HBV for 2, HCV for 6 and HBV+HDV for 2 samples. Not all of the information were available for all of the samples. There are missing information regarding the clinical data which was substituted by pathology examinations. Tissue samples were analyzed by pathologists at the hospital centers immediately after the tissues were resected. After samples arrived our lab, slides obtained from tissue samples were examined again by pathologist Dr. Önder Bozdoğan.

Table 4.3: Cirrhosis and hepatocellular carcinoma samples used for microarray analyses

Sample ID	**Sample Type**	**Age (yr)**	**Gender**	**Etiology**	**Pathology Pathology**
Ankara-1NT	Cirrhosis	45	male	HBV	cirrhosis
Ankara-6NT	Cirrhosis	50	male	HBV	cirrhosis
Izmir-3NT	Cirrhosis	65	male	HBV	cirrhosis
Izmir-4NT	Cirrhosis	52	female	HCV	cirrhosis
Izmir-1NT	Cirrhosis	56	male	HBV	cirrhosis
Izmir-6NT	Cirrhosis	64	male	HCV	cirrhosis
Izmir-7NT	Cirrhosis	41	male	HBV+HDV	cirrhosis
Izmir-8 NT	Cirrhosis	48	female	HBV	cirrhosis
Izmir-9NT	Cirrhosis	52	male	HBV	cirrhosis
Izmir-10NT	Cirrhosis	48	male	HBV	cirrhosis
Izmir-11NT	Cirrhosis	50	male	HBV	cirrhosis
Ankara-8NT	Cirrhosis	30	female	HBV	cirhosis
Ankara-12NT	Cirrhosis	41	male	HBV+HDV	cirrhosis
Ankara-2NT	Cirrhosis	52	male	HBV	N/A
Ankara-3NT	Cirrhosis	62	male	HCV	N/A
Ankara-4NT	Cirrhosis	60	male	HBV	N/A
Izmir-2NT	Cirrhosis	44	female	N/A	N/A
Ankara-5NT	Cirrhosis	N/A	male	N/A	N/A
Izmir-5NT	Cirrhosis	N/A	male	N/A	N/A
Izmir-12NT	Cirrhosis	N/A	female	N/A	N/A
Ankara-1T	HCC	45	male	HBV	WD HCC
Ankara-2T	HCC	52	male	HBV	HCC
Ankara-3T	HCC	62	male	HCV	HCC
Ankara-4T	HCC	60	male	HBV	HCC
Ankara-6T	HCC	50	male	HBV	HCC
Izmir-1T	HCC	56	male	HBV	Focal HCC
Izmir-2T	HCC	44	female	N/A	MD HCC
Izmir-3T	HCC	65	male	HBV	WD HCC
Izmir-4T	HCC	52	female	HCV	MD. HCC
Ankara-7T	HCC	69	male	HBV	MD HCC
Ankara-9T	HCC	62	male	HCV	MD HCC
Izmir-10T	HCC	49	male	HBV	MD HCC
Izmir-11T	HCC	59	male	HBV	MD HCC
Ankara-10T	HCC	N/A	male	HBV	MD HCC
Ankara-5T	HCC	N/A	male	N/A	N/A
Ankara-11T	HCC	N/A	male	N/A	N/A
Izmir-5T	HCC	N/A	male	N/A	N/A

4.2.2 Establishing a senescence and immortality gene network signature for cirrhosis and hepatocellular carcinoma.

We previously described the generation of immortal and senescence programmed clones from the HCC-derived Huh7 cell line. Immortal clones were tumorigenic, and were able to sustain cell proliferation beyond 150 population doublings (PD), while senescence programmed clones were not tumorigenic, and entered senescence-like permanent growth arrest after $\sim$ 80 PD [42]. To generate a SIGN expression data, we first obtained global gene expression profiles of immortal and senescence-programmed clones, as well as of liver cirrhosis and HCC tumor tissues. Then we integrated in vitro and in vivo datasets.

Two immortal clones were tested after 150 PD following clone isolation. Two senescence programmed clones were analyzed at both presenescent (20-30 PD before senescence arrest) and senescent ($\sim$ 80 PD) states. Three biological replicates were used for RNA extraction from clonal cells with a total of 18 cell line samples. A total of 6390 probe-sets showed differential expression between immortal, presenescent and senescent cells ($P < 0.05$; dataset not shown). We also identified 10185 probe-sets that displayed differential expression between cirrhosis and tumor samples ($p < 0.05$; dataset not shown). Next, we integrated significant probe-sets generated from in vitro cell line and in vivo clinical samples (Figure 4.23). 1909 probe-sets were found to be common.

To demonstrate the ability of 1909 probe-sets to differentiate between senescence and immortality, we performed unsupervised hierarchical cluster analyses. Immortal and senescence programmed (presenescent and senescent) Huh7 clones formed two separate clusters (Figure 4.24).

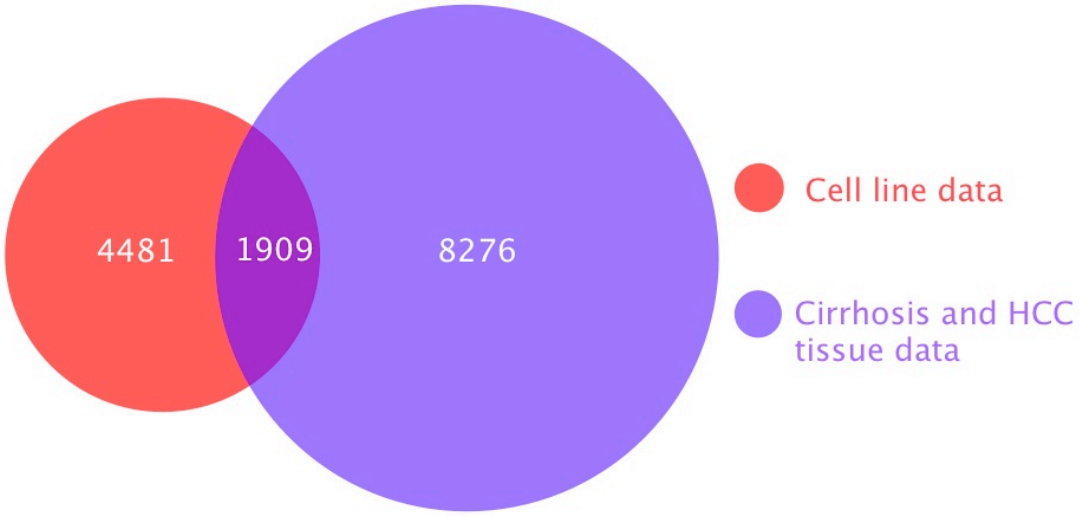

Figure 4.23: Venn diagram of probe-sets selected by two-tailed unpaired Welch's t-test and class comparison test in BRB array tools from in vitro cell line and in vivo tissue analysis data, respectively. Red circle represents the number of probe-sets differentially expressed between presenescent, senescent and immortal cells ($P < 0.05$). Blue circle represents number of probe-sets differentially expressed between cirrhosis and HCC tissue samples ($P < 0.05$). A total of 1909 probe-sets that display differential expression in both cell lines and tissues was selected as SIGN probe-sets.

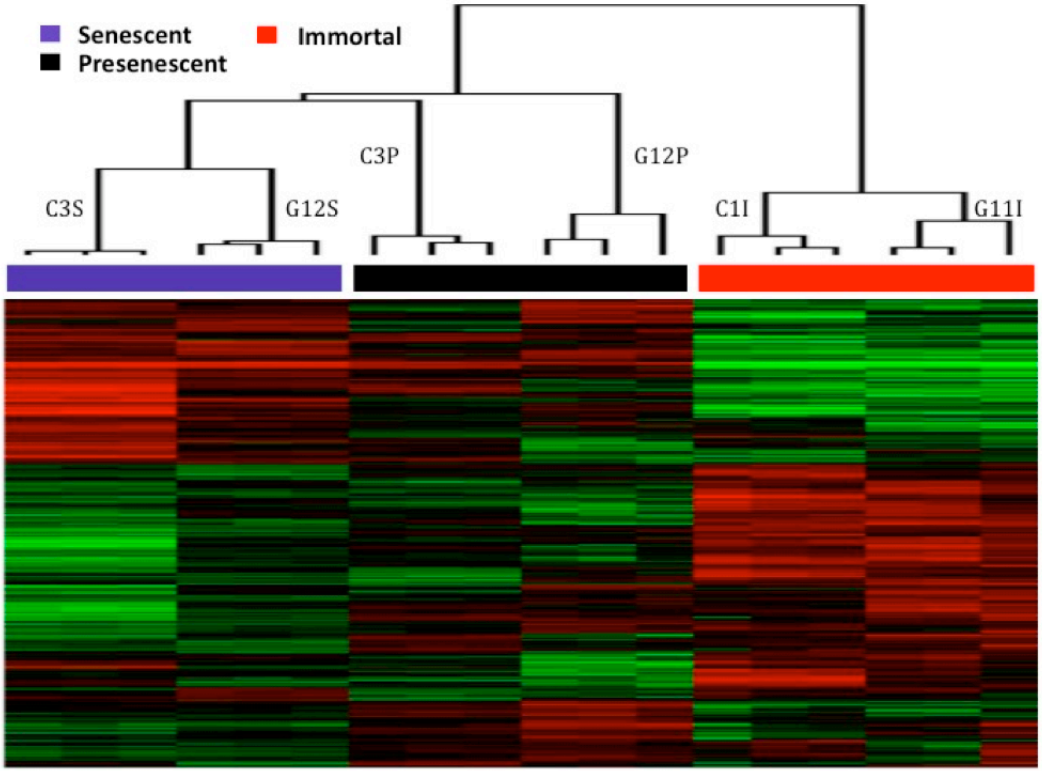

Figure 4.24: Unsupervised cluster analysis of Huh7-derived immortal, presenescent and senescent clones with 1909 probesets.

Next, we used our 1909 probe-sets for comparison of cirrhosis and HCC tissues. As expected, these samples also formed two major clusters. One cluster included 85% (17/20) of cirrhosis, and the other 71% (14/17) of HCC samples (Figure 4.25). Cirrhosis and HCC have been considered as in vivo states of hepatocellular senescence and immortality, respectively. Hence, our in vitro and in vivo data combined, identified a SIGN signature that could serve for classification of different hepatic lesions with respect to the states of senescence and immortality.

4.2.3 Discriminating between preneoplastic and neoplastic stages of hepatocellular carcinogenesis by the SIGN signature.

Because HCC typically develops in close association with pre-existing cirrhosis, it is widely believed that human hepatocellular carcinogenesis is a stepwise process starting with dysplastic nodules that lead to early HCC foci that in turn progress to advanced HCC by a process of dedifferentiation and increasing tumor size [4]. We tested the predictive power of the SIGN signature for the classification of these sequential events using an independent clinical dataset generated for the study of HCV-associated hepatocellular carcinogenesis [71]. We regrouped tissue samples into five stages; namely normal liver, cirrhosis, dysplasia, early HCC and advanced HCC. By unsupervised cluster analysis with the SIGN signature, the tissue samples formed two major clusters; one of all normal liver, cirrhosis and dysplasia samples, as well as two early HCCs, and the other all but two HCC samples (Figure 4.26, sample IDs are shown in Figure 4.27).

Thus, the SIGN signature was quite informative for discriminating between preneoplastic and neoplastic lesions of the liver. Indeed, a binary tree analysis ($P < 0.001$; Figure 4.28) distinguished normal liver and cirrhosis from dysplasia and

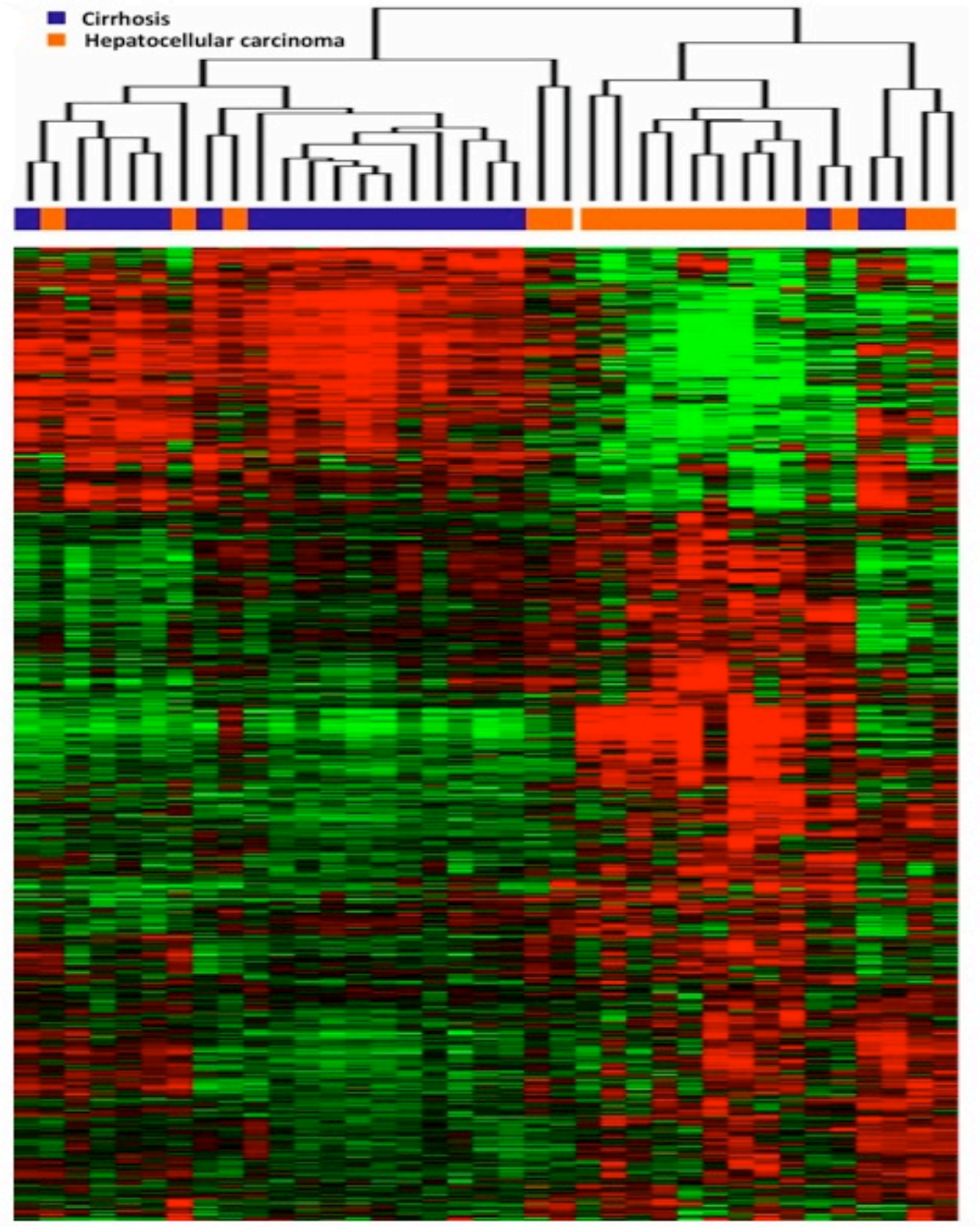

Figure 4.25: Unsupervised cluster analysis of HCC and cirrhosis samples with 1909 probesets. Experimental dendrogram showing the clustering of tissue samples into cirrhosis and HCC subgroups (top). The findings indicate that 1909 probesets represent the SIGN signature. Scaled-down representation of the entire cluster of gene probesets and samples based on similarities in gene expression were shown on the bottom of figure

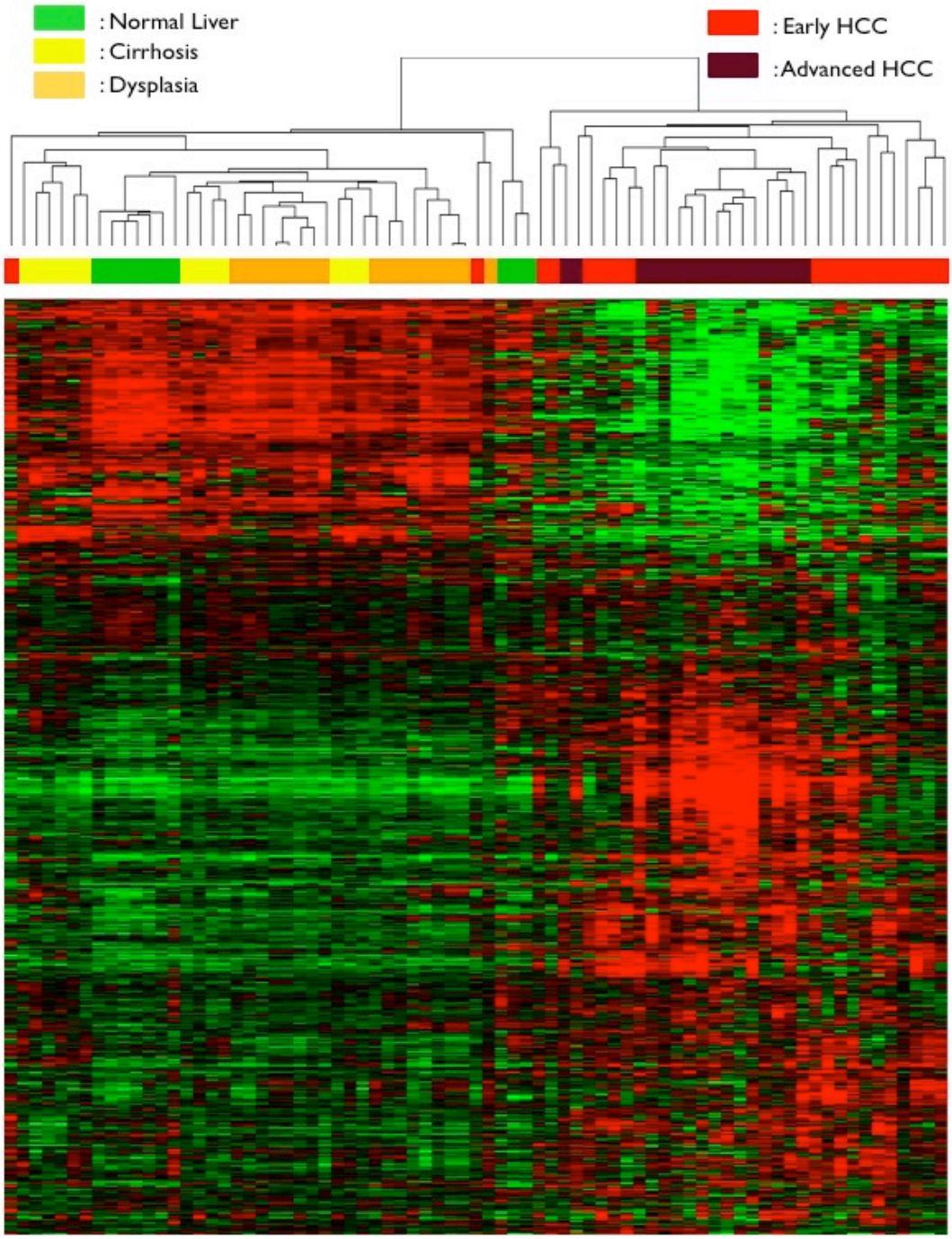

Figure 4.26: Hierarchical clustering of gene expression data from [71]. Experimental dendrogram showing the clustering of hepatocellular carcinoma (HCC) tissues separetely from normal liver, cirrhosis and dysplasia tissues (top), and scaled-down representation of the entire cluster of 1909 gene probesets and 72 tissue samples based on similarities in gene expression (bottom).

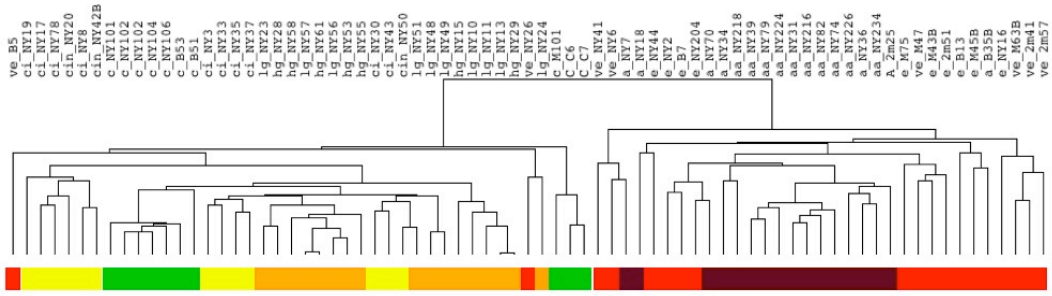

Figure 4.27: Unsupervised cluster analysis of 10 normal liver, 13 cirrhosis, 17 dysplasia, 18 early HCC, and 17 advanced HCC samples with SIGN probesets. This figure shows the sample clustering with sample IDs.

HCC (97% accurate classification), cirrhosis from normal liver (100% accuracy), and dysplasia from HCC (94% accuracy). Early and advanced HCCs were also differentiated from each other, but less accurately (74% accuracy).

These findings suggest that progressive steps of hepatocellular carcinogenesis are accompanied by significant changes in the expression of senescence- and immortality-associated genes. To study the significant changes between each step, we generated classifier probesets by a pair-wise class comparison analysis and identified genes that displayed a > 1.5-fold change between senescent and immortal cells. The ratios of the number of senescence- and immortality-associated genes between each successive step were compared (Figure 4.29).

The transition from normal liver to cirrhosis was associated with a significant enrichment in senescence genes ($P < 0.005$), in confirmation of the view that cirrhosis is a state of in vivo senescence [39]. Transition from cirrhosis to dysplasia did not affect the balance between senescence- and immortality-associated genes ($P = 0.189$). In contrast, the transition from dysplasia to the early HCC stage demonstrated a highly significant enrichment of immortality-associated genes ($P < 2X10^{-6}$). This 8 indicated that a senescence-to-immortality switch takes place

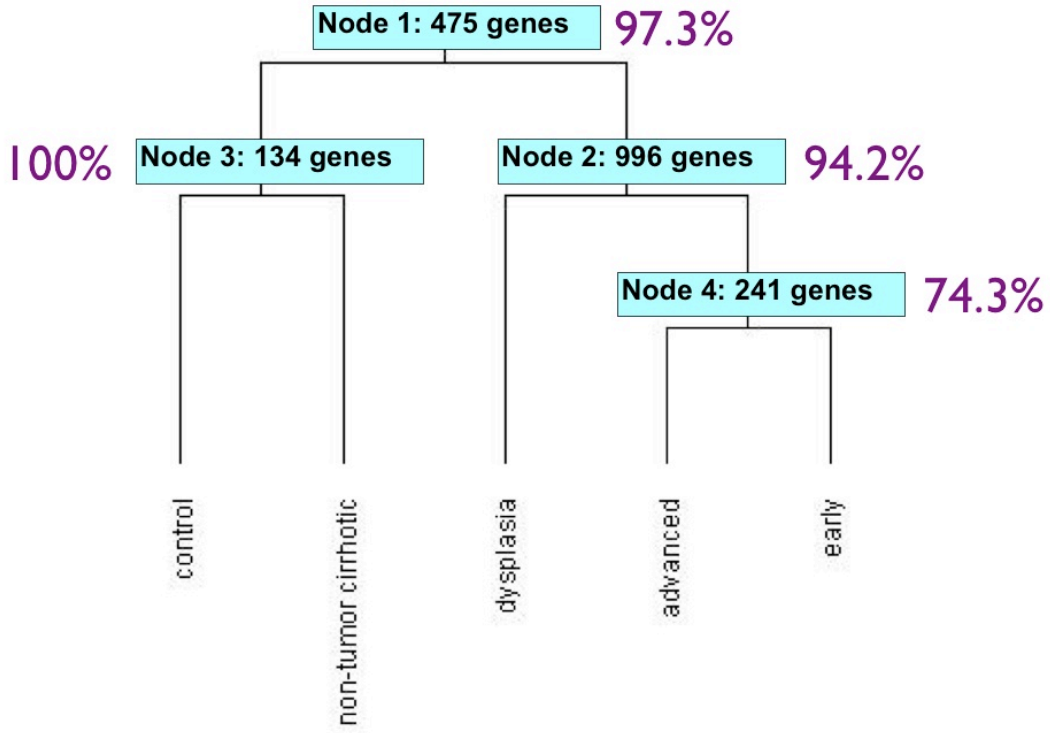

Figure 4.28: Classification of 72 liver tissue samples by binary tree analysis using SIGN probesets.

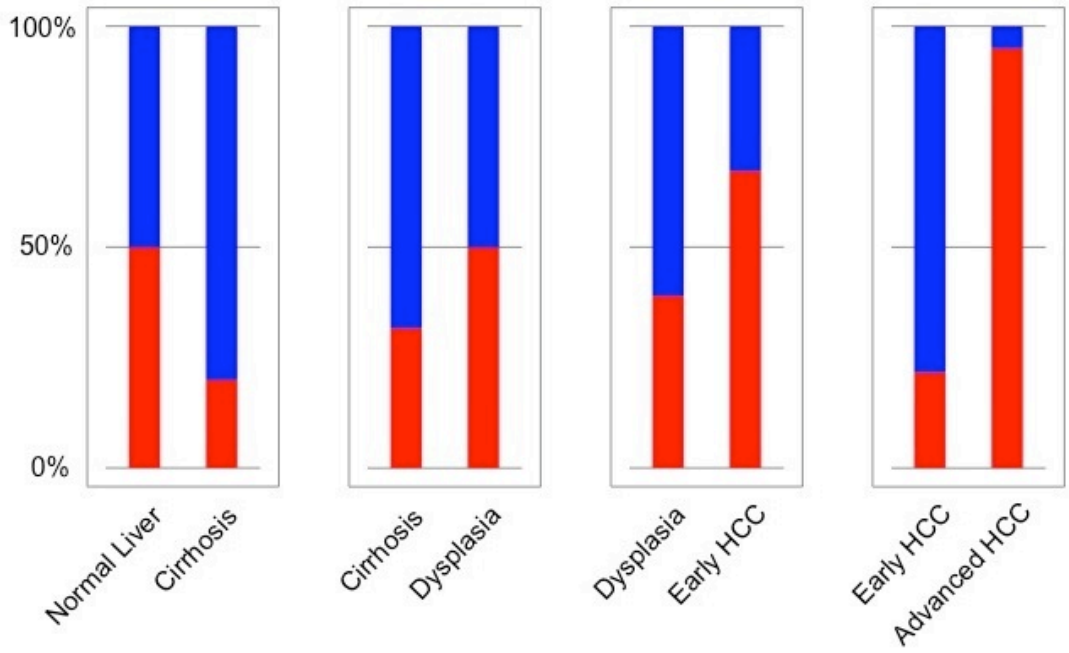

Figure 4.29: Differential expression of senescence- and immortality-associated genes between different liver lesions. Genes with more than 1.5-fold expression change between senescence-arrested and immortal cells were identified by a pair-wise class comparison of different lesions, and data were presented as % ratios of senescence-upregulated (blue) and immortality-upregulated (red) genes.

in the transition between the premalignant and malignant stages during hepatocellular carcinogenesis. Moreover, the immortality-associated genes were much more prominent in advanced HCCs compared to early HCCs ($P < 3X10^{-13}$), strongly suggesting that conversion to immortality is a continuous and progressive event in HCC.

4.2.4 The contribution of senescence- and immortality-related biological processes to hepatocellular carcinoma development and tumor heterogeneity.

The integration of senescence- and immortality-associated gene expression data with in vivo tissue data provided us a unique opportunity to address the contribution of senescence- and immortality-related biological processes to HCC. First, we identified cirrhosis- and HCC-associated classifier probesets among the SIGN probesets (dataset not shown). Then, we used Functional Annotation Clustering program provided by DAVID bioinformatics resources [70] to identify significant biological processes (dataset not shown). The genes that are upregulated in HCC formed significant clusters in chromosome organization (nucleosome assembly, chromatin assembly and modification), cytoskeletal organisation, proliferation related processes such as checkpoint control, spindle organization, mitotic sister chromatid segregation, centrosome cycling, DNA unwinding and replication, DNA damage response, ribosome biogenesis, protein export from nucleus, and phosphorylation. The genes downregulated in HCC identified another of set of biological processes. This set included lipid- steroid- amino acid-amine and alcohol metabolism, amino acid and aromatic compound catabolism, blood coagulation and immune response.

We used pair-wise classification data (dataset not shown) for gene annotation

cluster analyses for different lesions of hepatocellular carcinogenesis to identify significant biological process genes associated with each lesion (dataset not shown). As compared to a normal liver, cirrhosis was associated with downregulation of acute inflammatory response and classical complement activation genes, and with upregulation of anatomical structure morphogenesis genes.

The comparison of cirrhosis with dysplasia did not reveal any significant data, but the transition from dysplasia to early HCC was associated with significant changes in a large set of biological processes. The genes upregulated in early HCC clustered with cell proliferation-related processes including mitosis, cell cycle checkpoint, DNA packaging and DNA replication. Genes involved in ubiquitin cycle, RNA metabolism, RNA processing, and DNA repair were also upregulated. Early HCC development was associated also with downregulation of genes involved in different metabolic processes and hepatic functions. The most specifically affected processes were lipid, monocarboxylic acid, amine, fat-soluble vitamin, and alcohol metabolisms. Other affected processes included blood coagulation, classical complement activation, regulation of biological quality, and defense response.

4.2.5 DNA damage response genes as potential therapeutic targets

We repeatedly observed the upregulation of DDR genes in different steps and classes of HCC (datasets not shown). Although some genes such as TOP2A have been already associated to HCC [76], the role of these genes in HCC remains elusive. Therefore, we further analyzed the expression changes of DDR genes [77]. We identified 64 genes that were upregulated in HCC as compared to cirrhosis Figure 4.30. The most affected processes included DNA damage checkpoint (24 genes), double-strand DNA break repair (20 genes), base-excision repair (12 genes), nucleotide-excision repair (nine genes) and DNA mismatch repair (nine

genes). Some of these genes were upregulated during transition from dysplasia to early HCC, and others in advanced HCCs as compared to early HCCs. We also compared two major SIGN classes of HCC; normal-like 1A tumors versus 2A tumors. Class 2A tumors showed upregulation of 31 genes involved in DNA damage checkpoint, base-excision, nucleotide-excision, double-strand break and mismatch repair processes.

Genes	Checkpoint	DSBR	BER	NER	MMR	Other	HCC vs. Cirrhosis	Early HCC vs. Dysplasia	Adv. HCC vs. Early HCC
BARD1	(+)						(+)	(+)	
BAX	(+)						(+)	(+)	
CCNA2	(+)						(+)	(+)	(+)
CDC2	(+)						(+)	(+)	(+)
CHEK1	(+)						(+)		(+)
CHEK2	(+)						(+)		
DTL	(+)						(+)		(+)
DYRK2	(+)						(+)		
GTSE1	(+)						(+)		
H2AFX	(+)						(+)		
RAD1	(+)						(+)		(+)
KIN	(+)						(+)		
POLE2	(+)		(+)	(+)			(+)		
SFN	(+)						(+)		
SMC3	(+)						(+)		(+)
BRCA1	(+)	(+)					(+)		(+)
BRCA2	(+)	(+)					(+)		
DCLRE1A	(+)	(+)					(+)		
MRE11A	(+)	(+)					(+)		
RAD50	(+)	(+)					(+)	(+)	
PRKDC	(+)	(+)					(+)	(+)	
EME1	(+)	(+)					(+)		
SUPT16H	(+)	(+)					(+)	(+)	
FANCD2	(+)	(+)					(+)		(+)
FANCA		(+)					(+)		
FANCG		(+)					(+)	(+)	
FANCI		(+)					(+)		(+)
NSMCE2		(+)					(+)		
PRPF19		(+)					(+)	(+)	
RAD51		(+)					(+)		(+)
RAD54B		(+)					(+)		
RAD54L		(+)					(+)		
SMC6		(+)					(+)		
BRIP1		(+)					(+)		
HMGB1		(+)	(+)	(+)	(+)		(+)		
NEIL3			(+)				(+)	(+)	
PARP1			(+)				(+)		
PARP2			(+)				(+)	(+)	
LIG1			(+)	(+)			(+)	(+)	
PCNA			(+)	(+)			(+)		(+)
POLD3			(+)	(+)	(+)		(+)	(+)	
RFC3			(+)	(+)			(+)		(+)
RFC4			(+)	(+)			(+)	(+)	(+)
RUVBL2			(+)				(+)		
FEN1			(+)				(+)	(+)	(+)
CUL4A				(+)			(+)		
GTF2H1				(+)			(+)		
MCM7					(+)		(+)		(+)
MSH2					(+)		(+)	(+)	(+)
MSH6					(+)		(+)		
PMS1					(+)		(+)	(+)	
TIMELESS					(+)		(+)		(+)
UBR5					(+)		(+)	(+)	
EXO1					(+)		(+)		(+)
ALKBH2						(+)[1]	(+)		
CEBPG						(+)[2]	(+)		
CHAF1A						(+)[3]	(+)		
ESCO1						(+)[4]	(+)		
NUDT1						(+)[5]	(+)		
POLQ						(+)[6]	(+)		
TDP1						(+)[7]	(+)	(+)	
TOP2A						(+)[8]	(+)	(+)	(+)
UHRF1						(+)[9]	(+)		
UPF1						(+)[10]	(+)		

DSBR: Double-strand break repair; BER: base-excision repair; NER: nucleotide-excision repair; MMR: DNA mismatch repair.

[1]Direct repair

[2]Repair gene expression

[3]Chromatin assembly

[4]AcetylTransferase-sistercohesion

[5]Hydrolyzes oxidized purine nucleoside triphosphate

[6]Translesion synthesis

Figure 4.30: Upregulation of DNA damage response genes in hepatocellular carcinoma

Chapter 5

DISCUSSION

5.1 Downregulation and the anti-growth effect of ZEB2 in hepatocellular carcinoma.

ZEB2 was initially discovered as a SMAD-interacting multi-zinc finger protein with specific DNA-binding activity [78]. This protein also acted as a strong repressor of a set of genes [78], including E-cadherin [45]. As E-cadherin is involved in epithelial cell adhesion, its repression by ZEB2 was associated with disruption of cell-cell adhesion, induction of invasion and reduction of unidirectional cell migration, leading to the hypothesis that it may be a promoter of invasion in malignant epithelial tumors [45]. A potential tumor-promoting role for ZEB2 was also proposed for HCC. Miyoshi et al. [47] reported that ZEB2 expression in HCC cells suppressed E-cadherin expression, and enhanced the expression of several matrix proteinase family members. These changes were accompanied by morphologic changes into fibroblastoid features and acceleration of invasion activity. These findings led to the hypothesis that ZEB2 expression may be induced during HCC progression and activate cancer invasion [47]. The discovery of TERT as a novel repressed target of ZEB2 by Lin and Elledge [43] provided the first evidence for further involvement of this gene in cancer. Upregulation of TERT expression

is a critical, if not essential step for malignant transformation [20, 78]. Repression of TERT or inhibition of telomerase activity have been shown to induce tumor cell apoptosis or senescence almost consistently [78]. Here, we demonstrate that ectopic expression of ZEB2 in HCC-derived Hep3B cells induces not only TERT repression, but also senescence-like terminal growth arrest. In close correlation with these observations, cancer cells engineered to express ZEB2 ectopically did not survive during in vitro cell expansion and were replaced by ZEB2-negative progeny. Inversely, knockdown of endogenous ZEB2 by RNA interference in Huh7 cells resulted in increased clonogenicity and enhanced cell proliferation in Huh7 clones.

The mechanisms of ZEB2-induced senescence induction in HCC cells are not fully known. However, the induction of $p21^{Cip1}$ in ZEB2-expressing, senescence-positive Hep3B cells (Figure 4.7) strongly suggests that this well-known senescence inducing protein is involved in this process. Also unknown is the mechanism by which $p21^{Cip1}$ is induced in these cells. It is highly likely that ZEB2 is not directly involved in this induction. However, an indirect role via repression of TERT cannot be excluded. As ZEB2-expressing early clones displayed inhibited telomerase activity in correlation with TERT repression, deficient telomerase activity could trigger $p21^{Cip1}$ inductive signals, as observed previously in telomere-deficient cells [79].

In vivo relevance of our in vitro observations awaits further investigations. However, our in silico and RT-PCR studies with nontumor liver and HCC tumor samples indicate that relative levels of ZEB2 transcripts are high in cirrhosis, but low in HCC. Liver cirrhosis is characterized by telomerease deficiency, telomere shortening and senescence arrest of hepatocytes [2, 20, 39], whereas HCC cells are usually telomerase proficient and considered to be immortal [20]. Based on interesting similarities between our in vivo and in vitro observations, we propose that ZEB2 may display anti-tumor activities in HCC, at least under certain

conditions.

It is noteworthy that weak or undetectable expression of ZEB2 was limited to a subgroup of HCC cell lines, including Huh7, Hep3B, HepG2 and PLC/PRF/5 (Figure 5.1).

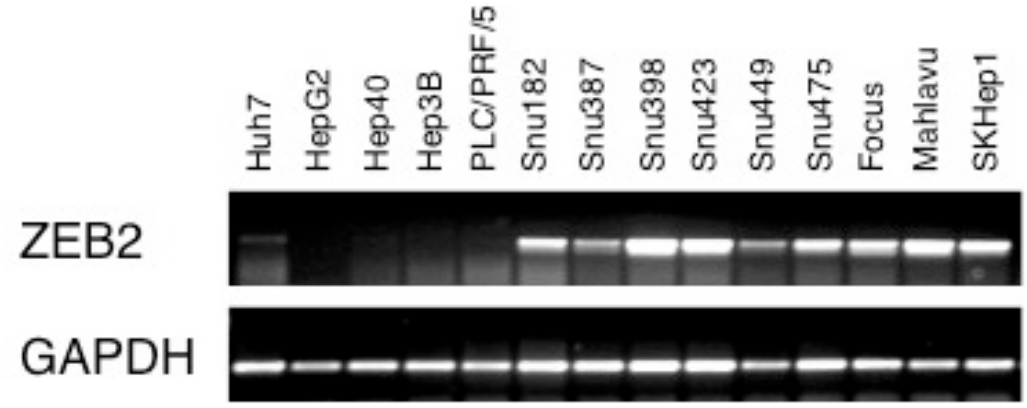

Figure 5.1: The expression of ZEB2 in HCC-derived cell lines. Total RNA from each cell lines was analyzed by RT-PCR using ZEB2-specific PCR primers.

This subgroup has recently been identified as epithelial HCC cell lines [80]. Here, we studied and observed growth-limiting effects in Huh7 and Hep3B cells belonging to this epithelial subgroup. Another subgroup of HCC cell lines, including SNU182, SNU387, SNU398, SNU449, SNU475, Focus and SKHep1 that express high levels of ZEB2 (Figure 5.1) has been classified as mesenchymal HCC cell lines. The effects of ZEB2 in this mesenchymal HCC cell line subgroup are presently unknown. However, it appears that these mesenchymal HCC cell lines can tolerate high levels of ZEB2 expression. Thus, we expect that ZEB2 plays different and/or additional roles in mesenchymal HCC cell lines. Taken together, these observations provide further evidence for differential roles of ZEB2 in epithelial and mesenchymal HCC cells. Further studies are underway for understanding additional implications of ZEB2 in HCC.

5.2 A Major Role for the Senescence and Immortality Gene Network in Hepatocellular Carcinoma

Hepatocellular senescence is a process gaining growing interest in the physiopathology field of chronic liver diseases [20], yet the observations are fragmented and somewhat contradictory. Telomere shortening and senescence have been observed in hepatocytes of cirrhotic liver, and replicative senescence was proposed as a key mechanism that contributes to cirrhosis development [10, 36, 38, 39]. However, a recent study reported that senescence in fibrosis and cirrhosis is limited primarily to stellate cells [81]. Controversies also exist regarding the role of senescence in HCC. These tumors display both TERT expression and telomerase activity [11], as an indication of telomere maintenance and cellular immortality. However, they often display extremely short telomeres, and even senescent cells at high levels [10, 36, 37, 38], as observed in aging tissues such as cirrhotic liver.

To better understand the role of cellular senescence in hepatocellular carcinogenesis, we explored the expression of senescence- and immortality-associated genes in HCC and its preneoplastic lesions, including cirrhosis. A complete set of genes associated with hepatocyte senescence and immortality was lacking. Therefore, we first determined differentially expressed genes in presenescent, senescent and immortal clones derived from a well-differentiated HCC cell line. We also determined differentially expressed genes between liver cirrhosis and HCC. Then, we obtained a set of genes by integrating the cell line and tissue data to generate a SIGN signature. This signature was tested against independent clinical datasets to analyze the role of senescence and immortality genes in hepatocellular carcinogenesis and tumor heterogeneity. This novel approach allowed us to show that cellular senescence and immortality mechanisms are deeply involved in HCC.

The SIGN signature alone was able to classify a normal liver, cirrhosis, dysplasia, and early HCC with high accuracy, and differentiated advanced HCC from early HCC with moderate accuracy. The cirrhosis was significantly enriched in senescence genes in confirmation of previous observations describing cirrhosis as a state of cellular senescence [39]. Hepatocellular carcinogenesis from cirrhotic lesions was associated with a significant increase in the ratio of upregulated immortality genes in early HCC, but not in dysplasia state. Thus, the development of dysplasia in cirrhotic liver is apparently a senescence-independent event. The prevalence of immortality genes became much more significant in advanced HCCs. This finding indicates that the transition from senescence to immortality is a progressive event in HCC, and it correlates with a recent report that shows higher telomerase activity and longer telomeres in advanced HCCs as compared to early HCCs [82]. Thus, the gain of immortality in cancer cells is not a single step event, but rather, a continuous and progressive event that goes along with tumor progression. This would not be totally unexpected, as four immortalization complementation groups have been described and a dozen chromosomes were shown to induce senescence, providing evidence for a multi-level control of senescence pathways [83]. It is highly likely that early HCC cells have bypassed some but not all senescence-inducing pathways, and that as tumors progress they bypass additional senescence controls.

We also identified critical senescence- and immortality-associated biological processes taking place in different steps of hepatocellular carcinogenesis. A large number of biological processes were significantly affected during transition from dysplasia to early HCC, and from early to advanced HCC. We observed a progressive decline in the expression of hepatocyte-specific genes involved in intermediary metabolism, complement activation and blood coagulation, indicative of hepatocyte dedifferentiation, a well-known feature of HCC [84]. Our findings connect this old concept to the gain of hepatocellular immortality. Hepatocyte

dedifferentiation was accompanied by the upregulation of genes involved cell proliferation, DDR, and chromatin modification. This may indicate that hepatocyte immortalization during hepatocellular carcinogenesis is associated with the gain of stem cell-like features [84]. In addition to the capacity of self-renewal, cancer stem cells display chromatin remodeling and resistance to DNA damage [85, 86].

The availability of large-scale genomic analysis and gene expression profiling methods contributed significantly to a better understanding of tumor heterogeneity and molecular classification of tumors [87]. Here, we show that senescence and immortality genes play a major role in the molecular heterogeneity of HCC. We reclassified a recently described HCC cohort using SIGN signature, detailed explanations on the classification of HCC samples from Boyault data set can be obtained from PhD Thesis by Sevgi Bağışlar, August 2009, Bilkent University].

The upregulation of a large set of DDR genes in HCC, and the association of this process with tumor progression indicate that liver malignancy is associated with acquired ability to deal with DNA damage. This finding correlates with well-known resistance of HCCs to currently available therapies. Thus, although DNA repair deficiency increases tumor susceptibility in normal cells, increased repair capacity may be beneficial for tumor cells. It will be interesting to investigate whether DNA damage response genes that are upregulated in HCC may serve as novel targets for combined therapies using DNA damaging agents together with DNA repair inhibitors.

In summary, our findings demonstrate that senescence and its bypass (i.e. immortality) play a central role in human hepatocellular carcinogenesis as well as in the molecular classification of HCC. These findings may serve in designing new prognostic and therapeutic approaches.

Bibliography

[1] D. M. Parkin, F. Bray, J. Ferlay, and P. Pisani, "Global cancer statistics, 2002." *CA Cancer J Clin*, vol. 55, no. 2, pp. 74–108, Mar-Apr 2005.

[2] H. B. El-Serag and K. L. Rudolph, "Hepatocellular carcinoma: epidemiology and molecular carcinogenesis." *Gastroenterology*, vol. 132, no. 7, pp. 2557–2576, Jun 2007.

[3] R. Capocaccia, M. Sant, F. Berrino, A. Simonetti, V. Santi, and F. Trevisani, "Hepatocellular carcinoma: trends of incidence and survival in europe and the united states at the end of the 20th century." *Am J Gastroenterol*, vol. 102, no. 8, pp. 1661–1670, Aug 2007.

[4] P. A. Farazi and R. A. DePinho, "Hepatocellular carcinoma pathogenesis: from genes to environment." *Nat Rev Cancer*, vol. 6, no. 9, pp. 674–687, Sep 2006.

[5] S. S. Thorgeirsson and J. W. Grisham, "Molecular pathogenesis of human hepatocellular carcinoma." *Nat Genet*, vol. 31, no. 4, pp. 339–346, Aug 2002.

[6] M. Ozturk, "Genetic aspects of hepatocellular carcinogenesis." *Semin Liver Dis*, vol. 19, no. 3, pp. 235–242, 1999.

[7] J. M. Llovet, A. Burroughs, and J. Bruix, "Hepatocellular carcinoma." *Lancet*, vol. 362, no. 9399, pp. 1907–1917, Dec 2003.

[8] K. Nouso, Y. Urabe, T. Higashi, H. Nakatsukasa, N. Hino, K. Ashida, N. Kinugasa, K. Yoshida, S. Uematsu, and T. Tsuji, "Telomerase as a tool for the differential diagnosis of human hepatocellular carcinoma." *Cancer*, vol. 78, no. 2, pp. 232–236, Jul 1996.

[9] H. Tahara, T. Nakanishi, M. Kitamoto, R. Nakashio, J. W. Shay, E. Tahara, G. Kajiyama, and T. Ide, "Telomerase activity in human liver tissues: comparison between chronic liver disease and hepatocellular carcinomas." *Cancer Res*, vol. 55, no. 13, pp. 2734–2736, Jul 1995.

[10] H. Kojima, O. Yokosuka, F. Imazeki, H. Saisho, and M. Omata, "Telomerase activity and telomere length in hepatocellular carcinoma and chronic liver disease." *Gastroenterology*, vol. 112, no. 2, pp. 493–500, Feb 1997.

[11] J. Nakayama, H. Tahara, E. Tahara, M. Saito, K. Ito, H. Nakamura, T. Nakanishi, E. Tahara, T. Ide, and F. Ishikawa, "Telomerase activation by htrt in human normal fibroblasts and hepatocellular carcinomas." *Nat Genet*, vol. 18, no. 1, pp. 65–68, Jan 1998.

[12] Y.-S. Cong, W. E. Wright, and J. W. Shay, "Human telomerase and its regulation." *Microbiol Mol Biol Rev*, vol. 66, no. 3, pp. 407–425, Sep 2002.

[13] P. A. Farazi, J. Glickman, S. Jiang, A. Yu, K. L. Rudolph, and R. A. DePinho, "Differential impact of telomere dysfunction on initiation and progression of hepatocellular carcinoma." *Cancer Res*, vol. 63, no. 16, pp. 5021–5027, Aug 2003.

[14] I. Horikawa and J. C. Barrett, "Transcriptional regulation of the telomerase htert gene as a target for cellular and viral oncogenic mechanisms." *Carcinogenesis*, vol. 24, no. 7, pp. 1167–1176, Jul 2003.

[15] Y. Murakami, K. Saigo, H. Takashima, M. Minami, T. Okanoue, C. Brechot, and P. Paterlini-Brechot, "Large scaled analysis of hepatitis b virus (hbv)

dna integration in hbv related hepatocellular carcinomas." *Gut*, vol. 54, no. 8, pp. 1162–1168, Aug 2005.

[16] H. Liu, F. Luan, Y. Ju, H. Shen, L. Gao, X. Wang, S. Liu, L. Zhang, W. Sun, and C. Ma, "In vitro transfection of the hepatitis b virus pres2 gene into the human hepatocarcinoma cell line hepg2 induces upregulation of human telomerase reverse transcriptase." *Biochem Biophys Res Commun*, vol. 355, no. 2, pp. 379–384, Apr 2007.

[17] Z.-L. Qu, S.-Q. Zou, N.-Q. Cui, X.-Z. Wu, M.-F. Qin, D. Kong, and Z.-L. Zhou, "Upregulation of human telomerase reverse transcriptase mrna expression by in vitro transfection of hepatitis b virus x gene into human hepatocarcinoma and cholangiocarcinoma cells." *World J Gastroenterol*, vol. 11, no. 36, pp. 5627–5632, Sep 2005.

[18] J.-M. Su, X.-M. Lai, K.-H. Lan, C.-P. Li, Y. Chao, S.-H. Yen, F.-Y. Chang, S.-D. Lee, and W.-P. Lee, "X protein of hepatitis b virus functions as a transcriptional corepressor on the human telomerase promoter." *Hepatology*, vol. 46, no. 2, pp. 402–413, Aug 2007.

[19] J. Campisi and F. d'Adda di Fagagna, "Cellular senescence: when bad things happen to good cells." *Nat Rev Mol Cell Biol*, vol. 8, no. 9, pp. 729–740, Sep 2007.

[20] M. Ozturk, A. Arslan-Ergul, S. Bagislar, S. Senturk, and H. Yuzugullu, "Senescence and immortality in hepatocellular carcinoma." *Cancer Lett*, vol. [Epub ahead of print], Dec 2008.

[21] T. de Lange, "Shelterin: the protein complex that shapes and safeguards human telomeres," *Genes Dev*, vol. 19, no. 18, pp. 2100–10, Sep 2005.

[22] E. H. Blackburn, "Structure and function of telomeres," *Nature*, vol. 350, no. 6319, pp. 569–73, Apr 1991.

[23] J. Karlseder, A. Smogorzewska, and T. de Lange, "Senescence induced by altered telomere state, not telomere loss," *Science*, vol. 295, no. 5564, pp. 2446–9, Mar 2002.

[24] F. d'Adda di Fagagna, P. M. Reaper, L. Clay-Farrace, H. Fiegler, P. Carr, T. Von Zglinicki, G. Saretzki, N. P. Carter, and S. P. Jackson, "A dna damage checkpoint response in telomere-initiated senescence," *Nature*, vol. 426, no. 6963, pp. 194–8, Nov 2003.

[25] M. Serrano, A. W. Lin, M. E. McCurrach, D. Beach, and S. W. Lowe, "Oncogenic ras provokes premature cell senescence associated with accumulation of p53 and p16ink4a," *Cell*, vol. 88, no. 5, pp. 593–602, Mar 1997.

[26] R. Di Micco, M. Fumagalli, and F. d'Adda di Fagagna, "Breaking news: high-speed race ends in arrest–how oncogenes induce senescence," *Trends Cell Biol*, vol. 17, no. 11, pp. 529–36, Nov 2007.

[27] Z. Chen, L. C. Trotman, D. Shaffer, H.-K. Lin, Z. A. Dotan, M. Niki, J. A. Koutcher, H. I. Scher, T. Ludwig, W. Gerald, C. Cordon-Cardo, and P. P. Pandolfi, "Crucial role of p53-dependent cellular senescence in suppression of pten-deficient tumorigenesis," *Nature*, vol. 436, no. 7051, pp. 725–30, Aug 2005.

[28] T. von Zglinicki, G. Saretzki, W. Döcke, and C. Lotze, "Mild hyperoxia shortens telomeres and inhibits proliferation of fibroblasts: a model for senescence?" *Exp Cell Res*, vol. 220, no. 1, pp. 186–93, Sep 1995.

[29] U. Herbig, W. A. Jobling, B. P. C. Chen, D. J. Chen, and J. M. Sedivy, "Telomere shortening triggers senescence of human cells through a pathway involving atm, p53, and p21(cip1), but not p16(ink4a)," *Mol Cell*, vol. 14, no. 4, pp. 501–13, May 2004.

[30] F. A. Mallette, M.-F. Gaumont-Leclerc, and G. Ferbeyre, "The dna damage signaling pathway is a critical mediator of oncogene-induced senescence," *Genes Dev*, vol. 21, no. 1, pp. 43–8, Jan 2007.

[31] J. Gil and G. Peters, "Regulation of the ink4b-arf-ink4a tumour suppressor locus: all for one or one for all," *Nat Rev Mol Cell Biol*, vol. 7, no. 9, pp. 667–77, Sep 2006.

[32] W. S. el Deiry, T. Tokino, V. E. Velculescu, D. B. Levy, R. Parsons, J. M. Trent, D. Lin, W. E. Mercer, K. W. Kinzler, and B. Vogelstein, "Waf1, a potential mediator of p53 tumor suppression," *Cell*, vol. 75, no. 4, pp. 817–25, Nov 1993.

[33] Y. Deng, S. S. Chan, and S. Chang, "Telomere dysfunction and tumour suppression: the senescence connection." *Nat Rev Cancer*, vol. 8, no. 6, pp. 450–458, Jun 2008.

[34] L. Fang, M. Igarashi, J. Leung, M. M. Sugrue, S. W. Lee, and S. A. Aaronson, "p21waf1/cip1/sdi1 induces permanent growth arrest with markers of replicative senescence in human tumor cells lacking functional p53," *Oncogene*, vol. 18, no. 18, pp. 2789–97, May 1999.

[35] H. Wege, H. T. Le, M. S. Chui, L. Liu, J. Wu, R. Giri, H. Malhi, B. S. Sappal, V. Kumaran, S. Gupta, and M. A. Zern, "Telomerase reconstitution immortalizes human fetal hepatocytes without disrupting their differentiation potential," *Gastroenterology*, vol. 124, no. 2, pp. 432–44, Feb 2003.

[36] V. Paradis, N. Youssef, D. Dargere, N. Ba, F. Bonvoust, J. Deschatrette, and P. Bedossa, "Replicative senescence in normal liver, chronic hepatitis c, and hepatocellular carcinomas." *Hum Pathol*, vol. 32, no. 3, pp. 327–332, Mar 2001.

[37] R. R. Plentz, M. Caselitz, J. S. Bleck, M. Gebel, P. Flemming, S. Kubicka, M. P. Manns, and K. L. Rudolph, "Hepatocellular telomere shortening correlates with chromosomal instability and the development of human hepatoma." *Hepatology*, vol. 40, no. 1, pp. 80–86, Jul 2004.

[38] R. R. Plentz, Y. N. Park, A. Lechel, H. Kim, F. Nellessen, B. H. E. Langkopf, L. Wilkens, A. Destro, B. Fiamengo, M. P. Manns, M. Roncalli, and K. L. Rudolph, "Telomere shortening and inactivation of cell cycle checkpoints characterize human hepatocarcinogenesis." *Hepatology*, vol. 45, no. 4, pp. 968–976, Apr 2007.

[39] S. U. Wiemann, A. Satyanarayana, M. Tsahuridu, H. L. Tillmann, L. Zender, J. Klempnauer, P. Flemming, S. Franco, M. A. Blasco, M. P. Manns, and K. L. Rudolph, "Hepatocyte telomere shortening and senescence are general markers of human liver cirrhosis." *FASEB J*, vol. 16, no. 9, pp. 935–942, Jul 2002.

[40] C.-H. Wu, J. van Riggelen, A. Yetil, A. C. Fan, P. Bachireddy, and D. W. Felsher, "Cellular senescence is an important mechanism of tumor regression upon c-myc inactivation." *Proc Natl Acad Sci U S A*, vol. 104, no. 32, pp. 13 028–13 033, Aug 2007.

[41] W. Xue, L. Zender, C. Miething, R. A. Dickins, E. Hernando, V. Krizhanovsky, C. Cordon-Cardo, and S. W. Lowe, "Senescence and tumour clearance is triggered by p53 restoration in murine liver carcinomas." *Nature*, vol. 445, no. 7128, pp. 656–660, Feb 2007.

[42] N. Ozturk, E. Erdal, M. Mumcuoglu, K. C. Akcali, O. Yalcin, S. Senturk, A. Arslan-Ergul, B. Gur, I. Yulug, R. Cetin-Atalay, C. Yakicier, T. Yagci,

M. Tez, and M. Ozturk, "Reprogramming of replicative senescence in hepatocellular carcinoma-derived cells." *Proc Natl Acad Sci U S A*, vol. 103, no. 7, pp. 2178–2183, 2006.

[43] S. Y. Lin and S. J. Elledge, "Multiple tumor suppressor pathways negatively regulate telomerase." *Cell*, vol. 113, no. 7, pp. 881–889, Jun 2003.

[44] R. Janknecht, "On the road to immortality: htert upregulation in cancer cells." *FEBS Lett*, vol. 564, no. 1-2, pp. 9–13, Apr 2004.

[45] J. Comijn, G. Berx, P. Vermassen, K. Verschueren, L. van Grunsven, E. Bruyneel, M. Mareel, D. Huylebroeck, and F. van Roy, "The two-handed e box binding zinc finger protein sip1 downregulates e-cadherin and induces invasion." *Mol Cell*, vol. 7, no. 6, pp. 1267–1278, Jun 2001.

[46] J. Mejlvang, M. Kriajevska, C. Vandewalle, T. Chernova, A. E. Sayan, G. Berx, J. K. Mellon, and E. Tulchinsky, "Direct repression of cyclin d1 by sip1 attenuates cell cycle progression in cells undergoing an epithelial mesenchymal transition." *Mol Biol Cell*, vol. 18, no. 11, pp. 4615–4624, 2007.

[47] A. Miyoshi, Y. Kitajima, K. Sumi, K. Sato, A. Hagiwara, Y. Koga, and K. Miyazaki, "Snail and sip1 increase cancer invasion by upregulating mmp family in hepatocellular carcinoma cells," *Br J Cancer*, vol. 90, no. 6, pp. 1265–73, Mar 2004.

[48] K. Verschueren, J. E. Remacle, C. Collart, H. Kraft, B. S. Baker, P. Tylzanowski, L. Nelles, G. Wuytens, M. T. Su, R. Bodmer, J. C. Smith, and D. Huylebroeck, "Sip1, a novel zinc finger/homeodomain repressor, interacts with smad proteins and binds to 5'-cacct sequences in candidate target genes," *J Biol Chem*, vol. 274, no. 29, pp. 20 489–98, Jul 1999.

[49] J. E. Remacle, H. Kraft, W. Lerchner, G. Wuytens, C. Collart, K. Verschueren, J. C. Smith, and D. Huylebroeck, "New mode of dna binding of

multi-zinc finger transcription factors: deltaef1 family members bind with two hands to two target sites," *EMBO J*, vol. 18, no. 18, pp. 5073–84, Sep 1999.

[50] T. Van de Putte, M. Maruhashi, A. Francis, L. Nelles, H. Kondoh, D. Huylebroeck, and Y. Higashi, "Mice lacking zfhx1b, the gene that codes for smad-interacting protein-1, reveal a role for multiple neural crest cell defects in the etiology of hirschsprung disease-mental retardation syndrome," *Am J Hum Genet*, vol. 72, no. 2, pp. 465–70, Feb 2003.

[51] K. Yamada, Y. Yamada, N. Nomura, K. Miura, R. Wakako, C. Hayakawa, A. Matsumoto, T. Kumagai, I. Yoshimura, S. Miyazaki, K. Kato, S. Sonta, H. Ono, T. Yamanaka, M. Nagaya, and N. Wakamatsu, "Nonsense and frameshift mutations in zfhx1b, encoding smad-interacting protein 1, cause a complex developmental disorder with a great variety of clinical features," *Am J Hum Genet*, vol. 69, no. 6, pp. 1178–85, Dec 2001.

[52] N. Wakamatsu, Y. Yamada, K. Yamada, T. Ono, N. Nomura, H. Taniguchi, H. Kitoh, N. Mutoh, T. Yamanaka, K. Mushiake, K. Kato, S. Sonta, and M. Nagaya, "Mutations in sip1, encoding smad interacting protein-1, cause a form of hirschsprung disease," *Nat Genet*, vol. 27, no. 4, pp. 369–70, Apr 2001.

[53] D. R. Mowat, M. J. Wilson, and M. Goossens, "Mowat-wilson syndrome," *J Med Genet*, vol. 40, no. 5, pp. 305–10, May 2003.

[54] L. Larue and A. Bellacosa, "Epithelial-mesenchymal transition in development and cancer: role of phosphatidylinositol 3' kinase/akt pathways," *Oncogene*, vol. 24, no. 50, pp. 7443–54, Nov 2005.

[55] G. Maeda, T. Chiba, M. Okazaki, T. Satoh, Y. Taya, T. Aoba, K. Kato, S. Kawashiri, and K. Imai, "Expression of sip1 in oral squamous cell carcinomas: implications for e-cadherin expression and tumor progression," *Int J Oncol*, vol. 27, no. 6, pp. 1535–41, Dec 2005.

[56] C. Vandewalle, J. Comijn, B. De Craene, P. Vermassen, E. Bruyneel, H. Andersen, E. Tulchinsky, F. Van Roy, and G. Berx, "Sip1/zeb2 induces emt by repressing genes of different epithelial cell-cell junctions," *Nucleic Acids Res*, vol. 33, no. 20, pp. 6566–78, 2005.

[57] S. Bindels, M. Mestdagt, C. Vandewalle, N. Jacobs, L. Volders, A. Noël, F. van Roy, G. Berx, J.-M. Foidart, and C. Gilles, "Regulation of vimentin by sip1 in human epithelial breast tumor cells," *Oncogene*, vol. 25, no. 36, pp. 4975–85, Aug 2006.

[58] S. Elloul, M. B. Elstrand, J. M. Nesland, C. G. Tropé, G. Kvalheim, I. Goldberg, R. Reich, and B. Davidson, "Snail, slug, and smad-interacting protein 1 as novel parameters of disease aggressiveness in metastatic ovarian and breast carcinoma," *Cancer*, vol. 103, no. 8, pp. 1631–43, Apr 2005.

[59] Y. Shi and J. Massagué, "Mechanisms of tgf-beta signaling from cell membrane to the nucleus," *Cell*, vol. 113, no. 6, pp. 685–700, Jun 2003.

[60] A. Sancar, L. A. Lindsey-Boltz, K. Unsal-Kaçmaz, and S. Linn, "Molecular mechanisms of mammalian dna repair and the dna damage checkpoints," *Annu Rev Biochem*, vol. 73, pp. 39–85, 2004.

[61] S. P. Hussain, J. Schwank, F. Staib, X. W. Wang, and C. C. Harris, "Tp53 mutations and hepatocellular carcinoma: insights into the etiology and pathogenesis of liver cancer," *Oncogene*, vol. 26, no. 15, pp. 2166–76, Apr 2007.

[62] M. J. van de Vijver, Y. D. He, L. J. van't Veer, H. Dai, A. A. M. Hart, D. W. Voskuil, G. J. Schreiber, J. L. Peterse, C. Roberts, M. J. Marton, M. Parrish, D. Atsma, A. Witteveen, A. Glas, L. Delahaye, T. van der Velde, H. Bartelink, S. Rodenhuis, E. T. Rutgers, S. H. Friend, and R. Bernards, "A gene-expression signature as a predictor of survival in breast cancer," *N Engl J Med*, vol. 347, no. 25, pp. 1999–2009, Dec 2002.

[63] E. Segal, N. Friedman, D. Koller, and A. Regev, "A module map showing conditional activity of expression modules in cancer," *Nat Genet*, vol. 36, no. 10, pp. 1090–8, Oct 2004.

[64] J.-S. Lee, I.-S. Chu, J. Heo, D. F. Calvisi, Z. Sun, T. Roskams, A. Durnez, A. J. Demetris, and S. S. Thorgeirsson, "Classification and prediction of survival in hepatocellular carcinoma by gene expression profiling," *Hepatology*, vol. 40, no. 3, pp. 667–76, Sep 2004.

[65] B. M. Bolstad, R. A. Irizarry, M. Astrand, and T. P. Speed, "A comparison of normalization methods for high density oligonucleotide array data based on variance and bias," *Bioinformatics*, vol. 19, no. 2, pp. 185–93, Jan 2003.

[66] M. B. Eisen, P. T. Spellman, P. O. Brown, and D. Botstein, "Cluster analysis and display of genome-wide expression patterns," *Proc Natl Acad Sci U S A*, vol. 95, no. 25, pp. 14 863–8, Dec 1998.

[67] N. Ozturk, "Heterogeneity of hepatocellular malignant phenotype," Ph.D. dissertation, Bilkent University, 2006.

[68] G. P. Dimri, X. Lee, G. Basile, M. Acosta, G. Scott, C. Roskelley, E. E. Medrano, M. Linskens, I. Rubelj, and O. Pereira-Smith, "A biomarker that identifies senescent human cells in culture and in aging skin in vivo." *Proc Natl Acad Sci U S A*, vol. 92, no. 20, pp. 9363–9367, 1995.

[69] *GeneChip Expression Analysis Technical Manual P/N 702232*, Rev.2 ed., Affymetrix, 2005-2006.

[70] D. W. Huang, B. T. Sherman, and R. A. Lempicki, "Systematic and integrative analysis of large gene lists using david bioinformatics resources." *Nat Protoc*, vol. 4, no. 1, pp. 44–57, 2009.

[71] E. Wurmbach, Y.-b. Chen, G. Khitrov, W. Zhang, S. Roayaie, M. Schwartz, I. Fiel, S. Thung, V. Mazzaferro, J. Bruix, E. Bottinger, S. Friedman, S. Waxman, and J. M. Llovet, "Genome-wide molecular profiles of hcv-induced dysplasia and hepatocellular carcinoma." *Hepatology*, vol. 45, no. 4, pp. 938–947, Apr 2007.

[72] S. Boyault, D. S. Rickman, A. de Reynies, C. Balabaud, S. Rebouissou, E. Jeannot, A. Herault, J. Saric, J. Belghiti, D. Franco, P. Bioulac-Sage, P. Laurent-Puig, and J. Zucman-Rossi, "Transcriptome classification of hcc is related to gene alterations and to new therapeutic targets." *Hepatology*, vol. 45, no. 1, pp. 42–52, Jan 2007.

[73] W. Wei and J. M. Sedivy, "Differentiation between senescence (m1) and crisis (m2) in human fibroblast cultures." *Exp Cell Res*, vol. 253, no. 2, pp. 519–522, Dec 1999.

[74] O. Hashimoto, T. Ueno, R. Kimura, M. Ohtsubo, T. Nakamura, H. Koga, T. Torimura, S. Uchida, K. Yamashita, and M. Sata, "Inhibition of proteasome-dependent degradation of wee1 in g2-arrested hep3b cells by tgf beta 1." *Mol Carcinog*, vol. 36, no. 4, pp. 171–182, Apr 2003.

[75] A. Schroeder, O. Mueller, S. Stocker, R. Salowsky, M. Leiber, M. Gassmann, S. Lightfoot, W. Menzel, M. Granzow, and T. Ragg, "The rin: an rna integrity number for assigning integrity values to rna measurements." *BMC Mol Biol*, vol. 7, p. 3, 2006.

[76] A. Watanuki, S. Ohwada, T. Fukusato, F. Makita, T. Yamada, A. Kikuchi, and Y. Morishita, "Prognostic significance of dna topoisomerase iialpha expression in human hepatocellular carcinoma. ." *Anticancer Res*, vol. 22, no. 2B, pp. 1113–1119, Mar-Apr 2002.

[77] A. Sancar, L. A. Lindsey-Boltz, K. Unsal-Kacmaz, and S. Linn, "Molecular mechanisms of mammalian dna repair and the dna damage checkpoints." *Annu Rev Biochem*, vol. 73, pp. 39–85, 2004.

[78] J. W. Shay and W. E. Wright, "Senescence and immortalization: role of telomeres and telomerase," *Carcinogenesis*, vol. 26, no. 5, pp. 867–74, May 2005.

[79] A. R. Choudhury, Z. Ju, M. W. Djojosubroto, A. Schienke, A. Lechel, S. Schaetzlein, H. Jiang, A. Stepczynska, C. Wang, J. Buer, H.-W. Lee, T. von Zglinicki, A. Ganser, P. Schirmacher, H. Nakauchi, and K. L. Rudolph, "Cdkn1a deletion improves stem cell function and lifespan of mice with dysfunctional telomeres without accelerating cancer formation," *Nat Genet*, vol. 39, no. 1, pp. 99–105, Jan 2007.

[80] B. C. Fuchs, T. Fujii, J. D. Dorfman, J. M. Goodwin, A. X. Zhu, M. Lanuti, and K. K. Tanabe, "Epithelial-to-mesenchymal transition and integrin-linked kinase mediate sensitivity to epidermal growth factor receptor inhibition in human hepatoma cells," *Cancer Res*, vol. 68, no. 7, pp. 2391–9, Apr 2008.

[81] V. Krizhanovsky, M. Yon, R. A. Dickins, S. Hearn, J. Simon, C. Miething, H. Yee, L. Zender, and S. W. Lowe, "Senescence of activated stellate cells limits liver fibrosis," *Cell*, vol. 134, no. 4, pp. 657–67, Aug 2008.

[82] B.-K. Oh, H. Kim, Y. N. Park, J. E. Yoo, J. Choi, K.-S. Kim, J. J. Lee, and C. Park, "High telomerase activity and long telomeres in advanced hepatocellular carcinomas with poor prognosis," *Lab Invest*, vol. 88, no. 2, pp. 144–52, Feb 2008.

[83] A. L. Fridman and M. A. Tainsky, "Critical pathways in cellular senescence and immortalization revealed by gene expression profiling," *Oncogene*, vol. 27, no. 46, pp. 5975–87, Oct 2008.

[84] S. Sell and H. L. Leffert, "Liver cancer stem cells," *J Clin Oncol*, vol. 26, no. 17, pp. 2800–5, Jun 2008.

[85] S. Bao, Q. Wu, R. E. McLendon, Y. Hao, Q. Shi, A. B. Hjelmeland, M. W. Dewhirst, D. D. Bigner, and J. N. Rich, "Glioma stem cells promote radioresistance by preferential activation of the dna damage response," *Nature*, vol. 444, no. 7120, pp. 756–60, Dec 2006.

[86] C. A. Iacobuzio-Donahue, "Epigenetic changes in cancer," *Annu Rev Pathol*, vol. 4, pp. 229–49, 2009.

[87] A. Villanueva, S. Toffanin, and J. M. Llovet, "Linking molecular classification of hepatocellular carcinoma and personalized medicine: preliminary steps," *Curr Opin Oncol*, vol. 20, no. 4, pp. 444–53, Jul 2008.

Appendix A

A.1 Aminoacid alignments for human and mouse SIP1 proteins

A.2 RIN values

A.2.1 RIN values of the samples that were used in the analysis

The Agilent Bioanalyzer plots given in Figure A.2 belong to the samples that were included in the bioinformatic analysis and used to define SIGN signature.

A.2.2 RIN values of the samples that are saved for future analysis

The samples listed in Figure A.3 have high RIN values and exhibited ideal RNA plots indicating high quality RNA. These samples were not included in microarray analysis but reserved for future experiments. They may be used in validation experiments.

BLAST 2 SEQUENCES RESULTS VERSION BLASTP 2.2.17 [Aug-26-2007]

Matrix BLOSUM62 gap open: 11 gap extension: 1
x_dropoff: 0 expect: 10.0 wordsize: 3 Filter View option Mismatch - highlighting

Masking character option Lower case Masking color option Red
Show CDS translation Align

Sequence 1: gi|7662184|ref|NP_055610.1| zinc finger homeobox 1b [Homo sapiens]
Length = 1213 (1 .. 1214)

Sequence 2: gi|40254564|ref|NP_056568.2| zinc finger homeobox 1b isoform 2 [Mus musculus]
Length = 1214 (1 .. 1215)

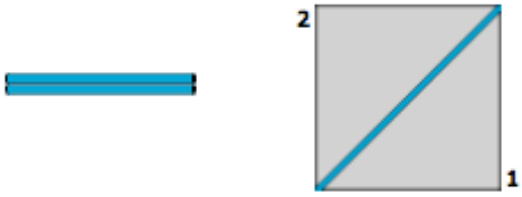

NOTE: Bitscore and expect value are calculated based on the size of the nr database.

```
 Score = 2095 bits (5427),  Expect = 0.0
 Identities = 1173/1213 (96%), Positives = 1193/1213 (98%), Gaps = 0/1213 (0%)

Query  2     KQPIMADGPRCKRRKQANPRRKNVVNYDNVVDTGSETDEEDKLHIAEDDGIANPLDQETS  61
Sbjct  2     ................................A................SL......D..  61

Query  62    PASVPNHESSPHVSQALLPREEEEDEIREGGVEHPWHNNEILQASVDGPEEMKEDYDTMG  121
Sbjct  62    ...M........M..G........E.L..SV...S..SG.......A..........A..  121

Query  122   PEATIQTAINNGTVKNANCTSDFEEYFAKRKLEERDGHAVSIEEYLQRSDTAIIYPEAPE  181
Sbjct  122   .......T.................................................  181

Query  182   ELSRLGTPEANGQEENDLPPGTPDAFAQLLTCPYCDRGYKRLTSLKEHIKYRHEKNEENF  241
Sbjct  182   ...................................................          241

Query  242   SCPLCSYTFAYRTQLERHMVTHKPGTDQHQMLTQGAGNRKFKCTECGKAFKYKHHLKEHL  301
Sbjct  242   ............................................................  301

Query  302   RIHSGEKPYECPNCKKRFSHSGSYSSHISSKKCIGLISVNGRMRNNIKTGSSPNSVSSSP  361
Sbjct  302   ...........................................................  361

Query  362   TNSAITQLRNKLENGKPLSMSEQTGLLKIKTEPLDFNDYKVLMATHGFSGTSPFMNGGLG  421
```

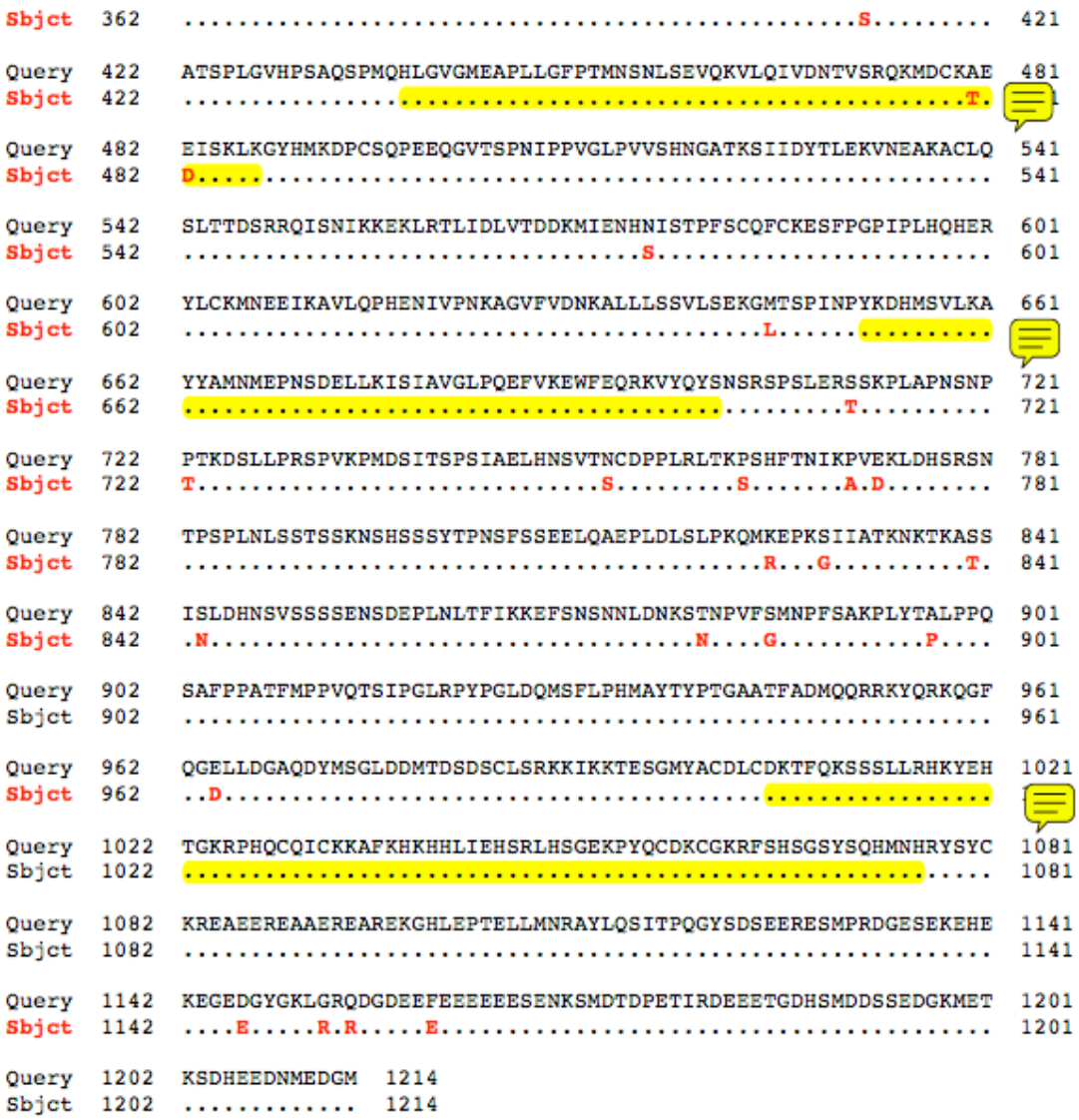

Figure A.1: Aminoacid alignments for human and mouse SIP1 proteins. Highlighted sequences indicate Zinc Finger Domain N-term, Smad Binding Domain, Homeodomain, and ZInc Finger C-term, respectively.

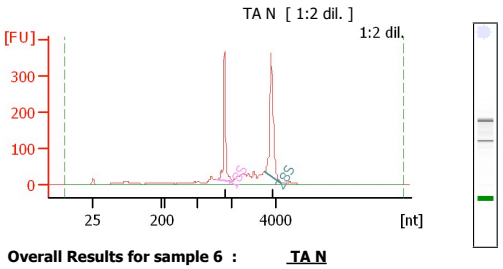

Overall Results for sample 6 : **TA N**

RNA Area:	1,471.8
RNA Concentration:	668 ng/µl
rRNA Ratio [28s / 18s]:	1.3
RNA Integrity Number (RIN):	8.8 (B.02.05)
Result Flagging Color:	
Result Flagging Label:	RIN: 8.80

Fragment table for sample 6 : **TA N**

Name	Start Size [nt]	End Size [nt]	Area	% of total Area
18S	1,582	2,028	304.1	20.7
28S	3,463	4,173	392.8	26.7

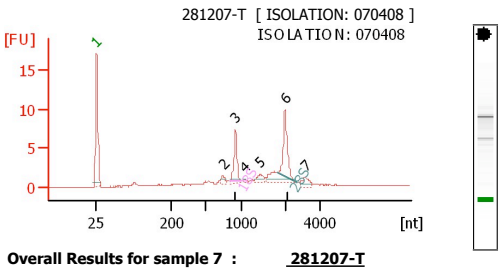

Overall Results for sample 7 : **281207-T**

RNA Area:	60.5
RNA Concentration:	55 ng/µl
rRNA Ratio [28s / 18s]:	1.5
RNA Integrity Number (RIN):	8.0 (B.02.05)
Result Flagging Color:	
Result Flagging Label:	

Fragment table for sample 7 : **281207-T**

Name	Start Size [nt]	End Size [nt]	Area	% of total Area
18S	840	1,001	7.2	11.9
28S	1,821	2,669	11.1	18.4

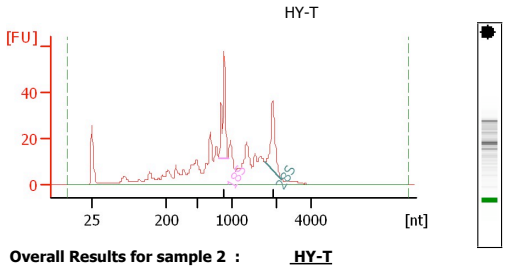

Overall Results for sample 2 : **HY-T**

RNA Area:	514.6
RNA Concentration:	2,206 ng/µl
rRNA Ratio [28s / 18s]:	0.8
RNA Integrity Number (RIN):	6.4 (B.02.05)
Result Flagging Color:	
Result Flagging Label:	

Fragment table for sample 2 : **HY-T**

Name	Start Size [nt]	End Size [nt]	Area	% of total Area
18S	806	943	53.6	10.4
28S	1,743	2,269	44.5	8.6

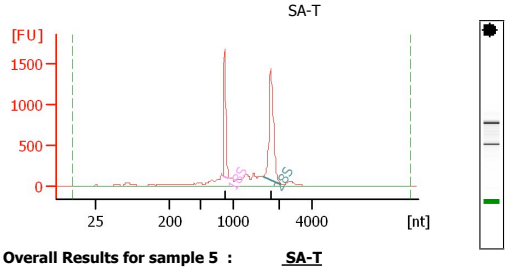

Overall Results for sample 5 : **SA-T**

RNA Area:	6,731.0
RNA Concentration:	28,859 ng/µl
rRNA Ratio [28s / 18s]:	1.7
RNA Integrity Number (RIN):	8.8 (B.02.05)
Result Flagging Color:	
Result Flagging Label:	

Fragment table for sample 5 : **SA-T**

Name	Start Size [nt]	End Size [nt]	Area	% of total Area
18S	839	930	1,220.4	18.1
28S	1,653	2,178	2,082.8	30.9

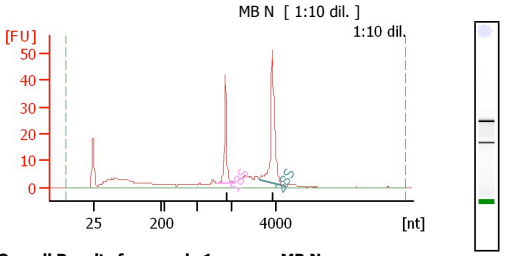

Overall Results for sample 1 : **MB N**

RNA Area:	253.0
RNA Concentration:	115 ng/µl
rRNA Ratio [28s / 18s]:	1.9
RNA Integrity Number (RIN):	8.5 (B.02.05)
Result Flagging Color:	
Result Flagging Label:	RIN: 8.50

Fragment table for sample 1 : **MB N**

Name	Start Size [nt]	End Size [nt]	Area	% of total Area
18S	1,624	2,131	33.2	13.1
28S	3,233	4,413	62.5	24.7

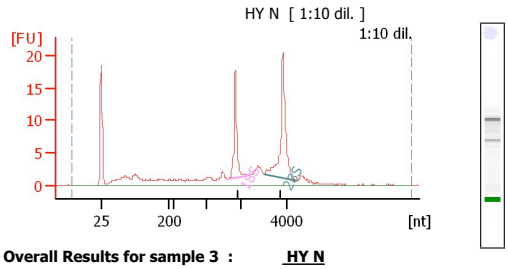

Overall Results for sample 3 : **HY N**

RNA Area:	140.0
RNA Concentration:	64 ng/µl
rRNA Ratio [28s / 18s]:	1.8
RNA Integrity Number (RIN):	8.2 (B.02.05)
Result Flagging Color:	
Result Flagging Label:	RIN: 8.20

Fragment table for sample 3 : **HY N**

Name	Start Size [nt]	End Size [nt]	Area	% of total Area
18S	1,608	2,265	17.7	12.6
28S	3,000	4,441	31.5	22.5

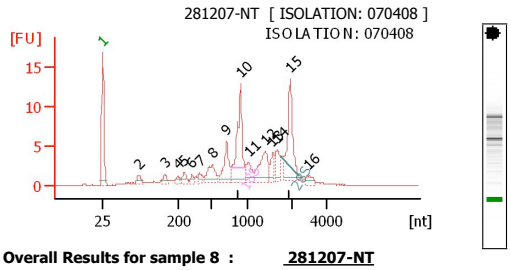

Overall Results for sample 8 : 281207-NT

RNA Area:	145.0
RNA Concentration:	132 ng/µl
rRNA Ratio [28s / 18s]:	1.0
RNA Integrity Number (RIN):	7.1 (B.02.05)
Result Flagging Color:	
Result Flagging Label:	

Fragment table for sample 8 : 281207-NT

Name	Start Size [nt]	End Size [nt]	Area	% of total Area
18S	767	966	15.1	10.4
28S	1,731	2,410	15.1	10.4

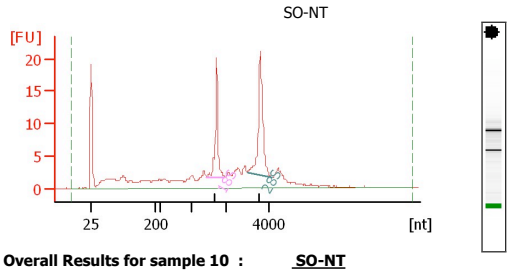

Overall Results for sample 10 : SO-NT

RNA Area:	176.3
RNA Concentration:	88 ng/µl
rRNA Ratio [28s / 18s]:	1.5
RNA Integrity Number (RIN):	7.8 (B.02.05)
Result Flagging Color:	
Result Flagging Label:	

Fragment table for sample 10 : SO-NT

Name	Start Size [nt]	End Size [nt]	Area	% of total Area
18S	1,456	1,977	19.3	10.9
28S	2,985	4,170	29.6	16.8

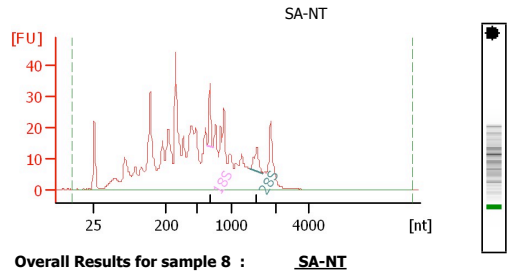

Overall Results for sample 8 : SA-NT

RNA Area:	750.4
RNA Concentration:	3,217 ng/µl
rRNA Ratio [28s / 18s]:	0.8
RNA Integrity Number (RIN):	4.3 (B.02.05)
Result Flagging Color:	
Result Flagging Label:	

Fragment table for sample 8 : SA-NT

Name	Start Size [nt]	End Size [nt]	Area	% of total Area
18S	649	726	15.8	2.1
28S	1,415	1,717	12.2	1.6

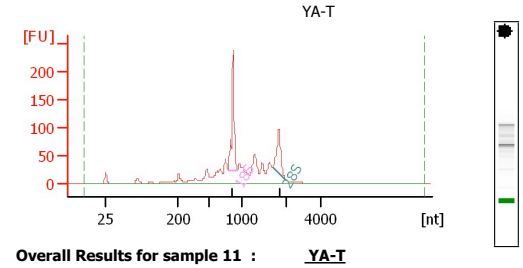

Overall Results for sample 11 : YA-T

RNA Area:	1,176.3
RNA Concentration:	5,043 ng/µl
rRNA Ratio [28s / 18s]:	0.5
RNA Integrity Number (RIN):	7.0 (B.02.05)
Result Flagging Color:	
Result Flagging Label:	

Fragment table for sample 11 : YA-T

Name	Start Size [nt]	End Size [nt]	Area	% of total Area
18S	781	920	204.2	17.4
28S	1,679	1,990	109.7	9.3

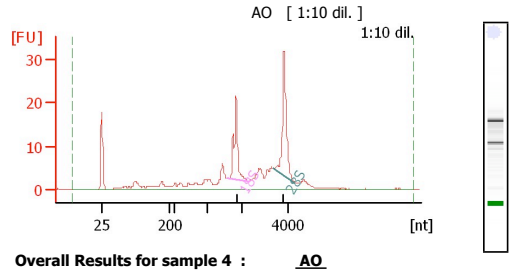

Overall Results for sample 4 : AO

RNA Area:	194.8
RNA Concentration:	88 ng/µl
rRNA Ratio [28s / 18s]:	1.4
RNA Integrity Number (RIN):	8.1 (B.02.05)
Result Flagging Color:	
Result Flagging Label:	RIN: 8.10

Fragment table for sample 4 : AO

Name	Start Size [nt]	End Size [nt]	Area	% of total Area
18S	1,579	2,249	28.1	14.4
28S	3,368	4,349	39.5	20.3

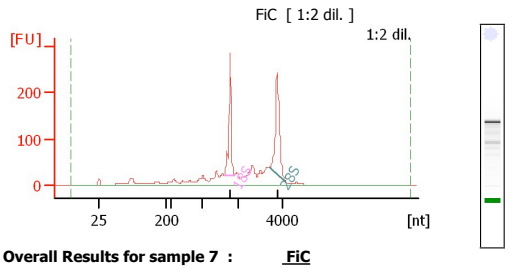

Overall Results for sample 7 : FiC

RNA Area:	1,508.8
RNA Concentration:	685 ng/µl
rRNA Ratio [28s / 18s]:	1.3
RNA Integrity Number (RIN):	7.8 (B.02.05)
Result Flagging Color:	
Result Flagging Label:	RIN: 7.80

Fragment table for sample 7 : FiC

Name	Start Size [nt]	End Size [nt]	Area	% of total Area
18S	1,628	1,900	241.0	16.0
28S	3,418	4,191	305.7	20.3

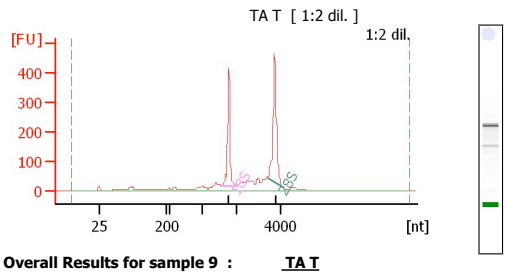

Overall Results for sample 9 : TA T

RNA Area:	1,852.0
RNA Concentration:	841 ng/µl
rRNA Ratio [28s / 18s]:	1.5
RNA Integrity Number (RIN):	8.8 (B.02.05)
Result Flagging Color:	
Result Flagging Label:	RIN: 8.80

Fragment table for sample 9 : TA T

Name	Start Size [nt]	End Size [nt]	Area	% of total Area
18S	1,558	1,986	352.8	19.0
28S	3,372	4,131	530.1	28.6

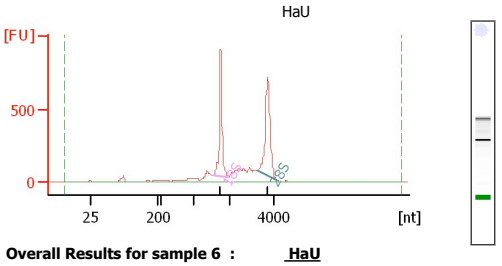

Overall Results for sample 6 : HaU

RNA Area:	4,065.0
RNA Concentration:	1,990 ng/µl
rRNA Ratio [28s / 18s]:	1.2
RNA Integrity Number (RIN):	8.9 (B.02.05)
Result Flagging Color:	
Result Flagging Label:	RIN: 8.90

Fragment table for sample 6 : HaU

Name	Start Size [nt]	End Size [nt]	Area	% of total Area
18S	1,543	1,974	924.8	22.8
28S	3,239	4,165	1,150.2	28.3

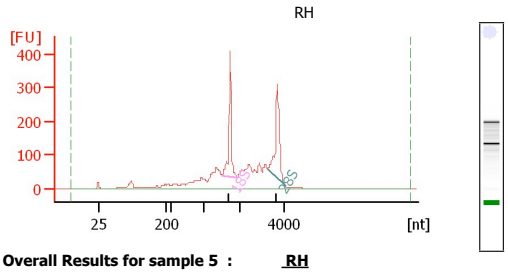

Overall Results for sample 5 : RH

RNA Area:	2,423.8
RNA Concentration:	1,187 ng/µl
rRNA Ratio [28s / 18s]:	1.1
RNA Integrity Number (RIN):	7.3 (B.02.05)
Result Flagging Color:	
Result Flagging Label:	RIN: 7.30

Fragment table for sample 5 : RH

Name	Start Size [nt]	End Size [nt]	Area	% of total Area
18S	1,521	1,930	356.2	14.7
28S	3,267	4,049	382.6	15.8

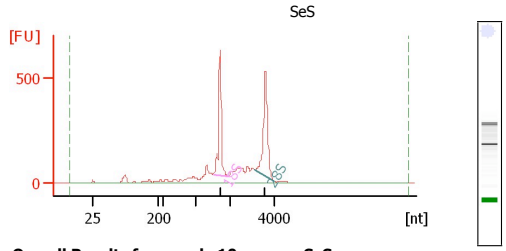

Overall Results for sample 10 : SeS

RNA Area:	3,114.1
RNA Concentration:	1,525 ng/µl
rRNA Ratio [28s / 18s]:	1.2
RNA Integrity Number (RIN):	8.2 (B.02.05)
Result Flagging Color:	
Result Flagging Label:	RIN: 8.20

Fragment table for sample 10 : SeS

Name	Start Size [nt]	End Size [nt]	Area	% of total Area
18S	1,513	1,943	599.9	19.3
28S	3,167	4,017	747.0	24.0

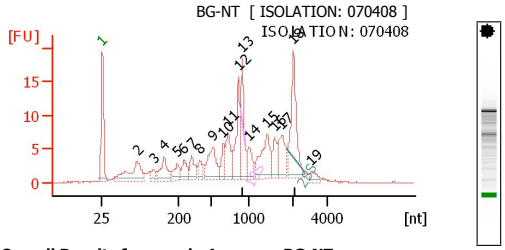

Overall Results for sample 4 : BG-NT

RNA Area:	282.6
RNA Concentration:	258 ng/µl
rRNA Ratio [28s / 18s]:	3.3
RNA Integrity Number (RIN):	4.9 (B.02.05)
Result Flagging Color:	
Result Flagging Label:	

Fragment table for sample 4 : BG-NT

Name	Start Size [nt]	End Size [nt]	Area	% of total Area
18S	892	962	6.7	2.4
28S	1,856	2,607	22.0	7.8

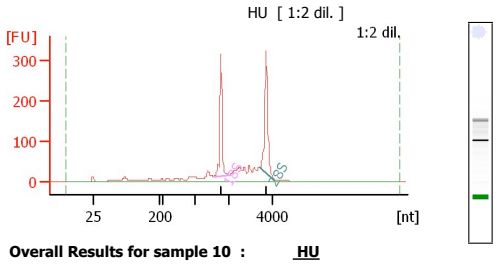

Overall Results for sample 10 : HU

RNA Area:	1,446.8
RNA Concentration:	657 ng/µl
rRNA Ratio [28s / 18s]:	1.2
RNA Integrity Number (RIN):	8.3 (B.02.05)
Result Flagging Color:	
Result Flagging Label:	RIN: 8.30

Fragment table for sample 10 : HU

Name	Start Size [nt]	End Size [nt]	Area	% of total Area
18S	1,549	1,976	262.6	18.2
28S	3,387	4,069	323.5	22.4

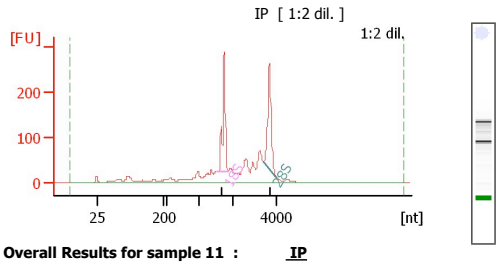

Overall Results for sample 11 : IP

RNA Area:	1,676.1
RNA Concentration:	761 ng/µl
rRNA Ratio [28s / 18s]:	1.0
RNA Integrity Number (RIN):	7.8 (B.02.05)
Result Flagging Color:	
Result Flagging Label:	RIN: 7.80

Fragment table for sample 11 : IP

Name	Start Size [nt]	End Size [nt]	Area	% of total Area
18S	1,556	1,868	281.4	16.8
28S	3,404	4,025	280.3	16.7

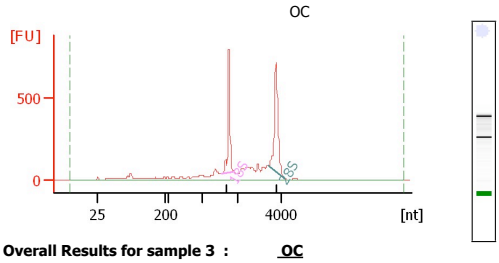

Overall Results for sample 3 : OC

RNA Area:	3,740.5
RNA Concentration:	1,832 ng/µl
rRNA Ratio [28s / 18s]:	1.3
RNA Integrity Number (RIN):	8.2 (B.02.05)
Result Flagging Color:	
Result Flagging Label:	RIN: 8.20

Fragment table for sample 3 : OC

Name	Start Size [nt]	End Size [nt]	Area	% of total Area
18S	1,556	1,868	642.3	17.2
28S	3,417	4,118	814.2	21.8

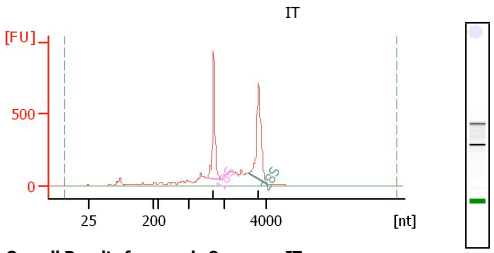

Overall Results for sample 8 : IT

RNA Area:	4,287.5
RNA Concentration:	2,099 ng/µl
rRNA Ratio [28s / 18s]:	1.2
RNA Integrity Number (RIN):	8.4 (B.02.05)
Result Flagging Color:	
Result Flagging Label:	RIN: 8.40

Fragment table for sample 8 : IT

Name	Start Size [nt]	End Size [nt]	Area	% of total Area
18S	1,510	1,937	855.4	20.0
28S	3,134	4,025	1,060.2	24.7

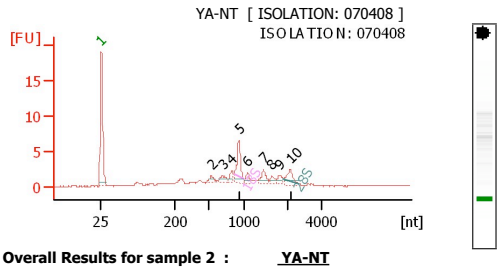

Overall Results for sample 2 : YA-NT

RNA Area:	56.6
RNA Concentration:	52 ng/µl
rRNA Ratio [28s / 18s]:	0.5
RNA Integrity Number (RIN):	6.8 (B.02.05)
Result Flagging Color:	
Result Flagging Label:	

Fragment table for sample 2 : YA-NT

Name	Start Size [nt]	End Size [nt]	Area	% of total Area
18S	864	1,001	5.9	10.5
28S	1,898	2,628	2.9	5.1

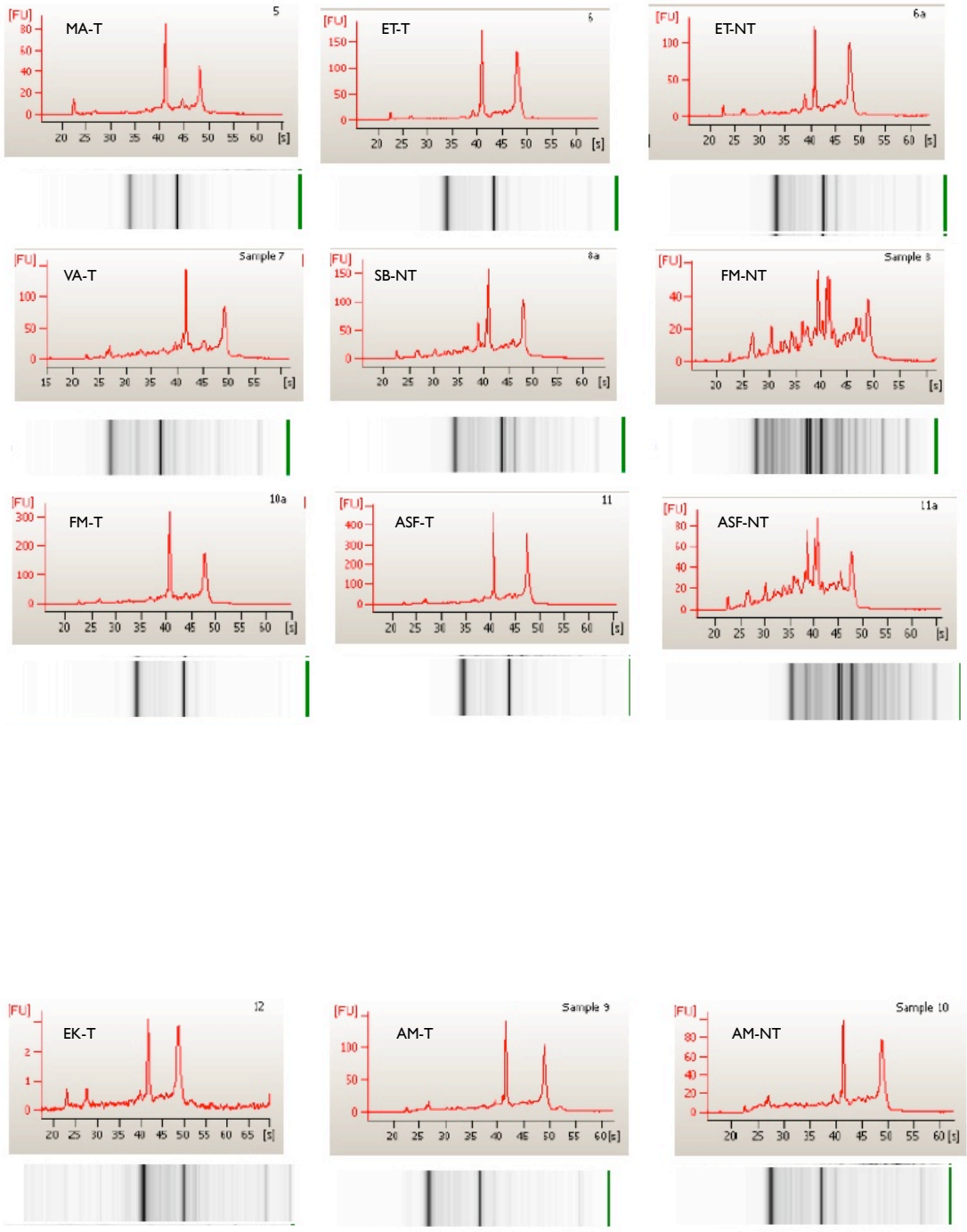

Figure A.2: Agilent Bioanalyzer plots of the samples that were included in microarray experiments

HK

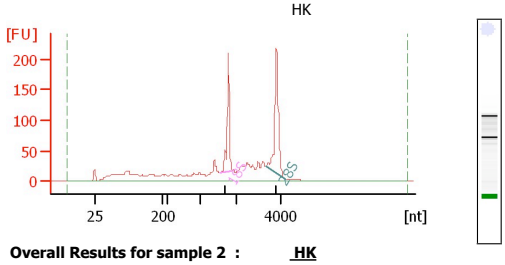

Overall Results for sample 2 : HK

RNA Area:	1,439.7
RNA Concentration:	705 ng/µl
rRNA Ratio [28s / 18s]:	1.5
RNA Integrity Number (RIN):	7.4 (B.02.05)
Result Flagging Color:	
Result Flagging Label:	RIN: 7.40

Fragment table for sample 2 : HK

Name	Start Size [nt]	End Size [nt]	Area	% of total Area
18S	1,561	1,884	173.5	12.1
28S	3,297	4,185	251.7	17.5

KaK [1:10 dil.]

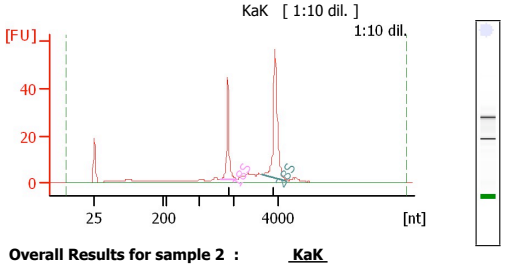

Overall Results for sample 2 : KaK

RNA Area:	227.1
RNA Concentration:	103 ng/µl
rRNA Ratio [28s / 18s]:	1.9
RNA Integrity Number (RIN):	9.1 (B.02.05)
Result Flagging Color:	
Result Flagging Label:	RIN: 9.10

Fragment table for sample 2 : KaK

Name	Start Size [nt]	End Size [nt]	Area	% of total Area
18S	1,631	2,167	38.4	16.9
28S	3,201	4,342	72.8	32.0

OU

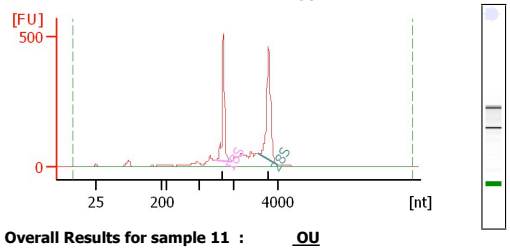

Overall Results for sample 11 : OU

RNA Area:	2,213.5
RNA Concentration:	1,084 ng/µl
rRNA Ratio [28s / 18s]:	1.4
RNA Integrity Number (RIN):	8.8 (B.02.05)
Result Flagging Color:	
Result Flagging Label:	RIN: 8.80

Fragment table for sample 11 : OU

Name	Start Size [nt]	End Size [nt]	Area	% of total Area
18S	1,503	1,923	465.0	21.0
28S	3,104	4,001	639.3	28.9

281207-NT

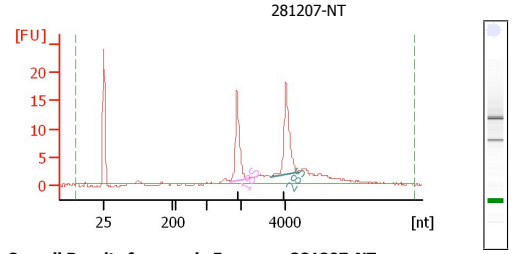

Overall Results for sample 5 : 281207-NT

RNA Area:	112.8
RNA Concentration:	153 ng/µl
rRNA Ratio [28s / 18s]:	1.1
RNA Integrity Number (RIN):	9.4 (B.02.05)
Result Flagging Color:	
Result Flagging Label:	RIN: 9.40

Fragment table for sample 5 : 281207-NT

Name	Start Size [nt]	End Size [nt]	Area	% of total Area
18S	1,665	2,277	25.1	22.3
28S	3,347	4,590	28.3	25.1

281207-N

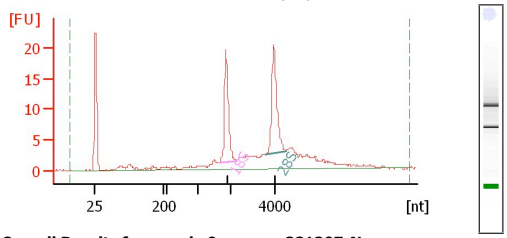

Overall Results for sample 9 : 281207-N

RNA Area:	150.0
RNA Concentration:	203 ng/µl
rRNA Ratio [28s / 18s]:	1.1
RNA Integrity Number (RIN):	9.2 (B.02.05)
Result Flagging Color:	
Result Flagging Label:	RIN: 9.20

Fragment table for sample 9 : 281207-N

Name	Start Size [nt]	End Size [nt]	Area	% of total Area
18S	1,640	2,265	28.2	18.8
28S	3,575	4,533	30.7	20.5

MB-N

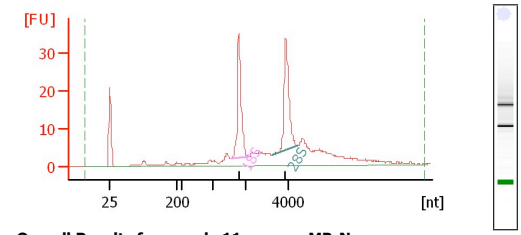

Overall Results for sample 11 : MB-N

RNA Area:	261.4
RNA Concentration:	354 ng/µl
rRNA Ratio [28s / 18s]:	1.0
RNA Integrity Number (RIN):	9.0 (B.02.05)
Result Flagging Color:	
Result Flagging Label:	RIN:9

Fragment table for sample 11 : MB-N

Name	Start Size [nt]	End Size [nt]	Area	% of total Area
18S	1,556	2,119	50.9	19.5
28S	3,239	4,440	49.8	19.1

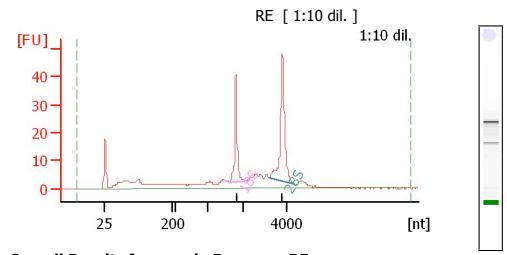

Overall Results for sample 5 : RE

RNA Area:	279.1
RNA Concentration:	127 ng/µl
rRNA Ratio [28s / 18s]:	1.7
RNA Integrity Number (RIN):	8.2 (B.02.05)
Result Flagging Color:	
Result Flagging Label:	RIN: 8.20

Fragment table for sample 5 : RE

Name	Start Size [nt]	End Size [nt]	Area	% of total Area
18S	1,623	2,107	37.5	13.4
28S	3,216	4,386	64.2	23.0

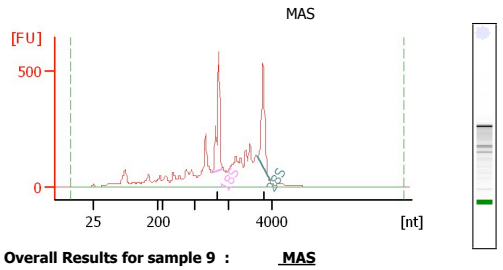

Overall Results for sample 9 : MAS

RNA Area:	4,989.6
RNA Concentration:	2,443 ng/µl
rRNA Ratio [28s / 18s]:	1.0
RNA Integrity Number (RIN):	6.6 (B.02.05)
Result Flagging Color:	
Result Flagging Label:	RIN: 6.60

Fragment table for sample 9 : MAS

Name	Start Size [nt]	End Size [nt]	Area	% of total Area
18S	1,513	1,816	557.5	11.2
28S	3,356	3,923	548.3	11.0

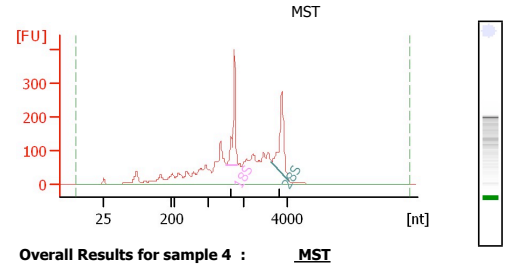

Overall Results for sample 4 : MST

RNA Area:	3,215.2
RNA Concentration:	1,574 ng/µl
rRNA Ratio [28s / 18s]:	1.1
RNA Integrity Number (RIN):	6.5 (B.02.05)
Result Flagging Color:	
Result Flagging Label:	RIN: 6.50

Fragment table for sample 4 : MST

Name	Start Size [nt]	End Size [nt]	Area	% of total Area
18S	1,518	1,849	335.3	10.4
28S	3,265	4,073	361.1	11.2

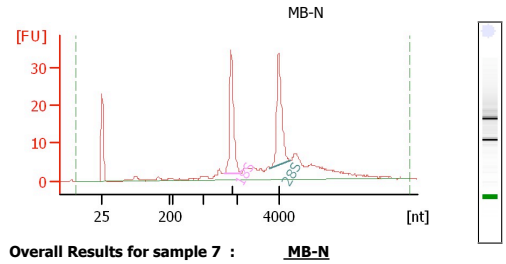

Overall Results for sample 7 : MB-N

RNA Area:	247.2
RNA Concentration:	334 ng/µl
rRNA Ratio [28s / 18s]:	1.0
RNA Integrity Number (RIN):	9.3 (B.02.05)
Result Flagging Color:	
Result Flagging Label:	RIN: 9.30

Fragment table for sample 7 : MB-N

Name	Start Size [nt]	End Size [nt]	Area	% of total Area
18S	1,616	2,206	51.0	20.6
28S	3,540	4,508	49.2	19.9

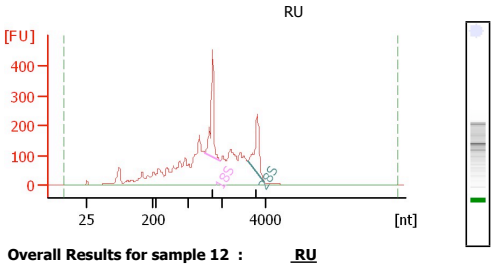

Overall Results for sample 12 : RU

RNA Area:	4,318.2
RNA Concentration:	2,114 ng/µl
rRNA Ratio [28s / 18s]:	0.8
RNA Integrity Number (RIN):	5.9 (B.02.05)
Result Flagging Color:	
Result Flagging Label:	RIN: 5.90

Fragment table for sample 12 : RU

Name	Start Size [nt]	End Size [nt]	Area	% of total Area
18S	1,486	1,925	398.0	9.2
28S	3,151	3,936	331.1	7.7

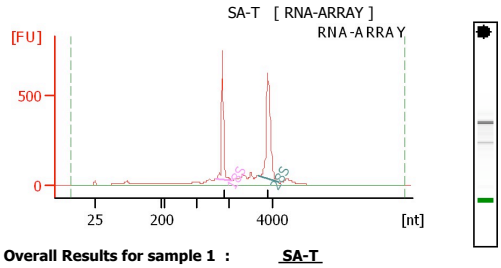

Overall Results for sample 1 : SA-T

RNA Area:	2,908.9
RNA Concentration:	1,895 ng/µl
rRNA Ratio [28s / 18s]:	1.4
RNA Integrity Number (RIN):	9.0 (B.02.05)
Result Flagging Color:	
Result Flagging Label:	

Fragment table for sample 1 : SA-T

Name	Start Size [nt]	End Size [nt]	Area	% of total Area
18S	1,599	2,116	607.6	20.9
28S	3,305	4,306	859.2	29.5

Figure A.3: Agilent Bioanalyzer plots of RNA samples that are saved for future experiments

A.2.3 RIN values of the samples with low RNA quality

Samples with low RIN value (< 4) or with highly degraded RNA plots were not included in the microarray analysis. These plots are shown in Figures A.4.

A.3 MA-plots

Representative MA-plots of microarray experiments are given in Figure A.5.

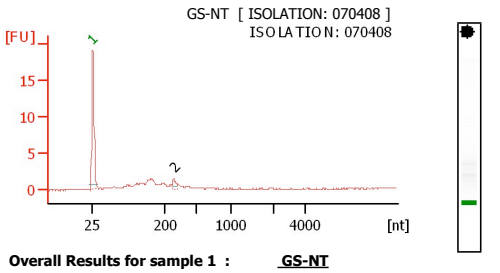

Overall Results for sample 1 : GS-NT

RNA Area:	28.5
RNA Concentration:	26 ng/µl
rRNA Ratio [28s / 18s]:	0.0
RNA Integrity Number (RIN):	1.1 (B.02.05)
Result Flagging Color:	
Result Flagging Label:	

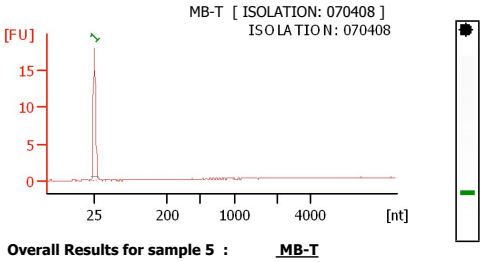

Overall Results for sample 5 : MB-T

RNA Area:	5.7
RNA Concentration:	5 ng/µl
rRNA Ratio [28s / 18s]:	0.0
RNA Integrity Number (RIN):	N/A (B.02.05)
Result Flagging Color:	
Result Flagging Label:	

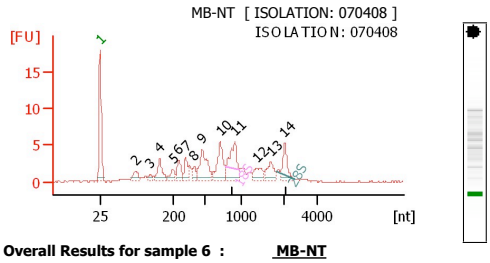

Overall Results for sample 6 : MB-NT

RNA Area:	116.4
RNA Concentration:	106 ng/µl
rRNA Ratio [28s / 18s]:	0.8
RNA Integrity Number (RIN):	6.2 (B.02.05)
Result Flagging Color:	
Result Flagging Label:	

Fragment table for sample 6 : MB-NT

Name	Start Size [nt]	End Size [nt]	Area	% of total Area
18S	786	983	7.8	6.7
28S	1,812	2,640	5.9	5.0

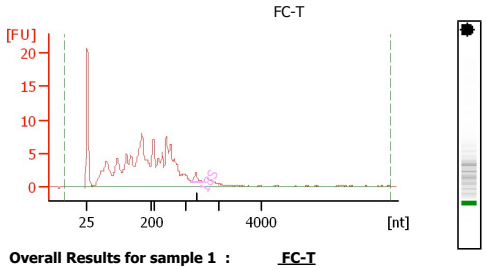

Overall Results for sample 1 : FC-T

RNA Area:	175.6
RNA Concentration:	87 ng/µl
rRNA Ratio [28s / 18s]:	0.0
RNA Integrity Number (RIN):	2.7 (B.02.05)
Result Flagging Color:	
Result Flagging Label:	

Fragment table for sample 1 : FC-T

Name	Start Size [nt]	End Size [nt]	Area	% of total Area
18S	1,170	1,522	2.1	1.2

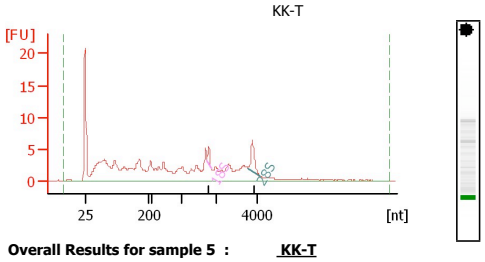

Overall Results for sample 5 : KK-T

RNA Area:	164.5
RNA Concentration:	82 ng/µl
rRNA Ratio [28s / 18s]:	3.7
RNA Integrity Number (RIN):	3.7 (B.02.05)
Result Flagging Color:	
Result Flagging Label:	

Fragment table for sample 5 : KK-T

Name	Start Size [nt]	End Size [nt]	Area	% of total Area
18S	1,749	1,868	1.7	1.0
28S	3,560	4,151	6.4	3.9

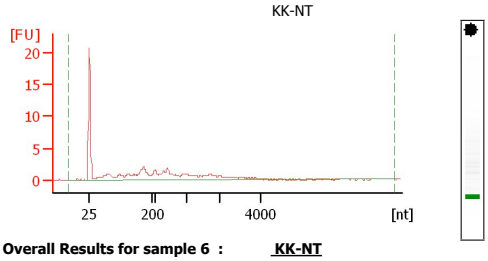

Overall Results for sample 6 : KK-NT

RNA Area:	52.6
RNA Concentration:	26 ng/µl
rRNA Ratio [28s / 18s]:	0.0
RNA Integrity Number (RIN):	1.1 (B.02.05)
Result Flagging Color:	
Result Flagging Label:	

IA-NT [ISOLATION: 070408]
ISOLATION: 070408

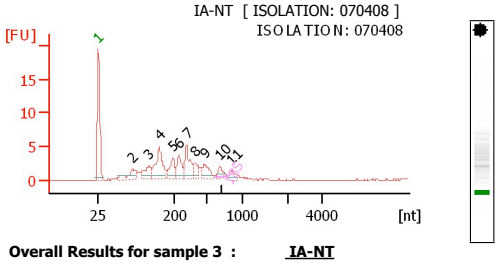

Overall Results for sample 3 : IA-NT

RNA Area:	91.3
RNA Concentration:	83 ng/µl
rRNA Ratio [28s / 18s]:	0.0
RNA Integrity Number (RIN):	3.1 (B.02.05)
Result Flagging Color:	
Result Flagging Label:	

Fragment table for sample 3 : IA-NT

Name	Start Size [nt]	End Size [nt]	Area	% of total Area
18S	610	806	2.5	2.8

SS-NT

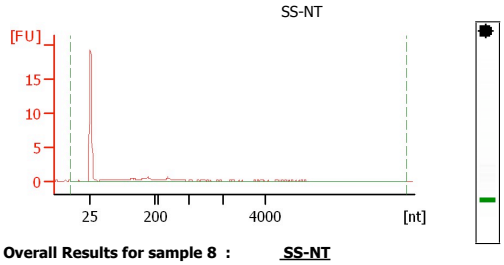

Overall Results for sample 8 : SS-NT

RNA Area:	11.4
RNA Concentration:	6 ng/µl
rRNA Ratio [28s / 18s]:	0.0
RNA Integrity Number (RIN):	N/A (B.02.05)
Result Flagging Color:	
Result Flagging Label:	

FC-NT

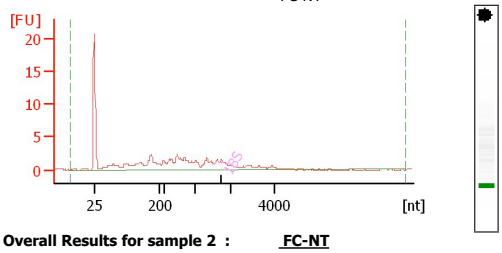

Overall Results for sample 2 : FC-NT

RNA Area:	65.3
RNA Concentration:	32 ng/µl
rRNA Ratio [28s / 18s]:	0.0
RNA Integrity Number (RIN):	2.1 (B.02.05)
Result Flagging Color:	
Result Flagging Label:	

Fragment table for sample 2 : FC-NT

Name	Start Size [nt]	End Size [nt]	Area	% of total Area
18S	1,673	1,789	0.3	0.5

GS-T

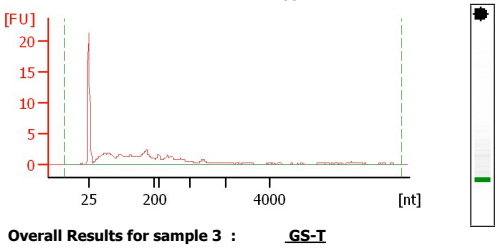

Overall Results for sample 3 : GS-T

RNA Area:	68.4
RNA Concentration:	34 ng/µl
rRNA Ratio [28s / 18s]:	0.0
RNA Integrity Number (RIN):	1.7 (B.02.05)
Result Flagging Color:	
Result Flagging Label:	

SS-T

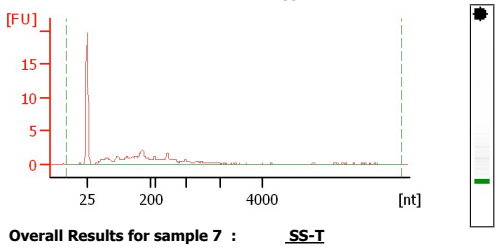

Overall Results for sample 7 : SS-T

RNA Area:	44.1
RNA Concentration:	22 ng/µl
rRNA Ratio [28s / 18s]:	0.0
RNA Integrity Number (RIN):	1.2 (B.02.05)
Result Flagging Color:	
Result Flagging Label:	

CO [1:2 dil.]

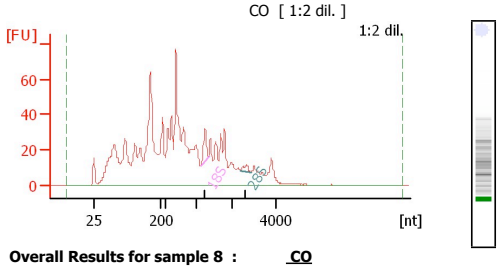

Overall Results for sample 8 : CO

RNA Area:	1,367.3
RNA Concentration:	621 ng/µl
rRNA Ratio [28s / 18s]:	0.3
RNA Integrity Number (RIN):	3.9 (B.02.05)
Result Flagging Color:	
Result Flagging Label:	RIN: 3.90

Fragment table for sample 8 : CO

Name	Start Size [nt]	End Size [nt]	Area	% of total Area
18S	1,114	1,337	22.5	1.6
28S	2,413	2,877	6.0	0.4

SO-T

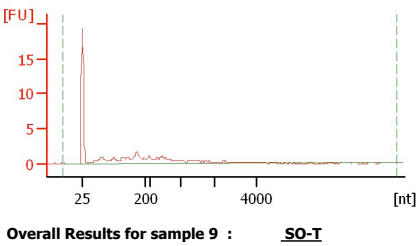

Overall Results for sample 9 : SO-T

RNA Area:	33.6
RNA Concentration:	17 ng/µl
rRNA Ratio [28s / 18s]:	0.0
RNA Integrity Number (RIN):	1.0 (B.02.05)
Result Flagging Color:	
Result Flagging Label:	

HY-NT

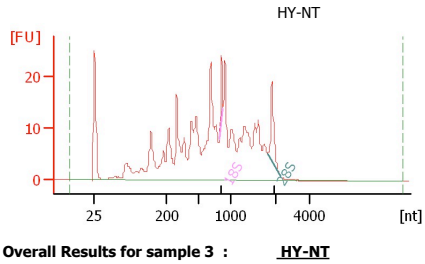

Overall Results for sample 3 : HY-NT

RNA Area:	421.1
RNA Concentration:	1,805 ng/µl
rRNA Ratio [28s / 18s]:	2.4
RNA Integrity Number (RIN):	4.0 (B.02.05)
Result Flagging Color:	
Result Flagging Label:	

Fragment table for sample 3 : HY-NT

Name	Start Size [nt]	End Size [nt]	Area	% of total Area
18S	827	878	6.6	1.6
28S	1,818	2,286	16.0	3.8

281207-T

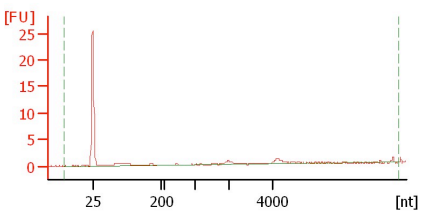

Overall Results for sample 4 : 281207-T

RNA Area:	9.0
RNA Concentration:	12 ng/µl
rRNA Ratio [28s / 18s]:	0.0
RNA Integrity Number (RIN):	8.1 (B.02.05)
Result Flagging Color:	
Result Flagging Label:	RIN: 8.10

HY-N [RNA-ARRAY]

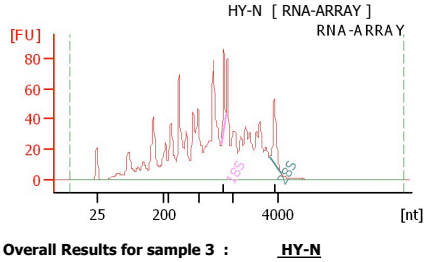

Overall Results for sample 3 : HY-N

RNA Area:	1,503.5
RNA Concentration:	979 ng/µl
rRNA Ratio [28s / 18s]:	1.6
RNA Integrity Number (RIN):	3.7 (B.02.05)
Result Flagging Color:	
Result Flagging Label:	

Fragment table for sample 3 : HY-N

Name	Start Size [nt]	End Size [nt]	Area	% of total Area
18S	1,646	1,766	28.4	1.9
28S	3,622	4,176	46.1	3.1

EK-NT

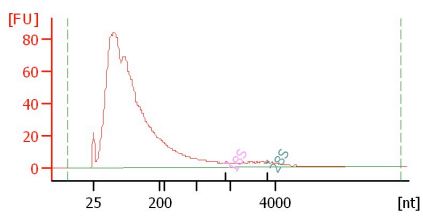

Overall Results for sample 1 : EK-NT

RNA Area:	1,796.9
RNA Concentration:	880 ng/µl
rRNA Ratio [28s / 18s]:	1.5
RNA Integrity Number (RIN):	2.3 (B.02.05)
Result Flagging Color:	
Result Flagging Label:	RIN: 2.30

Fragment table for sample 1 : EK-NT

Name	Start Size [nt]	End Size [nt]	Area	% of total Area
18S	1,801	1,916	0.3	0.0
28S	3,594	3,702	0.4	0.0

HG

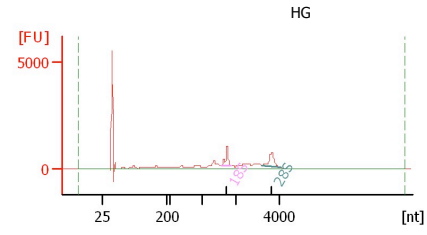

Overall Results for sample 7 : HG

RNA Area:	14,054.0
RNA Concentration:	6,882 ng/µl
rRNA Ratio [28s / 18s]:	1.1
RNA Integrity Number (RIN):	8.0 (B.02.05)
Result Flagging Color:	
Result Flagging Label:	RIN:8

Fragment table for sample 7 : HG

Name	Start Size [nt]	End Size [nt]	Area	% of total Area
18S	1,546	1,825	978.0	7.0
28S	3,194	4,065	1,123.1	8.0

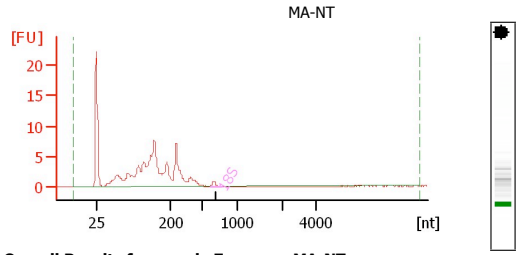

Overall Results for sample 7 : MA-NT

RNA Area:	101.2
RNA Concentration:	434 ng/µl
rRNA Ratio [28s / 18s]:	0.0
RNA Integrity Number (RIN):	2.6 (B.02.05)
Result Flagging Color:	
Result Flagging Label:	

Fragment table for sample 7 : MA-NT

Name	Start Size [nt]	End Size [nt]	Area	% of total Area
18S	611	790	1.1	1.1

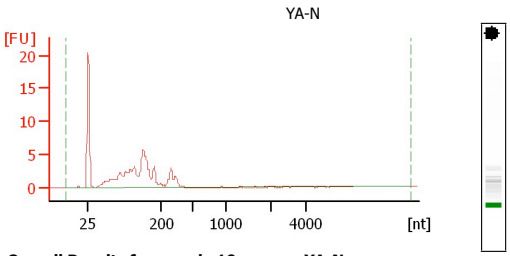

Overall Results for sample 10 : YA-N

RNA Area:	68.9
RNA Concentration:	295 ng/µl
rRNA Ratio [28s / 18s]:	0.0
RNA Integrity Number (RIN):	2.2 (B.02.05)
Result Flagging Color:	
Result Flagging Label:	

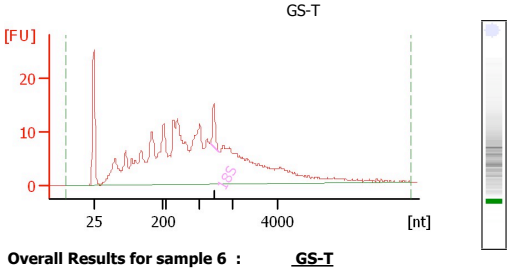

Overall Results for sample 6 : GS-T

RNA Area:	426.6
RNA Concentration:	577 ng/µl
rRNA Ratio [28s / 18s]:	0.0
RNA Integrity Number (RIN):	3.3 (B.02.05)
Result Flagging Color:	
Result Flagging Label:	RIN: 3.30

Fragment table for sample 6 : GS-T

Name	Start Size [nt]	End Size [nt]	Area	% of total Area
18S	1,339	1,591	9.4	2.2

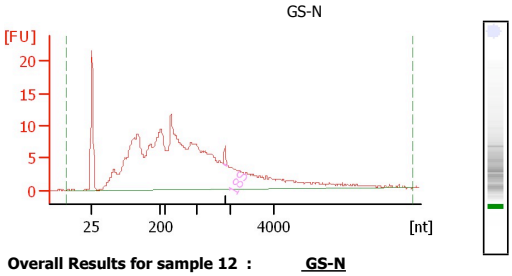

Overall Results for sample 12 : GS-N

RNA Area:	362.0
RNA Concentration:	490 ng/µl
rRNA Ratio [28s / 18s]:	0.0
RNA Integrity Number (RIN):	3.1 (B.02.05)
Result Flagging Color:	
Result Flagging Label:	RIN: 3.10

Fragment table for sample 12 : GS-N

Name	Start Size [nt]	End Size [nt]	Area	% of total Area
18S	1,780	1,902	1.7	0.5

Figure A.4: Agilent Bioanalyzer plots of RNA samples with low quality. These samples were not included in microarray experiments

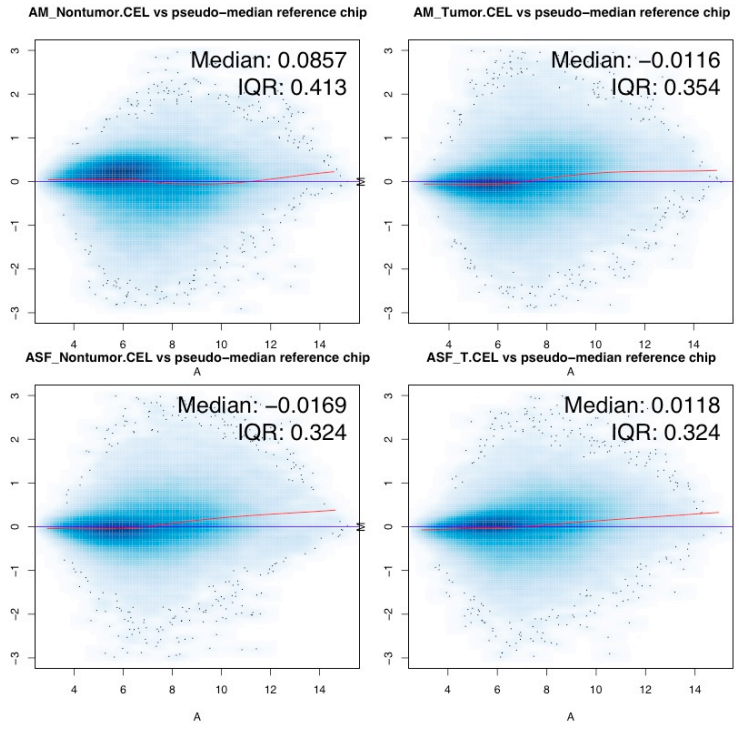
AM_Nontumor.CEL vs pseudo−median reference chip
Median: 0.0857
IQR: 0.413
AM_Tumor.CEL vs pseudo−median reference chip
Median: −0.0116
IQR: 0.354
ASF_Nontumor.CEL vs pseudo−median reference chip
Median: −0.0169
IQR: 0.324
ASF_T.CEL vs pseudo−median reference chip
Median: 0.0118
IQR: 0.324
M
A

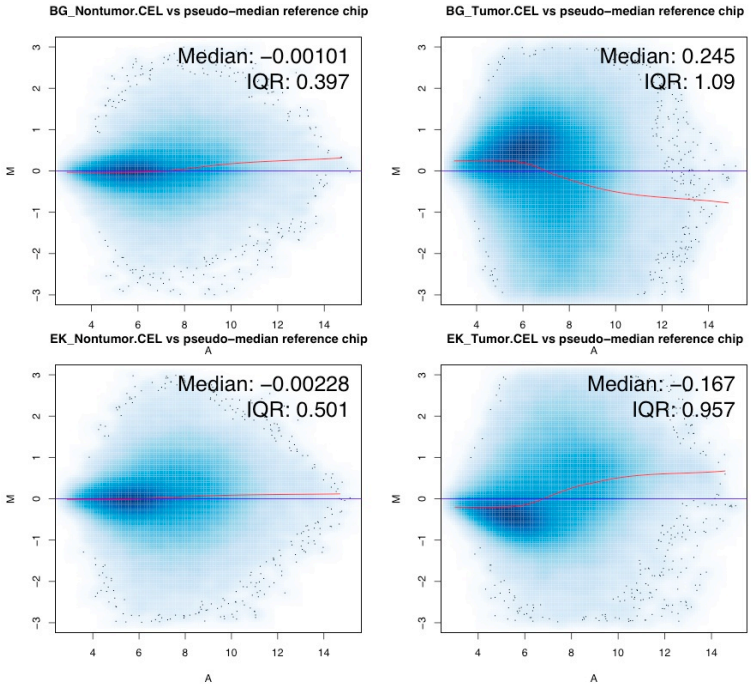
BG_Nontumor.CEL vs pseudo−median reference chip
Median: −0.00101
IQR: 0.397
BG_Tumor.CEL vs pseudo−median reference chip
Median: 0.245
IQR: 1.09
EK_Nontumor.CEL vs pseudo−median reference chip
Median: −0.00228
IQR: 0.501
EK_Tumor.CEL vs pseudo−median reference chip
Median: −0.167
IQR: 0.957
M
A

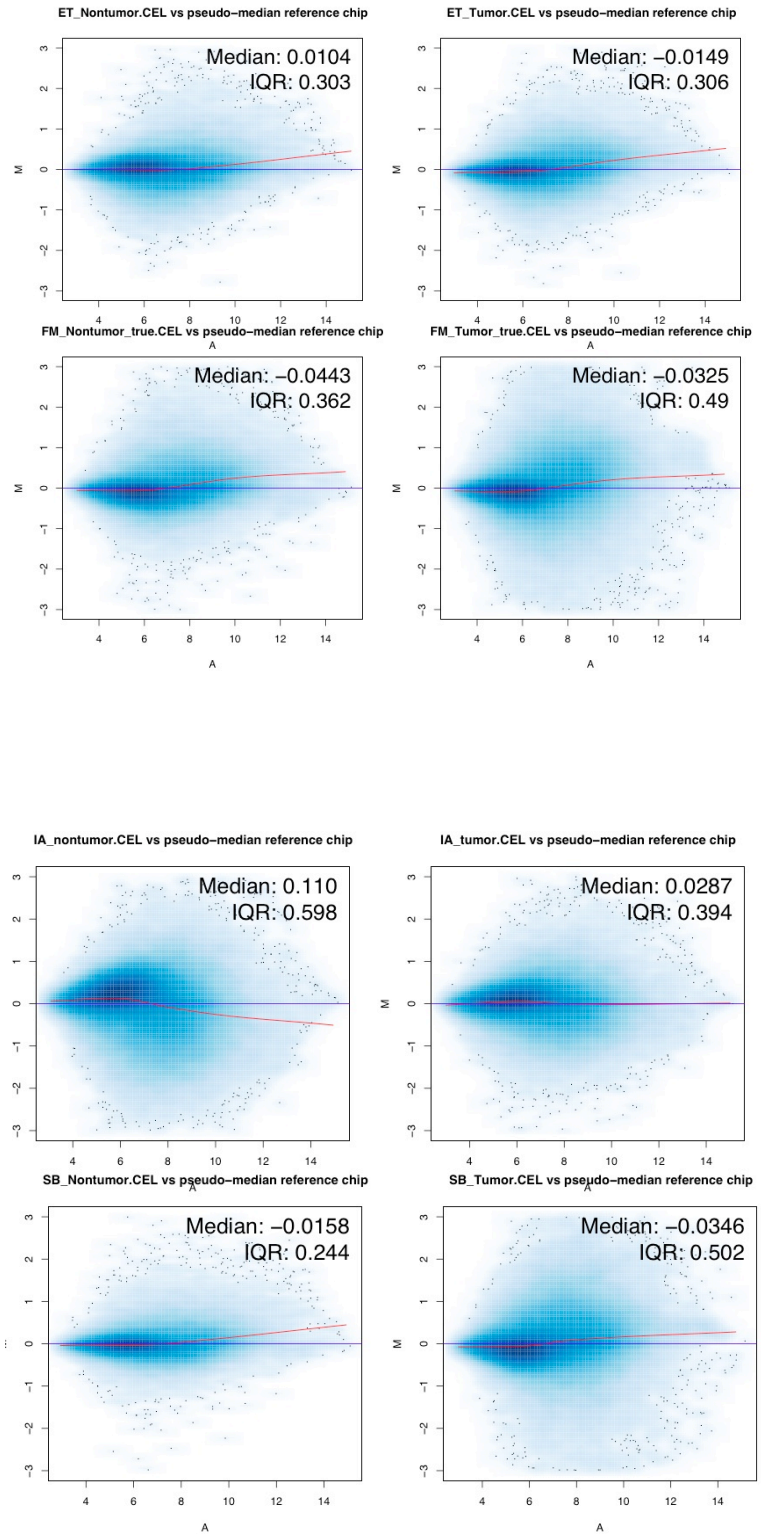

Figure A.5: MA-plots of tissues

Cancer Letters xxx (2008) xxx–xxx

Contents lists available at ScienceDirect

Cancer Letters

journal homepage: www.elsevier.com/locate/canlet

Mini-review

Senescence and immortality in hepatocellular carcinoma

Mehmet Ozturk [a,b,*], Ayca Arslan-Ergul [a], Sevgi Bagislar [a,b], Serif Senturk [a], Haluk Yuzugullu [a,b]

[a] Department of Molecular Biology and Genetics, Bilkent University, 06800 Ankara, Turkey
[b] Centre de Recherche INSERM-Université Joseph Fourrier U823, Institut Albert Bonniot, 38042 Grenoble, France

ARTICLE INFO

Article history:
Received 26 March 2008
Received in revised form 23 June 2008
Accepted 29 October 2008
Available online xxxx

Keywords:
Liver cancer
Senescence
Telomeres
DNA damage
p53
$p16^{INK4a}$
$p21^{Cip1}$
Retinoblastoma
Cirrhosis
Hepatocytes
Telomerase reverse transcriptase

ABSTRACT

Cellular senescence is a process leading to terminal growth arrest with characteristic morphological features. This process is mediated by telomere-dependent, oncogene-induced and ROS-induced pathways, but persistent DNA damage is the most common cause. Senescence arrest is mediated by $p16^{INK4a}$- and $p21^{Cip1}$-dependent pathways both leading to retinoblastoma protein (pRb) activation. p53 plays a relay role between DNA damage sensing and $p21^{Cip1}$ activation. pRb arrests the cell cycle by recruiting proliferation genes to facultative heterochromatin for permanent silencing. Replicative senescence that occurs in hepatocytes in culture and in liver cirrhosis is associated with lack of telomerase activity and results in telomere shortening. Hepatocellular carcinoma (HCC) cells display inactivating mutations of p53 and epigenetic silencing of $p16^{INK4a}$. Moreover, they re-express telomerase reverse transcriptase required for telomere maintenance. Thus, senescence bypass and cellular immortality is likely to contribute significantly to HCC development. Oncogene-induced senescence in premalignant lesions and reversible immortality of cancer cells including HCC offer new potentials for tumor prevention and treatment.

1. Introduction

Senescence is an evolutionary term meaning "the process of becoming old"; the phase from full maturity to death characterized by accumulation of metabolic products and decreased probability of reproduction or survival [1]. The term "cellular senescence" was initially used by Hayflick and colleagues to define cells that ceased to divide in culture [2]. Today, cellular senescence is recognized as a response of proliferating somatic cells to stress and damage from exogenous and endogenous sources. It is characterized by permanent cell cycle arrest. Senescent cells also display altered morphology and an altered pattern of gene expression, and can be recognized by the presence of senescence markers such as senescence-associated β-galactosidase (SABG), $p16^{INK4A}$, senescence-associated DNA-damage foci and senescence-associated heterochromatin foci (for a review see Ref. [3]). This cellular response has both beneficial (anti-cancer) and probably deleterious (such as tissue aging) effects on the organism. Most of our knowledge of cellular senescence is derived from in vitro studies performed with fibroblasts, and some epithelial cells such as mammary epithelial cells. Animal models are increasingly being used to study cellular senescence in vivo. Telomerase-deficient mouse models lacking RNA subunit (TERC−/−) have been very useful in demonstrating the critical role of telomeres in organ aging and tumor susceptibility [4]. Other mouse models including tumor suppressor gene-deficient and oncogene-expressing mice were also used extensively.

Compared to other tissues and cancer models, the role of senescence in liver cells and its implications in hepatocellular carcinogenesis have been less explored. One of

* Corresponding author. Address: Centre de Recherche INSERM-Université Joseph Fourrier U823, Institut Albert Bonniot, Grenoble 38000, France. Tel.: +33 (0) 4 76 54 94 10; fax: +33 (0) 4 76 54 94 54.
E-mail address: ozturkm@ujf-grenoble.fr (M. Ozturk).

0304-3835/$ - see front matter © 2008 Elsevier Ireland Ltd. All rights reserved.
doi:10.1016/j.canlet.2008.10.048

the main obstacles is the lack of adequate in vitro systems. As hepatocytes can not divide in cell culture, the study of their replicative senescence mechanisms is not easy. Nevertheless, these cells are able to quit their quiescent state in vivo and proliferate massively in response to partial hepatectomy or liver injury [5]. This capacity can be explored to study in vivo senescence of hepatocytes using rodent models. Studies with clinical samples indicate that hepatocyte senescence occurs in vivo in patients with chronic hepatitis, cirrhosis and HCC [6–8]. In contrast to the paucity of studies directly addressing cellular senescence, the critical role of telomere shortening (as a feature associated with replicative senescence) in cirrhosis and HCC development is well established [9]. Telomeres in normal liver show a consistent but slow shortening during aging. In contrast, hepatocyte DNA telomere shortening is accelerated in patients with chronic liver disease with shortest telomeres described in cirrhotic liver and HCC. Telomerase-deficient mice have also been used elegantly to demonstrate the critical roles of telomerase and telomeres in liver regeneration and experimentally induced cirrhosis [10,11]. A major accomplishment in recent years was the demonstration of critical role played by senescence for the clearance of ras-induced murine liver carcinomas following p53 restoration [12].

Despite a relatively important progress, the mechanisms of hepatocellular senescence and the role of cellular immortality in HCC remain ill-known issues. As one of the rare tissues with ample clinical data on senescence-related aberrations, liver may serve as an excellent model to further explore the relevance of cellular senescence in human biology. Moreover, a better understanding of senescence and immortality in hepatic tissues may help to develop new preventive and therapeutic approaches for severe liver diseases such as cirrhosis and HCC. Here we will review recent progress on senescence and immortality mechanisms with a specific emphasis on hepatocellular carcinogenesis.

2. Senescence pathways

Cellular senescence has long been considered as a mechanism that limits the number of cell divisions (or population doublings) in response to progressive telomere shortening. Most human somatic cells are telomerase-deficient because of the repression of telomerase reverse transcriptase (TERT) expression. Therefore, proliferating somatic cells undergo progressive telomere DNA erosion as a function of their number of cell divisions. This form of senescence is now called as replicative or telomere-dependent senescence (Fig. 1).

Human chromosome telomere ends are composed of TTAGGG repeats (5–20 kb) in a DNA-protein complex formed by six telomere-specific proteins, called "shelterin" [13]. Telomeric DNA has a structure called "t-loop" which is formed as a result of invasion of the single stranded G-rich sequence into the double-stranded telomeric tract. Since the 1930s, it has been known that telomeres, with telomere-binding proteins, prevent genomic instability and the loss of essential genetic information by "capping" chromosome ends. They are also indispensable for proper recombination and chromosomal segregation during cell division. Telomeres become shorter with every cell division in somatic cells, because of replication complex's inability to copy the ends of linear DNA, which also makes them a "cell cycle counter" for the cell [14]. Telomeres are added to the end of chromosomes with a complex containing the RNA template TERC and the reverse transcriptase TERT [15]. Most somatic cells lack telomerase activity because the expression of TERT is repressed, in contrast to TERC expression. The lack of sufficient TERT expression in somatic cells is the main cause of telomere shortening during cell replication. This telomerase activity also helps to maintain telomere integrity by telomere capping [15].

The loss of telomeres has long been considered to be the critical signal for senescence induction. It is now well known that telomere-dependent senescence is induced by a change in the protected status of shortened telomeres, whereby the loss of telomere DNA contributes to this change [16]. The loss of telomere protection or any other cause of telomere dysfunction results in inappropriate chromosomal end-to-end fusions through non-homologous end joining or homologous recombination DNA repair pathways [17]. These DNA repair pathways are used principally to repair double-strand DNA breaks (DSBs). Thus, it is highly likely that the open-ended telomere DNA is sensed as a DSB by the cell machinery when telomere structure becomes dysfunctional. Accordingly, dysfunctional telomeres elicit a potent DSB type DNA damage response by recruiting phosphorylated H2AX, 53BP1, NBS1 and MDC1 [18].

Telomere-dependent senescence is not the only form of senescence. At least two other forms of telomere-independent senescence are presently known: (1) oncogene-induced senescence; and (2) reactive oxygen species (ROS)-induced senescence (Fig. 1).

Oncogene-induced senescence had initially been identified as a response to expression of Ras oncogene in normal cells ([19], for a recent review see [20]). The expression of oncogenic Ras in primary human or rodent cells results in permanent G1 arrest. The arrest was accompanied by accumulation of p53 and $p16^{INK4a}$, and was phenotypically indistinguishable from cellular senescence. This landmark observation suggested that the onset of cellular senescence does not simply reflect the accumulation of cell divisions, but can be prematurely activated in response to an oncogenic stimulus [19]. In 10 years following this important discovery, telomere-independent forms of senescence have become a new focus of extensive research leading to the recognition of senescence as a common form of stress response. Moreover, oncogene-induced senescence is now recognized as a novel mechanism contributing to the cessation of growth of premalignant or benign neoplasms to prevent malignant cancer development [21]. In addition to Ras, other oncogenes including Raf, Mos, Mek, Myc and Cyclin E also induce senescence [20]. Conversely, the loss of PTEN tumor suppressor gene also leads to senescence [22]. Similar to telomere-dependent senescence, oncogene-induced senescence is also primarily a DNA damage response (Fig. 1). Experimental inactivation of DNA damage response abrogates Ras-induced senescence

Please cite this article in press as: M. Ozturk et al., Senescence and immortality in hepatocellular carcinoma, Cancer Lett. (2008), doi:10.1016/j.canlet.2008.10.048

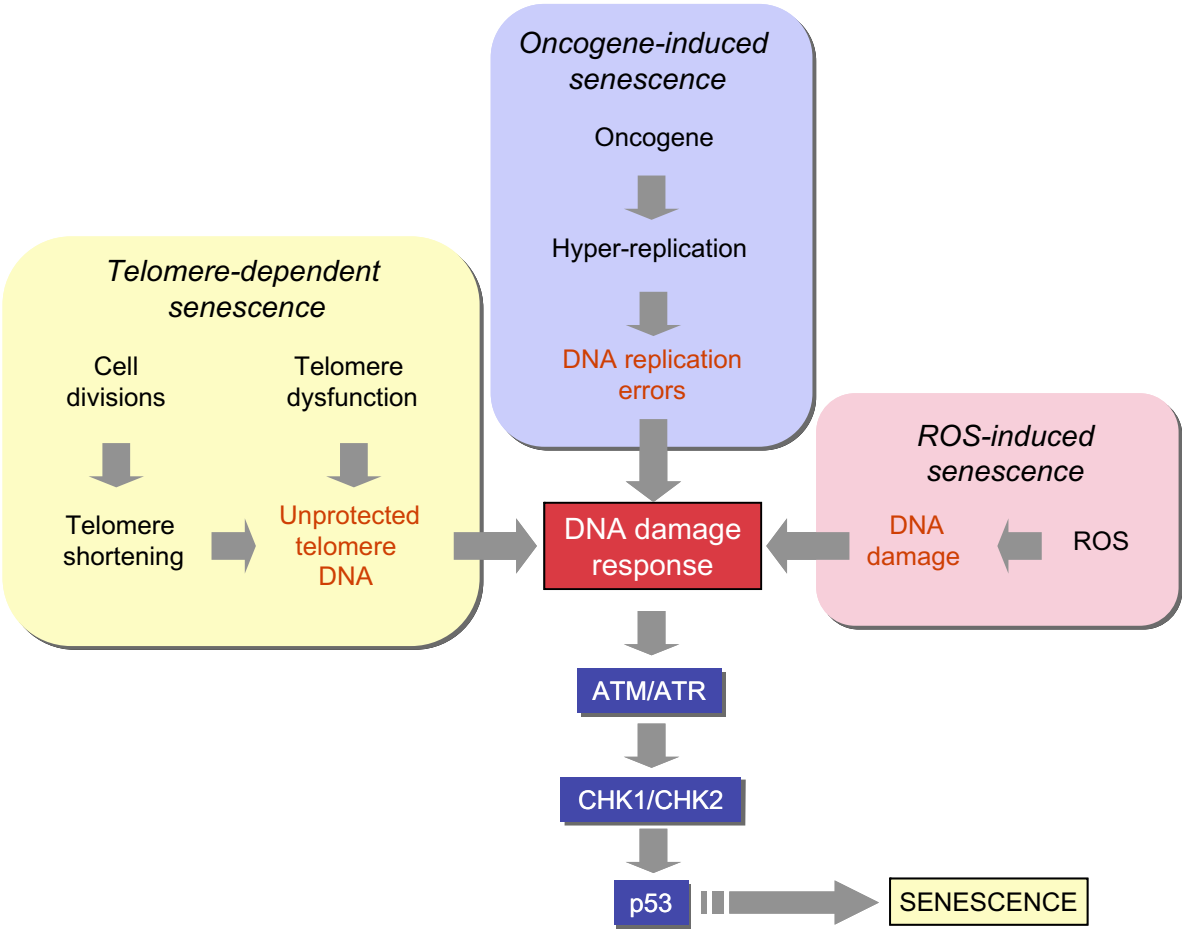

Fig. 1. DNA damage and p53 activation play a central role in different senescence pathways. DNA damage (often in the form of double-strand breaks) activate upstream kinases (ATM and ATR) leading to p53 phosphorylation by CHK1 and CHK2 kinases. Phosphoryated p53 is released from MDM, and stabilized in order to induce senescence arrest or apoptosis (not shown here).

and promotes cell transformation. DNA damage response and oncogene-induced senescence are established following DNA hyper-replication immediately after oncogene expression. Senescent cells arrest with partly replicated DNA, where DNA replication origins have fired multiple times, prematurely terminated DNA replication forks and DNA double-strand breaks are present [23,24].

ROS-induced senescence, the other telomere-independent senescence pathway is gaining importance (for a recent review see Ref. [25]). Mitochondria are the major intracellular sources of ROS which are mainly generated at the respiratory chain. Therefore, ROS have been suspected for many years as cellular metabolites involved in organismal aging [26]. ROS are also generated in the cytoplasm by the NOX family of enzymes [27]. Experimental induction of ROS accumulation in cells (for example by mild H2O2 treatment or glutathione depletion) induces senescence-like growth arrest in different cell types, whereas anti-oxidant treatment can inhibit senescence [25]. More importantly, ROS have been identified as critical mediators of both telomere-dependent and oncogene-induced senescence. Telomere-dependent senescence arrest is accelerated in cells grown under high O_2 conditions. Inversely, cells grown under low O_2 conditions display increased lifespan ([28], see Ref. [25]). ROS also play a critical role in Ras-induced senescence [29,30].

Currently, mechanisms of ROS-induced senescence are not fully understood. It is generally accepted that oxidative stress and ROS eventually cause DNA damage, whereby DNA damage response may contribute to senescence induction. The relationship between mitochondrial dysfunction, ROS, DNA damage and telomere-dependent senescence has recently been demonstrated [31]. However, ROS may also induce modifications in the cellular signaling pathways resulting in senescence arrest. For example, ROS induce senescence in hematopoietic stem cells by activating p38 MAPK [32].

Whether induced by telomere dysfunction, DNA replication stress following oncogene activation, or ROS accumulation, DNA damage is one of the common steps in the generation of senescence arrest via p53 activation (Fig. 1). Upstream checkpoint kinases, such as ATM or ATR are activated in response to DNA damage in the form of double-stand breaks. These kinases phosphorylate

Please cite this article in press as: M. Ozturk et al., Senescence and immortality in hepatocellular carcinoma, Cancer Lett. (2008), doi:10.1016/j.canlet.2008.10.048

downstream factors including CHK1 and CHK2 that in turn phosphorylate p53. Phosphorylation of p53 results in its activation by the displacement of the MDM2 protein. Critical involvement of this p53 activating pathway has been reported for both telomere-dependent [33], and oncogene-induced senescence [34].

Other mechanisms of senescence that are apparently not driven by DNA damage should also be discussed here. Of particular interest is the INK4 locus encoding two inhibitors of cyclin-dependent kinases ($p16^{INK4a}$, $p15^{INK4b}$), and ARF, a p53 regulatory protein (for a review see Ref. [35]). $p16^{INK4a}$ and $p15^{INK4b}$ connect some senescent initiating signals to the retinoblastoma (Rb) pathway, independent of p53 activation. These proteins are easily activated in cell culture and induce senescence arrest. Cells that escape senescence often display inactivation of $p16^{INK4a}$, and sometimes $p15^{INKb}$ and ARF either by homozygous deletion or by shutting-down gene expression. A prominent role for $p16^{INK4a}$ in senescence and tumor suppression in humans has emerged, despite some confusion due to the fact that a relatively small DNA segment encodes the 3 proteins of the INK4 locus. $p16^{INK4a}$ is activated during telomere-dependent and oncogene-induced senescence [19,36]. Moreover, its expression is induced in aging tissues [37]. The mechanisms of regulation of $p16^{INK4a}$ expression are not well known. Although individual components of INK4 locus can respond independently to positively – (for example to Ras) or negatively – (for example c-Myc) acting signals, the entire INK4 locus might be coordinately regulated by epigenetic mechanisms (reviewed in Ref. [35]).

A very recent addition to the list of senescence mechanisms is to be qualified as "senescence induced by secreted proteins". It was reported many years ago that TGF-β is a mediator of oncogene-induced senescence [38]. This mechanism of induction is of particular interest, because it suggests that not only intrinsic cellular factors, but also extracellular or secreted proteins can induce senescence. Recent discovery of several other secreted proteins, including IGFBP7 and IL6 as autocrine/paracrine mediators of oncogene-induced senescence arrest, provide strong support for an extracellularly induced form of senescence [39–41]. This new form of senescence regulation is reminiscent of the so called active apoptosis induction by death ligands. Thus, an active form of cellular senescence induced by "aging ligands" could be a major physiological regulator of tissue/organism aging.

3. Cyclin-dependent inhibitors as common mediators of senescence arrest

We have already stated that senescence and apoptosis share interesting similarities. Another similarity between these cellular processes is the convergence of different pathways in a common place to induce the same cell fate, independent of the initial signal. Similarly to caspase activation, prior to apoptosis induction by different stimuli, most if not all senescence pathways result in the activation of cyclin-dependent kinase inhibitors (CDKIs) in order to induce permanent cell cycle arrest. Senescent cells accumulate at G1 phase of the cell cycle due to an inability to enter into S phase in order to initiate DNA synthesis. The transition of proliferating cells from G1 to S phase requires the release of E2F factors from their inhibitory partner retinoblastoma protein (pRb) following phosphorylation by cyclin-dependent kinases (CDKs), in particular by CDK4/CDK6 and CDK2 at this stage of the cycle [35]. The senescence arrest is mediated by inhibition of pRb phosphorylation by CDK4 and CDK2. The activities of these enzymes are controlled by different mechanisms, but the major proteins involved in the control of senescence arrest are CDKIs. Almost all known CDKIs have been reported to be implicated in senescence arrest, but three of them are best characterized: $p16^{INK4a}$ and $p15^{INK4b}$ which inhibit CDK4/CDK6, and $p21^{Cip1}$ which inhibits CDK2 (Fig. 2).

$p21^{Cip1}$ is one of the main targets of p53 for the induction of cell cycle arrest following DNA damage [42]. Pathways that generate DNA damage response and p53 activation use $p21^{Cip1}$ as a major mediator of cellular senescence to control pRb protein [43]. Exceptionally, $p21^{Cip1}$ can be activated by p53-independent pathways to induce senescence [44].

The Rb protein plays two important and complementary roles that are necessary to initiate and to permanently maintain the cell cycle arrest in senescent cells. pRb proteins firstly contribute to the exit from the cell cycle by arresting cells at G1 phase, as expected [45]. In senescent cells, this exit is complemented with a dramatic remodeling of chromatin through the formation of domains of facultative heterochromatin called SAHF [46–48]. SAHF contain modifications and associated proteins characteristic of transcriptionally silent heterochromatin. Proliferation-promoting genes, such as E2F target genes are recruited into SAHF in a pRb protein-dependent manner. This recruitment is believed to contribute to irreversible silencing of these proliferation-promoting genes [49].

4. Senescence of hepatocytes and chronic liver disease

Hepatocytes in the adult liver are quiescent cells, they are renewed slowly, approximately once a year, as estimated by telomere loss which is 50–120 bp per year in healthy individuals [50,51]. However, the liver has an extremely powerful regenerative capacity, as demonstrated experimentally in rodents, and as observed in patients with chronic liver diseases [5]. This regenerative capacity is due mostly to the ability of mature hepatocytes to proliferate in response to a diminution of total liver mass either experimentally, or following exposure to viral and non viral hepatotoxic agents. In addition, the adult liver seems to harbor hepatocyte-progenitor cells (<0.10% of total hepatocyte mass) that are able to restore liver hepatocyte populations [52]. However, hepatocytes, like any other somatic cells, do not have unlimited replicative capacity, due to the lack of telomerase activity that is needed to avoid telomere shortening during successive cell divisions. This is best exemplified by decreased hepatocyte proliferation in liver cirrhosis stage of chronic liver diseases [53], providing in vivo evidence for the exhaustion of hepatocyte proliferation capacity. Senescence mechanisms in hepatocytes and in liver tissue are not well known. However, a limited

Please cite this article in press as: M. Ozturk et al., Senescence and immortality in hepatocellular carcinoma, Cancer Lett. (2008), doi:10.1016/j.canlet.2008.10.048

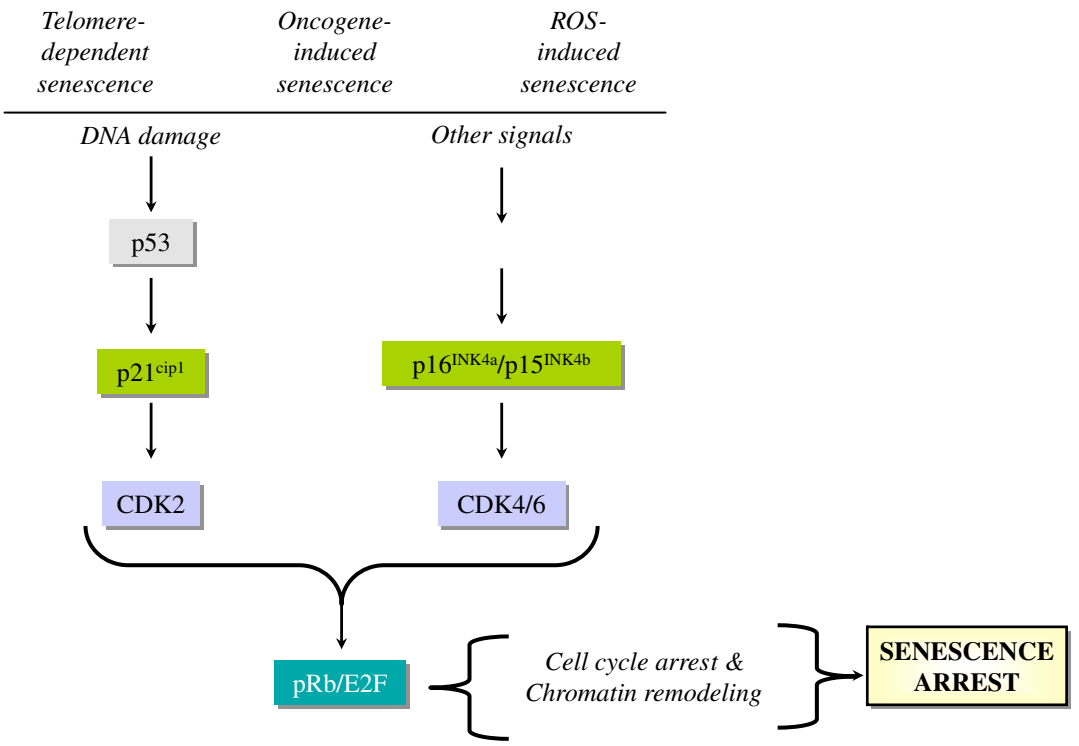

Fig. 2. All known senescence pathways converge at the level of activation of CDKIs ($p15^{INK4b}$, $p16^{INK4a}$ and $p21^{Cip1}$) that keep the pRb protein under the active form. The pRb protein inhibits E2F action and prevents the expression of growth-promoting genes for cell cycle exit. Furthermore, pRb recruits growth-promoting genes into a facultative chromatin structure for permanent silencing and growth arrest.

number of in vitro studies with hepatocytes, as well as numerous descriptive in vivo studies in liver tissue provide sufficient evidence that hepatocytes can undergo senescence type changes.

In vitro senescence in hepatocytes: as stated earlier, limited proliferative capacity of somatic cells is controlled by replicative senescence. The experimental study of replicative senescence is done traditionally by serial culture of primary cells. Initially observed in fibroblasts, this phenomenon has also been well understood in some epithelial cells, mammary epithelial cells in particular [54]. On the other hand, our knowledge of hepatocyte replicative senescence is highly limited. In contrast to in vivo conditions, mature hepatocytes are extremely resistant to cell proliferation in cell culture. Usually, more than 99.9% of adult liver hepatocytes do not divide and can only be maintained in culture for a few weeks at most. A small progenitor-type cell population (so called small hepatocytes) has been shown to proliferate in vitro, but they usually stop growing at passages 5–7, with an ill-defined senescence-like phenotype [55].

Fetal hepatocytes display better proliferation capacity in culture. A few studies have shown that these fetal cells enter replicative senescence, as shown by senescence-associated β-galactosidase assay (SABG) at population doubling (PD) 30–35 [55]. This is accompanied by progressive shortening of telomeres down to ~6 kbp, as these cells like adult hepatocytes lack telomerase activity. However, it was possible to immortalize these fetal hepatocytes by stable expression of TERT [55]. Such immortalized cells have been expanded beyond known senescence barriers (>300 PD).

In vivo senescence in liver tissue: in contrast to in vitro studies, in vivo senescence of human hepatocytes is better known. Indeed, the liver is one of the rare tissues where in vivo evidence for senescence has been convincingly and independently demonstrated by different investigators [6–9]. Replicative senescence (as tested by SABG assay) displayed a gradual increase from 10% in normal liver, to 84% in cirrhosis ([6,7]. It was also detected in 60% HCCs [6]. It has also been demonstrated that telomere shortening in cirrhosis is restricted to hepatocytes and this hepatocyte-specific shortening was correlated with SABG staining [7].

Potential mechanisms of senescence in hepatocytes and the liver: as presented in detail in the previous section, multiple pathways of senescence have been described in different experimental systems. Key molecules that are already involved in senescence arrest have also been summarized. The published data on different senescence pathways in the liver is fragmented and control mechanisms involved in hepatocyte senescence are not completely understood. Therefore, existing data on hepatocellular senescence together with potential mechanisms that may be involved in this process will be presented.

For reasons previously described, almost nothing is known about molecular mechanisms involved in replicative senescence and immortalization of hepatocytes in cul-

ture. There are only a few demonstrations of hepatocyte immortalization in vitro. Thus, ectopically expressed TERT may induce hepatocyte immortalization. However, as the published data using TERT immortalization is scarce, it is highly likely that the immortalization of hepatocytes is not an easy task even with a well-established protocol that works with other epithelial cell types such as mammary epithelial cells. The mechanisms of in vitro senescence induction in hepatocytes are also mostly unknown. Rapid induction of a senescence arrest in cultured hepatocytes suggests that these cells display robust telomere-independent senescence-inducing systems that are functional in vitro. However, they remain to be discovered. It is highly likely that, similar to other somatic cells, p53 and RB pathways in general, and some CDKIs in particular are also involved in hepatocyte senescence, but the evidence is lacking for the time being.

Telomere shortening during aging is slow (55–120 base pairs per year) and stabilizes at mid age in healthy liver, so that the loss of telomeric DNA does not reach a level to induce telomere dysfunction and DNA damage response [50,51]. Other forms of telomere-independent senescence such as ROS-induced senescence may also be rare under normal physiological conditions. On the other hand, telomere loss is accelerated in chronic liver disease to reach lowest levels in the cirrhotic liver [7,51]. Therefore, one plausible mechanism involved in cirrhosis is probably telomere-dependent senescence, or replicative senescence. The relevance of replicative senescence to liver tissue aging has been demonstrated experimentally using telomerase-deficient mice. Late generation telomerase-deficient mice display critically shortened telomeres and an impaired liver growth response to partial hepatectomy. A subpopulation of telomere-shortened hepatic cells displayed impaired proliferative capacity that is associated with SABG activity [11,56]. On the other hand, it has been reported that mouse liver cells are highly resistant to extensive telomere dysfunction. Conditional deletion of the telomeric protein TRF2 in hepatocytes resulted in telomeric accumulation of phospho-H2AX and frequent telomere fusions, indicating loss of telomere protection. However, there was no induction of p53 and liver function appeared unaffected. The loss of TRF2 did not compromise liver regeneration after partial hepatectomy. Liver regeneration occurred without cell division involving endoreduplication and cell growth, thereby circumventing the chromosome segregation problems associated with telomere fusions. Thus, it appears that hepatocytes display intrinsic resistance to telomere dysfunction, although they are apparently vulnerable to severe telomere loss [57].

Hepatocyte senescence that is observed in severe chronic liver diseases such as cirrhosis may also be induced by telomere-independent pathways. Chronic liver injury observed under such conditions is accompanied with inflammation, cell death, and oxidative stress [58–60]. Some of the etiological factors such as HCV and alcohol induce mitochondrial dysfunction may result in ROS accumulation [61,62]. Thus, ROS-induced senescence may also occur during cirrhosis, although this has not yet been reported. The status of DNA damage in chronic liver disease is less well-known. 8-Hydroxydeoxyguanosine, an indicator of DNA lesions produced by ROS, was reported to be increased in chronic liver disease [63]. On the other hand, the upregulation of DNA repair enzymes in cirrhosis has also been reported [64]. Increased DNA repair activity in cirrhosis which may reflect increased DNA damages as a consequence of chronic liver injury, but also inhibition of DNA damage responses such as senescence were observed. Taken together, these observations suggest that the primary cause of senescence in cirrhotic patients is telomere dysfunction and that ROS may also play additional roles.

Among senescence-related proteins, $p16^{INK4a}$ and $p21^{Cip1}$ expression was found to be high in cirrhosis, as compared to normal liver and tumor tissues [65], suggesting that these major senescence-inducing proteins accumulate in the cirrhotic liver. Promoter methylation of these CDKIs was also studied. Chronic liver disease samples displayed lower levels of methylation as compared to HCCs [66]. Thus, the progression of chronic liver disease towards cirrhosis is accompanied with a progressive activation of different CDKIs, as expected.

5. Senescence pathway aberrations and telomerase reactivation in hepatocellular carcinoma

As stated earlier, p53 and retinoblastoma (Rb) pathways play a critical role in senescence arrest as observed in different in vitro and in vivo models. Indirect evidence suggests that these pathways may also be important in hepatocellular senescence. The accumulation of p21 and p16 in cirrhotic liver tissues has been reported independently by different reports. On the other hand, HCC rarely develops in liver tissues absent of chronic liver disease. More than 80% of these cancers are observed in patients with cirrhosis [9]. As the appearance of proliferating malignant cells from this senescence stage requires the bypass of senescence, the status of both p53 and RB pathways in HCC is of great importance in terms of molecular aspects of hepatocellular carcinogenesis.

HCC is one of the major tumors displaying frequent p53 mutations [67,68]. The overall p53 mutation frequency in HCC is around 30%. Both the frequency and the spectrum of p53 mutations show great variations between tumors from different geographical areas of the World. A hotspot mutation (codon 249 AGG → AGT) has been linked to exposure to aflatoxins which are known to be potent DNA damaging agents (for a review see Ref. [67]). Although, it is unknown whether aflatoxins are able to generate a DNA damage-dependent senescence response in hepatocytes, their association with DNA damage and p53 mutation provides indirect evidence for such an ability. Other p53 mutations described in HCCs from low aflatoxin areas may similarly be correlated with other DNA damaging agents, such as ROS which are known to accumulate in the livers of patients with chronic liver diseases, including cirrhosis.

Another player of senescence arrest, the p16 gene is rarely mutated in HCC, but its epigenetic silencing by promoter methylation is highly frequent in this cancer. More than 50% of HCCs display de novo methylation of the promoter of CDKN2A gene, encoding p16 protein, resulting in

Please cite this article in press as: M. Ozturk et al., Senescence and immortality in hepatocellular carcinoma, Cancer Lett. (2008), doi:10.1016/j.canlet.2008.10.048

loss of gene expression [67]. Major components of p53 and Rb pathways in the same set of HCCs with different etiologies have been analyzed [69]. Retinoblastoma pathway alterations (p16 ^{INK4a}, p15^{INK4b} or RB1 genes) were present in 83% of HCCs, whereas p53 pathway alterations (p53 or ARF genes) were detected in only 31% of tumors. Alterations in both Rb and p53 pathways were present in 30% of HCCs. Thus, it appears that either the Rb and/or the p53 pathway are affected in the great majority of HCCs, and that both pathways are affected in at least one third of these tumors. Unfortunately, p53 and p16^{INK4a} aberrations observed in HCC have not yet been studied in relation to senescence aberrations. However, these observations provide supporting evidence on the critical role of senescence-controlling pathways in the development of HCC.

The lack of telomerase activity in normal and cirrhotic liver correlates with progressive loss of telomere sequences ending up with a senescence arrest. The emergence of malignant hepatocytes from this senescence-dominated cirrhotic milieu would require not only the bypass of senescence, but also a way of survival despite critically shortened telomeres. Additionally, the proliferative expansion of neoplastic cells in order to form sustained tumor masses would require telomeres at a minimal length required to maintain intact chromosomal structures.

Many studies showed that telomerase activity is a hallmark of all human cancers, including 80–90% of HCCs [70–72]. It is currently unclear how the TERT expression is repressed and released in normal hepatocytes and HCC cells, respectively. The integration of HBV DNA sequences into TERT gene provides evidence for a virus-induced deregulation of TERT expression, but this appears to rarely occur, as only four cases have been reported thus far [73–75]. Hbx and PreS2 proteins may upregulate TERT expression [76,77]. The molecular mechanisms involved in TERT suppression in somatic cells and its reactivation in cancer cells are ill-known. The TERT promoter displays binding sites for a dozen of transcriptional regulators: estrogen receptor, Sp1, Myc and ER81 acting positively, and vitamin D receptor, MZF-2, WT1, Mad, E2F1 and SMAD interacting protein-1 (SIP1, also called ZEB-2 or ZFHX1B) acting negatively [78]. Despite high telomerase activity, telomeres in HCC were repeatedly found to be highly shortened [65,79,80]. However, 3′ telomere overhangs were found to be increased in nearly 40% HCCs [80]. Moreover, the expression of several telomeric proteins is increased in HCC [80,81].

Another ill-known aspect of TERT activity in HCC cells is the cellular origin of these malignant cells. It is presently unclear whether HCC arises from mature hepatocytes which lack telomerase activity, or stem/progenitor cell-like cells that may already express TERT at sufficient levels to maintain telomere integrity. In the non-tumor area surrounding the cancer tissue, telomerase activity could not be detected, or was detected at very low levels.

The importance of telomerase activity in HCC development has been studied experimentally using telomerase-deficient mouse model. These mice show increased susceptibility to adenoma development (tumor initiation), but they are quite resistant to fully malignant tumor development [82]. Likewise, telomerase deletion limits the progression of p53-mutant HCCs with short telomeres [83]. These observations suggest that the aberrations affecting telomerase activity and senescence controlling genes such as p53 may cooperate during hepatocellular carcinogenesis.

In summary, HCC is characterized by mutational inactivation of p53, a major player in DNA damage-induced senescence. In addition, p15^{INK4b}, p16^{INK4a}, p21^{Cip1} CDKIs are often inactivated in this cancer mostly by epigenetic mechanisms involving promoter methylation. These changes may play a critical role in the bypass of senescence that is observed in most cirrhosis cases, allowing some initiated cells to escape senescence control and proliferate. In the absence of telomerase activity such cells would probably not survive due to telomere loss. However, since more than 80% of HCCs display telomerase activity, it is highly likely that the telomerase reactivation, together with the inactivation of major CDKIs, plays a critical role in HCC development by conferring premalignant or malignant cells the ability to proliferate indefinitely (Fig. 3). However, cellular immortality is not sufficient for full malignancy [84]. Thus, senescence-related aberrations that are observed in HCC cells, may confer a partial survival advantage that would need to be complemented by other genetic or epigenetic alterations.

6. Senescence as an anti-tumor mechanism in hepatocellular carcinoma

Senescence in normal somatic cells and tissues is expected. How about cancer cells and tumors? Initial studies using different cancer cell lines provided ample evidence for the induction of senescence by different genetic as well as chemical or biological treatments [85]. Thus, it appeared that cancer cells, immortalized by definition, do have a hidden senescence program that can be revealed by different senescence-inducing stimuli. These studies provided preliminary evidence for considering senescence induction as an anti-cancer therapy. The in vivo relevance of these observations and expectations became evident only very recently. Senescence was observed in tumors or pre-neoplastic lesions. SABG activity as well as several other senescence markers were detected in lung adenomas, but not in adenocarcinomas observed in oncogenic Ras ‘‘knock-in” mice [86]. Ras-driven mouse T-cell lymphomas entered senescence after drug therapy, when apoptosis was blocked [87]. The first direct evidence of cellular senescence in humans was reported for the melanocytic nevus [88].

Senescence response of HCC cells was not the subject of intensive study until very recently. Therefore the potential role of senescence in these tumors is less well understood. Treatment of HCC cell lines with 5-aza-2-deoxycytidine induced the expression of p16^{INK4a}, hypophosphorylation of pRb and G1 arrest associated with positive SABG staining [89]. Recent findings indicate that senescence induction is a powerful mechanism of HCC regression. Xue et al. expressed H-ras oncogene and suppressed endogenous p53 expression in mouse hepatoblasts which produced massive

Please cite this article in press as: M. Ozturk et al., Senescence and immortality in hepatocellular carcinoma, Cancer Lett. (2008), doi:10.1016/j.canlet.2008.10.048

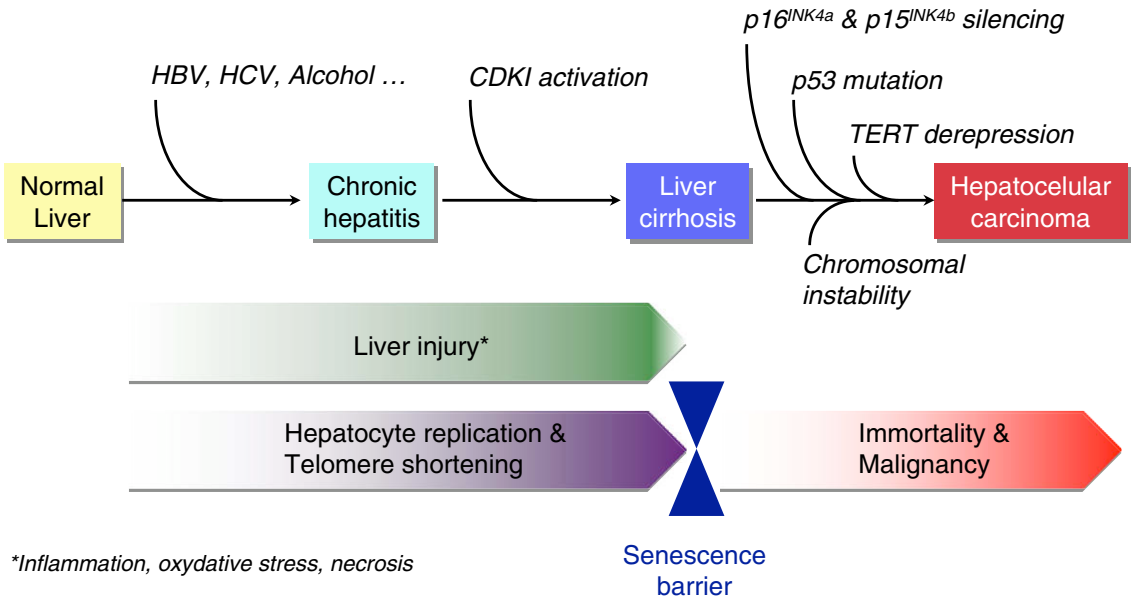

Fig. 3. Role of cellular senescence and immortalization in hepatocellular carcinogenesis. Chronic liver injury (triggered by major etiological factors HBV, HCV and alcohol) leading to cirrhosis is a common cause of HCC. Hepatocytes having no telomerase activity undergo progressive telomere shortening and DNA damage during this process. Consequently, CDKIs (primarily $p16^{INK4a}$ and $p21^{Cip1}$) are activated gradually to induce senescence in the preneoplastic cirrhosis stage. Mutation and expression analyses in HCC strongly suggest that neoplastic cells bypass the senescence barrier by inactivating major senescence-inducing genes (p53, $p16^{INK4a}$ and $p15^{INK4b}$). Moreover, they acquire the ability of unlimited proliferation (immortality) by re-expressing the TERT enzyme. Chromosomal instability that is generated by telomere erosion may contribute to additional mutations necessary for tumor progression.

HCCs upon implantation into livers of athymic mice [12]. However, these tumors regressed rapidly upon restoration of p53 expression. Tumor regression was due to differentiation and massive senescence induction, followed by immune-mediated clearance of senescent cells. These observations may indicate that oncogene-induced senescence is also involved in HCC. On the other hand, HCCs induced by tet-regulated c-Myc activation in mouse liver cells differentiate into mature hepatocytes and biliary cells or undergo senescence [90]. Thus, senescence induction may also be relevant to oncogene inactivation in HCC. In this regard, c-Myc down-regulation and senescence induction in several HCC cell lines as a response to TGF-β was observed (S. Senturk, M. Ozturk, unpublished data).

So far, all the reported examples of senescence induction in HCC cells are in the form of a telomere-independent permanent cell cycle arrest. Until recently, it was unknown whether replicative senescence could also be induced in immortal cancer cells. Ozturk et al. reported recently that immortal HCC cells can revert spontaneously to a replicative senescence phenotype [91]. Immortal HCC cells generated progeny that behaved, in vitro, similar to normal somatic cells. Such senescence-programmed progeny lacked telomerase activity due to TERT repression (probably mediated by SIP1 gene), and displayed progressive telomere shortening in cell culture, resulting in senescence arrest. It will be interesting to test whether such spontaneous reversal of replicative immortality is involved in well known tumor dormancy and/or spontaneous tumor regression.

7. Concluding remarks

Cellular senescence has gained great interest in recent years following the demonstration that it also occurs in vivo. It is also highly interesting that senescence can be mediated by a large number of pathways and molecules, as is the case for apoptosis. Recent findings that implicate secreted molecules in senescence induction strongly suggest that cellular senescence is not just a cellular event, but also a physiologically relevant process for the whole organism. In terms of tumor biology, oncogene-induced senescence that may serve as anti-tumor mechanism in pre-neoplastic lesions underlines its clinical relevance. On the other hand, induced or spontaneous senescence that is observed in cancer cells is promising to explore new approaches for tumor prevention and treatment. The role of senescence bypass and cellular immortality in hepatocellular carcinogenesis is not well defined. But, many findings (inactivation of senescence-mediator genes such as p53, $p16^{INK4a}$ and $p15^{INK4b}$, as well as reactivation of TERT) indicate that senescence mechanisms and their aberrations are critically involved in HCC. We may expect that this field will attract more attention in coming years for a better definition of senescence implications in hepatocellular carcinogenesis.

Please cite this article in press as: M. Ozturk et al., Senescence and immortality in hepatocellular carcinoma, Cancer Lett. (2008), doi:10.1016/j.canlet.2008.10.048

AcknowledgmentS

Authors' research is supported by grants from TUBITAK, DPT and TUBA (Turkey), and InCA (France). We thank D. Ozturk for language editing.

References

[1] D.E. Crew (Ed.), Human senescence-evolutionary and biocultural perspectives, Cambridge University Press, Cambridge, 2003.
[2] L. Hayflick, The limited in vitro lifetime of human diploid cell strains, Exp. Cell Res. 37 (1965) 614–636.
[3] J. Campisi, F. d'Adda di Fagagna, Cellular senescence: when bad things happen to good cells, Nat. Rev. Mol. Cell Biol. 8 (2007) 729–740.
[4] K.L. Rudolph, S. Chang, H.W. Lee, M. Blasco, G.J. Gottlieb, C. Greider, R.A. DePinho, Longevity, stress response, and cancer in aging telomerase-deficient mice, Cell 96 (1999) 701–712.
[5] G.K. Michalopoulos, Liver regeneration, J. Cell Physiol. 213 (2007) 286–300.
[6] V. Paradis, N. Youssef, D. Dargere, N. Ba, F. Bonvoust, J. Deschatrette, P. Bedossa, Replicative senescence in normal liver, chronic hepatitis C, and hepatocellular carcinomas, Hum. Pathol. 32 (2001) 327–332.
[7] S.U. Wiemann, A. Satyanarayana, M. Tsahuridu, H.L. Tillmann, L. Zender, J. Klempnauer, P. Flemming, S. Franco, M.A. Blasco, M.P. Manns, K.L. Rudolph, Hepatocyte telomere shortening and senescence are general markers of human liver cirrhosis, FASEB J. 16 (2002) 935–942.
[8] V. Trak-Smayra, J. Contreras, F. Dondero, F. Durand, S. Dubois, D. Sommacale, P. Marcellin, J. Belghiti, C. Degott, V. Paradis, Role of replicative senescence in the progression of fibrosis in hepatitis C virus (HCV) recurrence after liver transplantation, Transplantation 77 (2004) 1755–1760.
[9] H.B. El-Serag, K.L. Rudolph, Hepatocellular carcinoma: epidemiology and molecular carcinogenesis, Gastroenterology 132 (2007) 2557–2576.
[10] K.L. Rudolph, S. Chang, M. Millard, N. Schreiber-Agus, R.A. DePinho, Inhibition of experimental liver cirrhosis in mice by telomerase gene delivery, Science 287 (2000) 1253–1258.
[11] A. Satyanarayana, S.U. Wiemann, J. Buer, J. Lauber, K.E. Dittmar, T. Wüstefeld, M.A. Blasco, M.P. Manns, K.L. Rudolph, Telomere shortening impairs organ regeneration by inhibiting cell cycle re-entry of a subpopulation of cells, EMBO J. 22 (2003) 4003–4013.
[12] W. Xue, L. Zender, C. Miething, R.A. Dickins, E. Hernando, V. Krizhanovsky, C. Cordon-Cardo, S.W. Lowe, Senescence and tumour clearance is triggered by p53 restoration in murine liver carcinomas, Nature 445 (2007) 656–660.
[13] T. de Lange, Shelterin: the protein complex that shapes and safeguards human telomeres, Genes Dev. 19 (2005) 2100–2110.
[14] E.H. Blackburn, Structure and function of telomeres, Nature 350 (1991) 569–573.
[15] Y.S. Cong, W.E. Wright, J.W. Shay, Human telomerase and its regulation, Microbiol. Mol. Biol. Rev. 66 (2002) 407–425.
[16] J. Karlseder, A. Smogorzewska, T. de Lange, Senescence induced by altered telomere state, Not telomere loss, Science 295 (2002) 2446–2449.
[17] R.E. Verdun, J. Karlseder, Replication and protection of telomeres, Nature 447 (2007) 924–931.
[18] F. d'Adda di Fagagna, P.M. Reaper, L. Clay-Farrace, H. Fiegler, P. Carr, T. Von Zglinicki, G. Saretzki, N.P. Carter, S.P. Jackson, A DNA damage checkpoint response in telomere-initiated senescence, Nature 426 (2003) 194–198.
[19] M. Serrano, A.W. Lin, M.E. McCurrach, D. Beach, S.W. Lowe, Oncogenic ras provokes premature cell senescence associated with accumulation of p53 and p16INK4a, Cell 88 (1997) 593–602.
[20] R. Di Micco, M. Fumagalli, d'Adda F. di Fagagna, Breaking news: high-speed race ends in arrest-how oncogenes induce senescence, Trends Cell Biol. 17 (2007) 529–536.
[21] W.J. Mooi, D.S. Peeper, Oncogene-induced cell senescence-halting on the road to cancer, N. Engl. J. Med. 355 (2006) 1037–1046.
[22] Z. Chen, L.C. Trotman, D. Shaffer, H.K. Lin, Z.A. Dotan, M. Niki, J.A. Koutcher, H.I. Scher, T. Ludwig, W. Gerald, C. Cordon-Cardo, P.P. Pandolfi, Crucial role of p53-dependent cellular senescence in suppression of Pten-deficient tumorigenesis, Nature 436 (2005) 725–730.
[23] R. Di Micco, M. Fumagalli, A. Cicalese, S. Piccinin, P. Gasparini, C. Luise, C. Schurra, M. Garre', P.G. Nuciforo, A. Bensimon, R. Maestro, P.G. Pelicci, F. d'Adda di Fagagna, Oncogene-induced senescence is a DNA damage response triggered by DNA hyper-replication, Nature 444 (2006) 638–642.
[24] J. Bartkova, N. Rezaei, M. Liontos, P. Karakaidos, D. Kletsas, N. Issaeva, L.V. Vassiliou, E. Kolettas, K. Niforou, V.C. Zoumpourlis, M. Takaoka, H. Nakagawa, F. Tort, K. Fugger, F. Johansson, M. Sehested, C.L. Andersen, L. Dyrskjot, T. Ørntoft, J. Lukas, C. Kittas, T. Helleday, T.D. Halazonetis, J. Bartek, V.G. Gorgoulis, Oncogene-induced senescence is part of the tumorigenesis barrier imposed by DNA damage checkpoints, Nature 444 (2006) 633–637.
[25] T. Lu, T. Finkel, Free radicals and senescence, Exp. Cell Res. 314 (2008) 1918–1922.
[26] M. Giorgio, M. Trinei, E. Migliaccio, P.G. Pelicci, Hydrogen peroxide: a metabolic by-product or a common mediator of ageing signals?, Nat Rev. Mol. Cell Biol. 8 (2007) 722–728.
[27] C. Blanchetot, J. Boonstra, The ROS-NOX connection in cancer and angiogenesis, Crit. Rev. Eukaryot. Gene Expr. 18 (2008) 35–45.
[28] T. von Zglinicki, G. Saretzki, W. Döcke, C. Lotze, Mild hyperoxia shortens telomeres and inhibits proliferation of fibroblasts: a model for senescence?, Exp Cell Res. 220 (1995) 186–193.
[29] A.C. Lee, B.E. Fenster, H. Ito, K. Takeda, N.S. Bae, T. Hirai, Z.X. Yu, V.J. Ferrans, B.H. Howard, T. Finkel, Ras proteins induce senescence by altering the intracellular levels of reactive oxygen species, J. Biol. Chem. 274 (1999) 7936–7940.
[30] S. Courtois-Cox, S.L. Jones, K. Cichowski, Many roads lead to oncogene-induced senescence, Oncogene 27 (2008) 2801–2809.
[31] J.F. Passos, G. Saretzki, S. Ahmed, G. Nelson, T. Richter, H. Peters, I. Wappler, M.J. Birket, G. Harold, K. Schaeuble, M.A. Birch-Machin, T.B. Kirkwood, T. von Zglinicki, Mitochondrial dysfunction accounts for the stochastic heterogeneity in telomere-dependent senescence, PLoS Biol. 5 (2007) e110.
[32] K. Ito, A. Hirao, F. Arai, K. Takubo, S. Matsuoka, K. Miyamoto, M. Ohmura, K. Naka, K. Hosokawa, Y. Ikeda, T. Suda, Reactive oxygen species act through p38 MAPK to limit the lifespan of hematopoietic stem cells, Nat. Med. 12 (2006) 446–451.
[33] U. Herbig, W.A. Jobling, B.P. Chen, D.J. Chen, J.M. Sedivy, Telomere shortening triggers senescence of human cells through a pathway involving ATM, p53, and p21(CIP1), but not p16(INK4a) but not p16(INK4a), Mol. Cell. 14 (2004) 501–513.
[34] F.A. Mallette, M.F. Gaumont-Leclerc, G. Ferbeyre, The DNA damage signaling pathway is a critical mediator of oncogene-induced senescence, Genes Dev. 21 (2007) 43–48.
[35] J. Gil, G. Peters, Regulation of the INK4b-ARF-INK4a tumour suppressor locus: all for one or one for all, Nat. Rev. Mol. Cell Biol. 7 (2006) 667–677.
[36] D.A. Alcorta, Y. Xiong, D. Phelps, G. Hannon, D. Beach, J.C. Barrett, Involvement of the cyclin-dependent kinase inhibitor p16 (INK4a) in replicative senescence of normal human fibroblasts, Proc. Natl. Acad. Sci. U S A 93 (1996) 13742–13747.
[37] F. Zindy, D.E. Quelle, M.F. Roussel, C.J. Sherr, Expression of the p16INK4a tumor suppressor versus other INK4 family members during mouse development and aging, Oncogene 15 (1997) 203–211.
[38] R. Tremain, M. Marko, V. Kinnimulki, H. Ueno, E. Bottinger, A. Glick, Defects in TGF-beta signaling overcome senescence of mouse keratinocytes expressing v-Ha-ras, Oncogene 19 (2000) 1698–1709.
[39] N. Wajapeyee, R.W. Serra, X. Zhu, M. Mahalingam, M.R. Green, Oncogenic BRAF induces senescence and apoptosis through pathways mediated by the secreted protein IGFBP7, Cell 132 (2008) 363–374.
[40] J.C. Acosta, A. O'Loghlen, A. Banito, M.V. Guijarro, A. Augert, S. Raguz, M. Fumagalli, M. Da Costa, C. Brown, N. Popov, Y. Takatsu, J. Melamed, F. d'Adda di Fagagna, D. Bernard, E. Hernando, J. Gil, Chemokine signaling via the CXCR2 receptor reinforces senescence, Cell 133 (2008) 1006–1018.
[41] T. Kuilman, C. Michaloglou, L.C. Vredeveld, S. Douma, R. van Doorn, C.J. Desmet, L.A. Aarden, W.J. Mooi, D.S. Peeper, Oncogene-induced senescence relayed by an interleukin-dependent inflammatory network, Cell 133 (2008) 1019–1031.
[42] W.S. el-Deiry, T. Tokino, V.E. Velculescu, D.B. Levy, R. Parsons, J.M. Trent, D. Lin, W.E. Mercer, K.W. Kinzler, B. Vogelstein, WAF1, a potential mediator of p53 tumor suppression, Cell 75 (1993) 817–825.
[43] Y. Deng, S.S. Chan, S. Chang, Telomere dysfunction and tumor suppression: the senescence connection, Nat. Rev. Cancer 8 (2008) 450–458.
[44] L. Fang, M. Igarashi, J. Leung, M.M. Sugrue, S.W. Lee, S.A. Aaronson, p21Waf1/Cip1/Sdi1 induces permanent growth arrest with markers

of replicative senescence in human tumor cells lacking functional p53, Oncogene 18 (1999) 2789–2797.
[45] C. Giacinti, A. Giordano, RB and cell cycle progression, Oncogene 25 (2006) 5220–5227.
[46] M. Narita, S. Nunez, E. Heard, A.W. Lin, S.A. Hearn, D.L. Spector, G.J. Hannon, S.W. Lowe, Rb-mediated heterochromatin formation and silencing of E2F target genes during cellular senescence, Cell 113 (2003) 703–716.
[47] R. Zhang, M.V. Poustovoitov, X. Ye, H.A. Santos, W. Chen, S.M. Daganzo, J.P. Erzberger, I.G. Serebriiskii, A.A. Canutescu, R.L. Dunbrack, J.R. Pehrson, J.M. Berger, P.D. Kaufman, P.D. Adams, Formation of MacroH2A-containing senescence-associated heterochromatin foci and senescence driven by ASF1a and HIRA, Dev. Cell 8 (2005) 19–30.
[48] M. Narita, M. Narita, V. Krizhanovsky, S. Nunez, A. Chicas, S.A. Hearn, M.P. Myers, S.W. Lowe, A novel role for high-mobility group a proteins in cellular senescence and heterochromatin formation, Cell 126 (2006) 503–514.
[49] P.D. Adams, Remodeling of chromatin structure in senescent cells and its potential impact on tumor suppression and aging, Gene 397 (2007) 84–93.
[50] K. Takubo, N. Izumiyama-Shimomura, N. Honma, M. Sawabe, T. Arai, M. Kato, M. Oshimura, K. Nakamura, Telomere lengths are characteristic in each human individual, Exp. Gerontol. 37 (2002) 523–531.
[51] H. Aikata, H. Takaishi, Y. Kawakami, S. Takahashi, M. Kitamoto, T. Nakanishi, Y. Nakamura, F. Shimamoto, G. Kajiyama, T. Ide, Telomere reduction in human liver tissues with age and chronic inflammation, Exp. Cell Res. 256 (2000) 578–582.
[52] R. Utoh, C. Tateno, C. Yamasaki, N. Hiraga, M. Kataoka, T. Shimada, K. Chayama, K. Yoshizato, Susceptibility of chimeric mice with livers repopulated by serially subcultured human hepatocytes to hepatitis B virus, Hepatology 47 (2008) 435–446.
[53] M. Delhaye, H. Louis, C. Degraef, O. Le Moine, J. Devière, B. Gulbis, D. Jacobovitz, M. Adler, P. Galand, Relationship between hepatocyte proliferative activity and liver functional reserve in human cirrhosis, Hepatology 23 (1996) 1003–1011.
[54] M.R. Stampfer, P. Yaswen, Human epithelial cell immortalization as a step in carcinogenesis, Cancer Lett. 194 (2003) 199–208.
[55] H. Wege, H.T. Le, M.S. Chui, L. Lui, J. Wu, G. Giri, H. Malhi, B.S. Sappal, V. Kumaran, S. Gupta, M.A. Zern, Telomerase reconstitution immortalized human fetal hepatocytes without disrupting their differentiation potential, Gastroenterology 124 (2003) 432–444.
[56] A. Lechel, A. Satyanarayana, Z. Ju, R.R. Plentz, S. Schaetzlein, C. Rudolph, L. Wilkens, S.U. Wiemann, G. Saretzki, N.P. Malek, M.P. Manns, J. Buer, K.L. Rudolph, The cellular level of telomere dysfunction determines induction of senescence or apoptosis in vivo, EMBO Rep. 6 (2005) 275–281.
[57] E. Lazzerini Denchi, G. Celli, T. de Lange, Hepatocytes with extensive telomere deprotection and fusion remain viable and regenerate liver mass through endoreduplication, Genes Dev. 20 (2006) 2648–2653.
[58] G. Szabo, P. Mandrekar, A. Dolganiuc, Innate immune response and hepatic inflammation, Semin. Liver Dis. 27 (2007) 339–350.
[59] H. Malhi, G.J. Gores, Cellular and molecular mechanisms of liver injury, Gastroenterology 134 (2008) 1641–1654.
[60] D. Schuppan, N.H. Afdhal, Liver cirrhosis, Lancet 371 (2008) 838–851.
[61] F. Farinati, R. Cardin, M. Bortolami, P. Burra, F.P. Russo, M. Rugge, M. Guido, A. Sergio, R. Naccarato, Hepatitis C virus: from oxygen free radicals to hepatocellular carcinoma, J. Viral Hepat. 14 (2007) 821–829.
[62] A. Reuben, Alcohol and the liver, Curr. Opin. Gastroenterol. 24 (2008) 328–338.
[63] R. Shimoda, M. Nagashima, M. Sakamoto, N. Yamaguchi, S. Hirohashi, J. Yokota, H. Kasai, Increased formation of oxidative DNA damage, 8-hydroxydeoxyguanosine, in human livers with chronic hepatitis, Cancer Res. 54 (1994) 3171–3172.
[64] P. Zindy, L. Andrieux, D. Bonnier, O. Musso, S. Langouët, J.P. Campion, B. Turlin, B. Clément, N. Théret, Upregulation of DNA repair genes in active cirrhosis associated with hepatocellular carcinoma, FEBS Lett. 579 (2005) 95–99.
[65] R.R. Plentz, Y.N. Park, A. Lechel, H. Kim, F. Nellessen, B.H. Langkopf, L. Wilkens, A. Destro, B. Fiamengo, M.P. Manns, M. Roncalli, K.L. Rudolph, Telomere shortening and inactivation of cell cycle checkpoints characterize human hepatocarcinogenesis, Hepatology 45 (2007) 968–976.
[66] M. Roncalli, P. Bianchi, B. Bruni, L. Laghi, A. Destro, S. Di Gioia, L. Gennari, M. Tommasini, A. Malesci, G. Coggi, Methylation framework of cell cycle gene inhibitors in cirrhosis and associated hepatocellular carcinoma, Hepatology 36 (2002) 427–432.
[67] M. Ozturk, Genetic aspects of hepatocellular carcinogenesis, Semin. Liver Dis. 19 (1999) 235–242.
[68] T. Soussi, p53 alterations in human cancer: more questions than answers, Oncogene 26 (2007) 2145–2156.
[69] Y. Edamoto, A. Hara, W. Biernat, L. Terracciano, G. Cathamos, H.M. Riehle, M. Matsuda, H. Fuji, J.M. Scoazec, H. Ohgaki, Alterations of RB1, p53 and Wnt pathways in Hepatocellular carcinomas associated with HCV, HBV and alcoholic liver cirrhosis, Int. J. Cancer 106 (2003) 334–341.
[70] H. Tahara, T. Nakanishi, M. Kitamoto, R. Nakashio, J.W. Shay, E. Tahara, G. Kajiyama, T. Ide, Telomerase activity in human liver tissues: Comparison between chronic liver disease and hepatocellular carcinomas, Cancer Res. 55 (1995) 2734–2736.
[71] H. Kojima, O. Yokosuka, F. Imazeki, H. Saisho, M. Omata, Telomerase activity and telomere length in hepatocellular carcinoma and chronic liver disease, Gastroenterology 112 (1997) 493–500.
[72] J. Nakayama, H. Tahara, E. Tahara, M. Saito, K. Ito, H. Nakamura, T. Nakanishi, E. Tahara, T. Ide, F. Ishikawa, Telomerase activation by hTERT in human normal fibroblasts and hepatocellular carcinomas, Nat. Genet. 18 (1998) 65–68.
[73] D. Gozuacik, Y. Murakami, K. Saigo, M. Chami, C. Mugnier, D. Lagorce, T. Okanoue, T. Urashima, C. Bréchot, P. Paterlini-Bréchot, Identification of human cancer-related genes by naturally occurring Hepatitis B Virus DNA tagging, Oncogene 20 (2001) 6233–6240.
[74] I. Horikawa, JC. Barrett, Transcriptional regulation of the telomerase hTERT gene as a target for cellular and viral oncogenic mechanisms, Carcinogenesis 24 (2003) 1167–1176.
[75] Y. Murakami, K. Saigo, H. Takashima, M. Minami, T. Okanoue, C. Bréchot, P. Paterlini-Bréchot, Large scaled analysis of hepatitis B virus (HBV) DNA integration in HBV related hepatocellular carcinomas, Gut 54 (2005) 1162–1168.
[76] Z.L. Qu, S.Q. Zou, N.Q. Cui, X.Z. Wu, M.F. Qin, D. Kong, Z.L. Zhou, Upregulation of human telomerase reverse transcriptase mRNA expression by in vitro transfection of hepatitis B virus X gene into human hepatocarcinoma and cholangiocarcinoma cells, World J. Gastroenterol. 11 (2005) 5627–5632.
[77] H. Liu, F. Luan, Y. Ju, H. Shen, L. Gao, X. Wang, S. Liu, L. Zhang, W. Sun, C. Ma, In vitro transfection of the hepatitis B virus PreS2 gene into the human hepatocarcinoma cell line HepG2 induces upregulation of human telomerase reverse transcriptase, Biochem. Biophys. Res. Commun. 355 (2007) 379–384.
[78] R. Janknecht, On the road to immortality: hTERT upregulation in cancer cells, FEBS Lett. 564 (2004) 9–13.
[79] N. Miura, I. Horikawa, A. Nishimoto, H. Ohmura, H. Ito, S. Hirohashi, J.W. Shay, M. Oshimura, Progressive telomere shortening and telomerase reactivation during hepatocellular carcinogenesis, Cancer Genet. Cytogenet. 93 (1997) 56–62.
[80] J.E. Lee, B.K. Oh, J. Choi, Y.N. Park, Telomeric 3' overhangs in chronic HBV-related hepatitis and hepatocellular carcinoma, Int. J. Cancer 123 (2008) 264–272.
[81] B.K. Oh, Y.J. Kim, C. Park, Y.N. Park, Up-regulation of telomere-binding proteins, TRF1, TRF2, and TIN2 is related to telomere shortening during human multistep hepatocarcinogenesis, Am. J. Pathol. 166 (2005) 73–80.
[82] A. Satyanarayana, M.P. Manns, K.L. Rudolph, Telomeres and Telomerase: a Dual role in hepatocarcinogenesis, Hepatology 40 (2004) 276–283.
[83] A. Lechel, H. Holstege, Y. Begus, A. Schienke, K. Kamino, U. Lehmann, S. Kubicka, P. Schirmacher, J. Jonkers, K.L. Rudolph, Telomerase deletion limits progression of p53-mutant hepatocellular carcinoma with short telomeres in chronic liver disease, Gastroenterology 132 (2007) 1465–1475.
[84] W.C. Hahn, C.M. Counter, A.S. Lundberg, R.L. Beijersbergen, M.W. Brooks, R.A. Weinberg, Creation of human tumor cells with defined genetic elements, Nature 400 (1999) 464–468.
[85] J.W. Shay, I.B. Roninson, Hallmarks of senescence in carcinogenesis and cancer therapy, Oncogene 23 (2004) 2919–2933.
[86] M. Collado, J. Gil, A. Efeyan, C. Guerra, A.J. Schuhmacher, M. Barradas, A. Benguría, A. Zaballos, J.M. Flores, M. Barbacid, D. Beach, M. Serrano, Tumour biology: senescence in premalignant tumours, Nature 436 (2005) 642.
[87] M. Braig, S. Lee, C. Loddenkemper, C. Rudolph, A.H. Peters, B. Schlegelberger, H. Stein, B. Dörken, T. Jenuwein, C.A. Schmitt, Oncogene-induced senescence as an initial barrier in lymphoma development, Nature 436 (2005) 660–665.

Please cite this article in press as: M. Ozturk et al., Senescence and immortality in hepatocellular carcinoma, Cancer Lett. (2008), doi:10.1016/j.canlet.2008.10.048

[88] C. Michaloglou, L.C. Vredeveld, M.S. Soengas, C. Denoyelle, T. Kuilman, C.M. van der Horst, D.M. Majoor, J.W. Shay, W.J. Mooi, D.S. Peeper, BRAFE600-associated senescence-like cell cycle arrest of human naevi, Nature 436 (2005) 720–724.

[89] S.I. Suh, H.Y. Pyun, J.W. Cho, W.K. Baek, J.B. Park, T. Kwon, J.W. Park, M.H. Suh, D.A. Carson, 5-Aza-2'-deoxycytidine leads to down-regulation of aberrant p16 RNA transcripts and restores the functional retinoblastoma protein pathway in hepatocellular carcinoma cell lines, Cancer Lett. 160 (2000) 81–88.

[90] C.H. Wu, J. van Riggelen, A. Yetil, A.C. Fan, P. Bachireddy, D.W. Felsher, Cellular senescence is an important mechanism of tumor regression upon c-Myc inactivation, Proc. Natl. Acad. Sci. USA 104 (2007) 13028–13033.

[91] N. Ozturk, E. Erdal, M. Mumcuoglu, K.C. Akcali, O. Yalcin, S. Senturk, A. Arslan-Ergul, B. Gur, I. Yulug, R. Cetin-Atalay, C. Yakicier, T. Yagci, M. Tez, M. Ozturk, Reprogramming of replicative senescence in hepatocellular carcinoma-derived cells, Proc. Natl. Acad. Sci. USA 103 (2006) 2178–2183.

Please cite this article in press as: M. Ozturk et al., Senescence and immortality in hepatocellular carcinoma, Cancer Lett. (2008), doi:10.1016/j.canlet.2008.10.048

Reprogramming of replicative senescence in hepatocellular carcinoma-derived cells

Nuri Ozturk*, Esra Erdal*†, Mine Mumcuoglu*, Kamil C. Akcali*, Ozden Yalcin*‡, Serif Senturk*, Ayca Arslan-Ergul*, Bala Gur*, Isik Yulug*, Rengul Cetin-Atalay*, Cengiz Yakicier*, Tamer Yagci*, Mesut Tez§, and Mehmet Ozturk*¶

*Department of Molecular Biology and Genetics, Bilkent University, Bilkent, Ankara 06800, Turkey; and §Department of 5th Surgery, Numune Training and Research Hospital, Sihhiye, Ankara 06100, Turkey

Communicated by Aziz Sancar, University of North Carolina, Chapel Hill, NC, December 18, 2005 (received for review October 10, 2005)

Tumor cells have the capacity to proliferate indefinitely that is qualified as replicative immortality. This ability contrasts with the intrinsic control of the number of cell divisions in human somatic tissues by a mechanism called replicative senescence. Replicative immortality is acquired by inactivation of p53 and $p16^{INK4a}$ genes and reactivation of hTERT gene expression. It is unknown whether the cancer cell replicative immortality is reversible. Here, we show the spontaneous induction of replicative senescence in p53-and $p16^{INK4a}$-deficient hepatocellular carcinoma cells. This phenomenon is characterized with hTERT repression, telomere shortening, senescence arrest, and tumor suppression. SIP1 gene (*ZFHX1B*) is partly responsible for replicative senescence, because short hairpin RNA-mediated SIP1 inactivation released hTERT repression and rescued clonal hepatocellular carcinoma cells from senescence arrest.

immortality | liver cancer | SIP1 | telomerase | p53

Tumor cells are clonal (1), and tumorigenesis usually requires three to six independent mutations in the progeny of precancerous cells (2). For this to occur, preneoplastic somatic cells would need to breach the replicative senescence barriers. Replicative senescence is a telomere-dependent process that sets a limit to the successive rounds of cell division in human somatic cells (3). Progressive telomere shortening is observed in almost all dividing normal cells. This phenomenon is linked to the lack of efficient *hTERT* expression that is observed in most human somatic cells (3). Replicative senescence (permanent growth arrest also called M_1 stage) is believed to be initiated by a DNA damage-type signal generated by critically shortened telomeres, or by the loss of telomere integrity, leading to the activation of cell cycle checkpoint pathways involving p53, $p16^{INK4a}$, and/or retinoblastoma (pRb) proteins (4, 5). In the absence of functional p53 and $p16^{INK4a}$/pRb pathway responses, telomeres continue to shorten resulting in crisis (also called M2 stage). Cells that bypass the M_2 stage by reactivating *hTERT* expression gain the ability for indefinite cell proliferation, also called immortality (3, 4, 6). There is accumulating evidence that cancer cells undergo a similar process during carcinogenesis to acquire immortality. Telomerase activity associated with *hTERT* reexpression is observed in ≈80% of human tumors (7), and senescence controlling *p53* and $p16^{INK4A}$ genes are commonly inactivated in the majority of human cancers (8). Moreover, experimental transformation of normal human cells to tumor cells requires hTERT-mediated immortalization, as well as inactivation of *p53* and *pRb* genes (9).

Aberrant expression of hTERT, together with the loss of p53 and $p16^{INK4a}$/pRb control mechanisms, suggests that the replicative immortality is a permanent and irreversible characteristic of cancer cells. Although some cancer cells may react to extrinsic factors by a senescence-like stress response, this response is immediate, telomere-independent, and cannot be qualified as replicative senescence (10). Experimental inactivation of telomerase activity in cancer cells mostly results in cell death (11), whereas ectopic expression of p53, $p16^{INK4a}$, or pRb provokes an immediate senescence-like growth arrest or cell death (10). Thus, to date there is no experimental evidence for spontaneous reprogramming of replicative senescence in immortalized cancer cells. Using hepatocellular carcinoma (HCC)-derived Huh7 cells as a model system, here we show that cancer cells with replicative immortality are able to spontaneously generate progeny with replicative senescence. Thus, we provide preliminary evidence for the reversibility of cancer cell immortality. The replicative senescence of cancer cells shares many features with normal cell replicative senescence such as repression of *hTERT* expression, telomere shortening, and permanent growth arrest with morphological hallmarks of senescence. However, the *p53* gene is mutated, whereas $p16^{INK4a}$ promoter is hypermethylated in these cells. Thus, we show that fully malignant and tumorigenic HCC cells that display aberrant hTERT expression and lack functional *p53* and $p16^{INK4a}$ genes are able to revert from replicative immortality to replicative senescence by an intrinsic mechanism. Furthermore, we demonstrate that the *SIP1* gene, encoding a zinc-finger homeodomain transcription factor protein involved in TGF-β signaling (12, 13) and *hTERT* regulation (14), serves as a molecular switch between replicative immortality and replicative senescence fates in HCC cells.

Results

When analyzing clones from established cancer cell lines, we observed that some clones change morphology and cease proliferation at late passages with features reminiscent of cellular senescence (data not shown). We reasoned that this could be an indication for generation of progeny programmed for replicative senescence. We surveyed a panel of HCC and breast carcinoma cell lines and hTERT-immortalized human mammary epithelial cells (hTERT-HME). Plated at low clonogenic density, cells were maintained in culture until they performed 6–10 population doublings (PD), and tested for senescence-associated β-galactosidase (SABG) activity (15). Different cancer cell lines generated progeny with greatly contrasting SABG staining patterns. The first group, represented here by HCC-derived Huh7 and breast cancer-derived T-47D and BT-474 cell lines, generated heterogeneously staining colonies. Cells of some colonies were mostly positive for SABG, but others displayed significantly diminished or complete lack of staining (Fig. 1*A*). The second group, represented by HCC-derived Hep3B and Mahlavu, and hTERT-HME generated only SABG-negative colonies (Fig. 1*B*). Manual counting of randomly selected colonies demonstrated that mean SABG-labeling indexes for Huh7,

Conflict of interest statement: No conflicts declared.

Abbreviations: HCC, hepatocellular carcinoma; PD, population doubling; SABG, senescence-associated β-galactosidase; shRNA, short hairpin RNA.

†Present address: Department of Medical Biology and Genetics, Faculty of Medicine, Dokuz Eylul University, 35210 Izmir, Turkey.

‡Present address: Swiss Institute for Experimental Cancer Research, Ch. des Boveresses 155, CH-1066 Epalinges, Lausanne, Switzerland.

¶To whom correspondence should be addressed. E-mail: ozturk@fen.bilkent.edu.tr.

www.pnas.org/cgi/doi/10.1073/pnas.0510877103

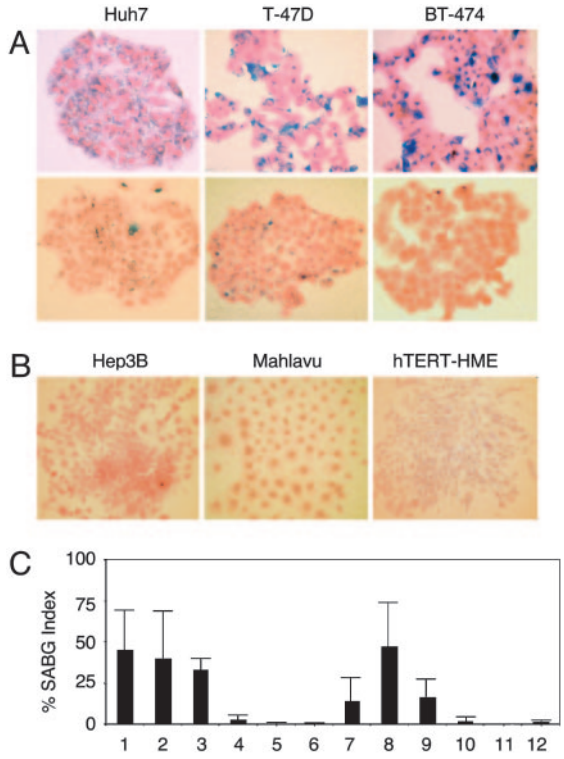

Fig. 1. Established human cancer cell lines generate senescence-associated β-galactosidase (SABG)-expressing progeny. (*A*) Representative pictures of HCC (Huh7) and breast cancer (T-47D and BT-474) cell lines that generate both SABG-positive (*Upper*) and SABG-negative (*Lower*) colonies. (*B*) Representative pictures of HCC (Hep3B and Mahlavu) and telomerase-immortalized mammary epithelial (hTERT-HME) cell lines that generate only SABG-negative colonies. Cells were plated at clonogenic density to generate colonies with 6–10 population doublings, and stained for SABG activity (blue), followed by eosin counterstaining (red). (*C*) Quantification of SABG-positive cells in colonies. Randomly selected colonies ($n \geq 10$) obtained from parental (lanes 1–6) cell lines and expanded clones (lanes 7–12) were counted to calculate the average % SABG positive cells per colony (% SABG index). Lanes 1–6 designate Huh7, T-47D, BT-474, Hep3B, Mahlavu, and hTERT-HME, respectively. Lanes 7–9 are Huh7-derived C1, C3, and C11 clones, and lanes 10–12 are Hep3B-derived 3B-C6, 3B-C11, and 3B-C13 clones. Error bars indicate SD.

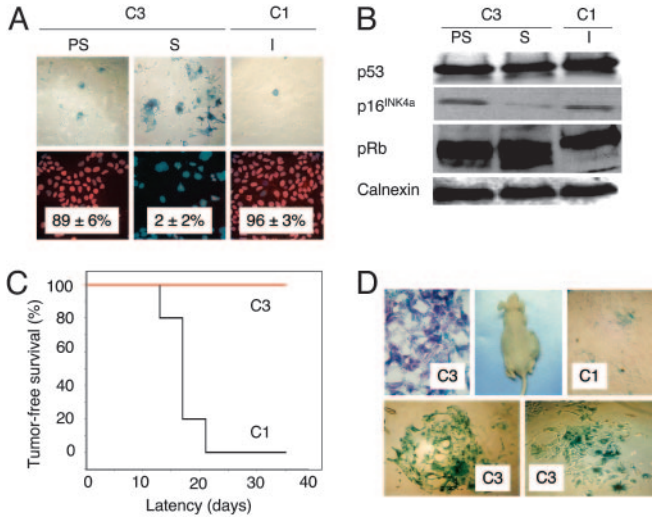

Fig. 2. p53-and p16^{INK4a}-deficient Huh7 cells generate progeny that undergo *in vitro* and *in vivo* replicative senescence resulting in loss of tumorigenicity. (*A*) Huh7-derived clones C3 and C1 were tested for replicative senescence arrest by SABG and BrdUrd staining at different passages. Presenescent C3 and immortal C1 cells display low SABG staining (*Upper*) and high BrdUrd incorporation (*Lower*), whereas senescent C3 cells are fully positive for SABG (*Upper*) and fail to incorporate BrdUrd into DNA after mitogenic stimuli (*Lower*). (*B*) p53 and p16^{INK4a} protein levels show no increase in senescent C3 cells, compared to presenescent C3 and immortal C1 cells, but senescent C3 cells display partial hypophosphorylation of pRb. Calnexin was used as a loading control. Proteins were tested by Western blotting. PS, presenescent (PD 57); S, senescent (PD 80); I, immortal (PD 179). (*C*) C1 cells (black line) were fully tumorigenic, but C3 cells (red line) were not in *nude* mice. (*D*) C1 tumors displayed low SABG staining (*Upper Right*), whereas implanted C3 cells remaining at the injection site are fully positive for SABG *in situ* (*Upper Left*), as well as after short-term *in vitro* selection (*Lower*). Animals were injected with presenescent C3 (PD 59) and immortal C1 (PD 119) cells, and tumors and nontumorigenic cell samples were collected at day 35 and analyzed.

T-47D and BT-474 progenies were 45 ± 23%, 40 ± 29%, and 33 ± 7%, respectively (Fig. 1*C*, lanes 1–3). In contrast, Hep3B, Mahlavu, and hTERT-HME progenies displayed <3 ± 3% mean SABG-labeling indexes (Fig. 1*C*, lanes 4–6). Clones from representative cell lines were expanded and subjected to the same analysis. SABG-staining patterns of all clones tested were closely similar to the patterns of their respective parental cell lines. For example, mean SABG staining indexes of Huh7-derived clones were 14 ± 15%, 47 ± 27%, and 17 ± 11% (Fig. 1*C*, lanes 7–9), whereas Hep3B-derived clones generated <2 ± 3% SABG-positive progenies (Fig. 1*C*, lanes 10–12). We speculated that the first group of cell lines comprised progenies in different stages of replicative senescence process at the time of analysis, whereas the second group of cell lines were composed mostly of immortal cells. The results obtained with the first group were unexpected. These cell lines have been established >20 years ago (16–18) and expanded in culture over many years, with PD well beyond the known senescence barriers for normal human cells (3), but they were still capable of generating presumably senescent progeny.

The study of a potentially active replicative senescence program in the progeny of immortal cancer cell lines requires the long-term follow up of single cell-derived clones. To this end, we chose to focus our investigations on Huh7 cell line. We expanded different Huh7-derived clones in long-term culture and examined their potential to undergo replicative senescence. Some clones performed >100 PD in culture with stable proliferation rates and heterogeneous SABG staining, whereas others sustained a limited number of PD, then entered a growth arrest phase with full SABG staining patterns. For example, C3 clone performed only 80 PD, whereas C1 clone replicated >150 PD. Permanently arrested C3 cells (PD 80) displayed enlarged size, flattened shape, and fully positive SABG staining, whereas early passage C3 (PD 57) and C1 (PD 179) cells displayed normal morphology with heterogeneous SABG staining (Fig. 2*A Upper*). Normal human cells at replicative senescence (M_1) are refractory to mitotic stimulation and display <5% BrdUrd index (19). Growth-arrested C3 cells displayed very low BrdUrd staining (2 ± 2%), in contrast to early passage C3 and late passage C1 cells, which exhibited 89 ± 6%, and 96 ± 3% BrdUrd indexes, respectively (Fig. 2*A Lower*). Senescent C3 cells remained growth arrested, but alive when maintained in culture for at least 3 months, with no emergence of immortal clones (data not shown).

Biological mechanisms of replicative senescence observed here are of particular interest, because senescence-regulatory *p53* is inactivated (20–22) and *p16^{INK4a}* promoter is hypermethylated (23) in Huh7 cells. Accordingly, there was no change in p53 levels, whereas the low level p16^{INK4a} expression did not increase, but decreased in senescent C3 (PD 80) cells, when compared to presenescent C3 (PD 57) or immortal C1 (PD 179) cells. Retinoblastoma protein (pRb) displayed partial hypophos-

phorylation in senescent C3 cells, apparently in a p53- and $p16^{INK4a}$-independent manner (Fig. 2*B*). Cyclin E and A levels were also decreased, but $p21^{cip1}$ levels were elevated in both presenescent and senescent C3 cells (Fig. 5*A*, which is published as supporting information on the PNAS web site). Cyclin D1, CDK4, and CDK2 protein levels (Fig. 5*A*) and $p14^{ARF}$ transcript levels (Fig. 5*B*) did not change.

Cancer cell senescence that we characterized here shared many features with normal cell replicative senescence (3), except that it was not accompanied with wild-type *p53* or *p16*^{INK4a} induction. However, *in vivo* relevance of the replicative senescence observed in cell culture is debated (6). Therefore, we compared *in vivo* replicative potentials of C3 (PD 59) and C1 (PD 119) cells in CD-1 *nude* mice. C3 cells did not form visible tumors, whereas C1 cells were fully tumorigenic in the same set of animals (Fig. 2*C*), like parental Huh7 cells (data not shown; ref. 24). C1 tumors collected at day 35 displayed scattered but low-rate SABG-positive staining, but remnant C3 cell masses collected from their injection sites were fully SABG-positive (Fig. 2*D Upper*). For confirmation, these remnants were removed from two different animals, passaged twice in cell culture for selection, and examined. Nearly all cells displayed senescence features including enlarged size, flattened shape, and highly positive SABG staining (Fig. 2*D Lower*). We concluded that loss of C3 tumorigenicity was due to replicative senescence *in vivo*.

Replicative senescence, also called telomere-dependent senescence is associated with progressive telomere shortening due to inefficient telomerase activity (3). When compared to parental Huh7 cells, presenescent C3 cells at PD 57 had telomeres that have already been shortened to ≈7 kbp from ≈12 kbp. These cells eroded their telomeres to <5 kbp at the onset of senescence. In contrast, immortal C1 clone (PD 179) telomeres did not shorten (Fig. 3*A*). These observations showed a perfect correlation with telomerase activity and *hTERT* expression. Immortal C1 cells displayed robust telomerase activity, whereas both presenescent and senescent C3 cells had no detectable telomerase activity (Fig. 3*B*). Accordingly, the expression of *hTERT* gene was high in C1, but barely detectable in C3 cells (Fig. 3*C*). Thus, senescence observed with C3 cells was characterized with the loss of *hTERT* expression and telomerase activity, associated with telomere shortening.

Mechanisms of *hTERT* expression are presently unclear, but several genes including *SIP1*, *hSIR2*, *c-myc*, *Mad1*, *Menin*, *Rak*, and *Brit1* have been implicated (14, 25). Therefore, we analyzed their expression in C1 and C3 clones. All tested genes, except *SIP1*, were expressed at similar levels in both C1 and C3 clones, independent of *hTERT* expression (Fig. 6, which is published as supporting information on the PNAS web site). SIP1 transcripts were undetectable in C1 cells, but elevated in C3 cells, moderately in presenescent, but strongly in senescent stages (Fig. 3*C*). We verified these findings with another Huh7-derived clone (G12) that displayed replicative senescence resulting in permanent cell proliferation arrest. Like C3, presenescent G12 cells that displayed low SABG staining with high BrdUrd index (98 ± 1%), became fully positive for SABG, and nearly negative for BrdUrd (3 ± 2%) at the onset of senescence (Fig. 7, which is published as supporting information on the PNAS web site). Presenescent G12 cells displayed only a weak *hTERT* repression associated with a slight increase in *SIP1* expression, whereas SIP1 was strongly elevated in hTERT-negative senescent cells (Fig. 3*D*). Thus, there was a close correlation between *SIP1* expression and *hTERT* repression in all Huh7 clones tested. The analysis of *SIP1* and *hTERT* expression in primary HCCs and their corresponding nontumor liver tissues confirmed this relationship. SIP1 transcript levels were high, but *hTERT* expression was low in nontumor liver tissues, whereas respective HCC tumors displayed diminished *SIP1* expression associated with up-regulated *hTERT* expression (Fig. 3*E*).

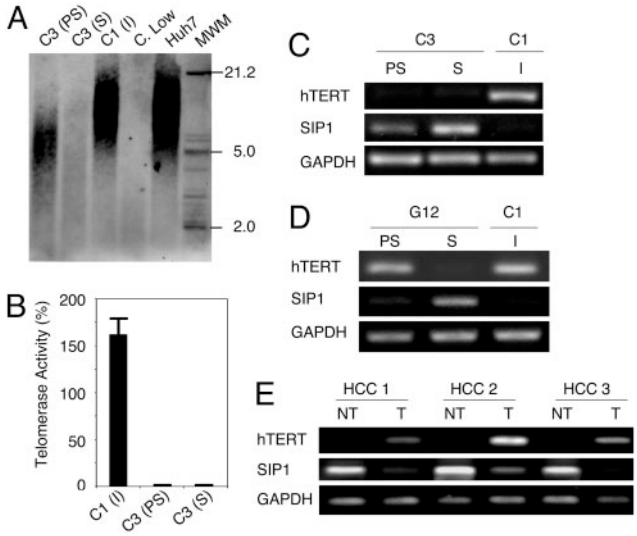

Fig. 3. C3 clonal cells undergo telomere-dependent replicative senescence associated with SIP1 expression and hTERT repression. SIP1 expression is lost, whereas hTERT is induced in primary HCC tumors. (*A*) Genomic DNAs from parental Huh7 and immortal C1 cells display long telomeres, whereas C3 telomeres are progressively shortened in presenescent and senescent stages, respectively. Equal amounts of genomic DNAs were blotted with a telomere repeat probe. C. Low, short telomere control DNA. (*B*) Presenescent and senescent C3 cells have lost telomerase activity, as measured by TRAP assay. Telomerase activity was shown as % value of test samples (± SD) compared to ''high positive'' control sample. (*C*) hTERT expression as tested by RT-PCR was high in immortal C1, but decreased to weakly detectable levels in C3 cells. Inversely, SIP1 expression tested by RT-PCR was undetectable in C1 cells, but showed a progressive increase in presenescent and senescent C3 cells. (*D*) Inverse relationship between SIP1 and hTERT expression was confirmed with another senescence-programmed Huh7 clone named G12 (for SABG and BrdUrd assays, see Fig. 7). hTERT expression in G12 showed a slight decrease in presenescent stage, followed by a loss at the onset of senescence. Inversely, the expression of SIP1 gene was weakly positive in presenescent G12, but highly positive in senescent G12 cells. C1 was used as control. PS, presenescent; S, senescent; I, immortal. (*E*) Negative correlation between hTERT and SIP1 expression in primary tumors (T) and nontumor liver tissues (NT).

The *SIP1* gene (Zinc finger homeobox 1B; *ZFHX1B*) encodes a transcriptional repressor protein that interacts with SMAD proteins of the TGF-β signaling pathway and CtBP corepressor (12, 13). This gene has recently been implicated in TGF-β-dependent regulation of *hTERT* expression in breast cancer cells (14). Our observations implicated *SIP1* gene as a candidate regulator of replicative senescence in HCC cells. To investigate whether *SIP1* expression constitutes a protective barrier against hTERT expression and senescence bypass, we constructed SIP1 short hairpin RNA (shRNA)-expressing plasmids, based on a reported effective SIP1 siRNA sequence (14). SIP1 shRNA was expressed by using either G-418-resistance plasmid pSuper.retro.neo+GFP or puromycin-resistance plasmid pSUPER.puro (see *shRNA* in *Methods*). Presenescent C3 cells at PD 75 were used for transfections, 3–4 weeks before expected senescence arrest stage. pSuper.retro.neo+GFP-based SIP1 shRNA suppressed the accumulation in SIP1 when expressed transiently (Fig. 4*A*, day 5). This resulted in a weak increase in *hTERT* expression. Transfected cells were maintained in culture in the presence of 500 μg/ml G-418 and observed for 30 days. At this period, C3 cells transfected with a control plasmid reached senescence-arrested stage with further up-regulation of *SIP1* expression (Fig. 4*A*, day 30) and resistance to BrdUrd incorporation after mitogenic stimuli (BrdUrd index = 3 ± 1%; Fig. 4*B Upper Left*). In sharp contrast, SIP1 shRNA-transfected cells lost

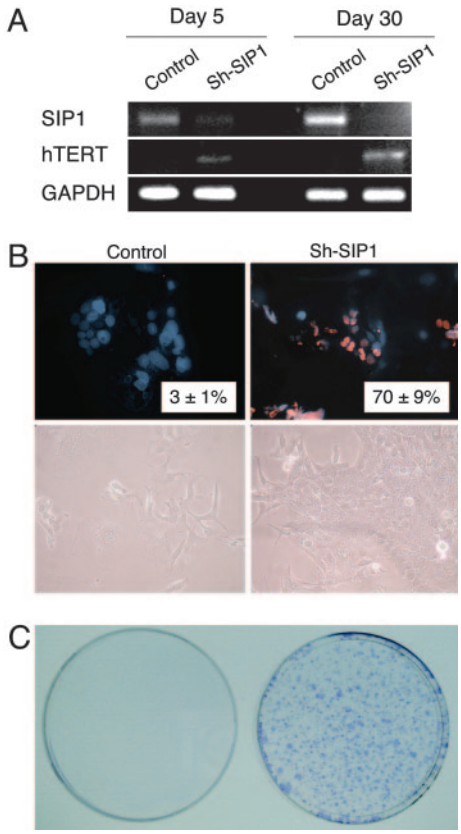

Fig. 4. ShRNA-mediated down-regulation of endogeneous SIP1 transcripts releases hTERT repression and rescues C3 cells from senescence arrest. (*A*) At day 5 after transfection, SIP1 shRNA-transfected cells (Sh-SIP1) show decreased expression of SIP1 and weak up-regulation of hTERT expression. At day 30, the expression of SIP1 is lost completely, and hTERT expression is stronger. (*B*) Cells transfected with empty vector (Control) are senescence-arrested as evidenced by resistance to BrdUrd incorporation (*Upper Left*) and morphological changes (*Lower Left*), but cells transfected with SIP1 shRNA vector (Sh-SIP1) escaped senescence arrest as indicated by high BrdUrd index (*Upper Right*) and proliferating cell clusters (*Lower Right*). (*C*) Colony-forming assay shows that C3 cells formed large number of colonies following puromycin selection after transfection with a puromycin-resistant SIP1-shRNA-expressing plasmid (*Right*), whereas cells transfected with empty vector did not survive (*Left*). SIP1 shRNA was expressed by using either G-418-resistance plasmid pSuper.retro.neo+GFP (*A* and *B*) or puromycin-resistance plasmid pSUPER. puro (*C*). Presenescent C3 cells at PD 75 were transfected with either SIP1 shRNA-expressing or empty plasmid vectors, maintained in culture in the presence of appropriate selection media and tested at days 5 (*A*) and 30 (*A–C*).

SIP1 expression and up-regulated *hTERT* transcripts (Fig. 4*A*, day 30). Furthermore, *SIP1*-inactivated cells escaped senescence, as evidenced with 70 ± 9% BrdUrd index (Fig. 4*B Upper Right*). Morphologically, SIP1 shRNA-transfected cells formed proliferating clusters, whereas cells transfected with control plasmid displayed hallmarks of senescence such as scattering, enlargement, and multiple nuclei (Fig. 4*B Lower*). Twelve independent clones were selected from SIP1 shRNA-transfected C3 cells. All but one of these clones have performed so far >15 PD beyond the expected senescence barrier (data not shown). As an additional confirmatory assay, C3 cells were transfected with the puromycin-selectable *pSUPER.puro-based* SIP1 shRNA vector and subjected to puromycin selection. SIP1 shRNA-transfected cells survived and formed large number of colonies after 30 days of puromycin selection. In contrast, no surviving colony was obtained from cells transfected with the control plasmid, as expected (Fig. 4*C*).

Discussion

Our observations provide experimental evidence for the generation of senescence-arrested clones from immortal HCC and breast cancer cell lines. Detailed analysis of clones from HCC-derived Huh7 cell line further indicates that what we observe is a replicative senescence, but not a stress-induced premature senescence-like arrest. Clonal C3 cells displayed telomerase repression, progressive telomere shortening, and permanent growth arrest after ≈80 PD with senescence-associated morphological changes and positive SABG staining. Similar changes have also been observed with G12, another independently derived clone. Thus, we demonstrate that immortal cancer cells have the intrinsic ability to reprogram the replicative senescence. As expected, this shift in cell fate results in a complete loss of tumorigenicity. The replicative senescence arrest that we identified with clonal C3 cells was not accompanied with the induction of the *p53*, $p16^{INK4a}$, $p14^{ARF}$, or $p21^{Cip1}$ gene. The nonparticipation of *p53* and $p16^{INK4a}$ to the senescence arrest described here was expected, in the light of published observations showing that Huh7 cells express a mutant p53 protein (20–22) and they are deficient in $p16^{INK4a}$ expression (23). Although the levels of $p21^{Cip1}$ protein displayed a slight increase in C3 cells, this was not related to senescence arrest, as early passage proliferating C3 cells also displayed this slight increase (Fig. 5). The early loss of *hTERT* expression in this clone could contribute to early $p21^{Cip1}$ up-regulation, because hTERT is known to down-regulate $p21^{Cip1}$ promoter activity (26). *p53*, $p16^{INK4a}$, $p14^{ARF}$, and $p21^{Cip1}$ form a group of replicative senescence-related cell cycle checkpoint genes. The lack of induction of these genes in senescence-arrested C3 cells clearly indicates that there are additional genes involved in senescence arrest in these tumor-derived cells.

The loss of *hTERT* expression in senescence programmed clones prompted us to analyze the expression of genes that have been implicated in *hTERT* regulation. Among seven candidate genes studied, only one, the *SIP1* gene, displayed a differential expression between immortal and senescence-programmed clones. This gene has been identified as a mediator of TGF-β-regulated repression of *hTERT* expression in a breast cancer cell line, although it was not effective in an osteosarcoma cell line (14). In our studies, SIP1 was not expressed in immortal hTERT-expressing C1 clone, but expressed in senescence-programmed hTERT-repressed C3 and G12 clones (Fig. 3 *B* and *C*). Furthermore, experimental depletion of SIP1 transcripts resulted in hTERT up-regulation in C3 clonal cells (Fig. 4*A*). This effect has been confirmed by using SKHep1, another HCC cell line (data not shown). Thus, we demonstrate that the *SIP1* gene acts as an hTERT repressor in HCC cells. More importantly, we also showed the bypass of senescence arrest after functional inactivation of SIP expression by shRNA in senescence-programmed C3 clonal cells. In contrast to C3 cells transfected with a control plasmid, SIP1 shRNA-treated cells displayed continued proliferation beyond PD ≈80 as evidenced by 70% BrdUrd incorporation index, and formation of large number of colonies. Selected shRNA-transfected clones from these experiments have already performed >15 PD beyond the senescence barrier. Thus, our findings indicate that the functional inactivation of *SIP1* in senescence-programmed cancer cells is sufficient to bypass senescent arrest.

SIP1 is a zinc finger and homeodomain containing transcription factor that exerts a repressive activity by binding to CACCT sequences in regulatory elements of target genes (12, 27). The *SIP1* gene is expressed at high levels in almost all human somatic tissues tested, including liver (28). Therefore, we also performed comparative analysis of hTERT and *SIP1* expression in nontumor liver and primary HCC tissues. *SIP1*

was strongly positive in nontumor liver samples, but its expression was significantly decreased in corresponding HCC samples. Inversely, *hTERT* expression was negative or low in nontumor liver samples, but highly positive in HCC tumors (Fig. 3*E*). We also detected complete loss of *SIP1* expression in 5 of 14 (36%) of HCC cell lines (data not shown). Taken together with *in vitro* studies, these observations strongly suggest that *SIP1* acts as a tumor suppressor gene in HCC. Although SIP1, as a repressor of *E-cadherin* promoter, has been suggested to be a promoter of invasion in malignant epithelial tumors (29), a tumor suppressive activity by the repression of *hTERT* and inhibition of senescence arrest is not precluded.

Hepatocellular carcinoma is one of the most common cancers worldwide. Liver cirrhosis is the major etiology of this tumor with limited therapeutic options (30, 31). Telomere shortening and senescence play a major role in liver cirrhosis, from which the neoplastic HCC cells emerge with high rates of telomerase reactivation (32). Furthermore, *p53* and $p16^{INK4a}$ are the most frequently inactivated genes in these tumors. This fact enhances the importance of our findings for potential therapeutic applications of replicative senescence programming in HCC.

Methods

Tissues, Cells, and Clones. Snap-frozen HCC and nontumor liver tissues were used. HCC and breast cancer cell lines T-47D (ATCC) and BT-474 (ATCC) were cultivated as described (33). hTERT-HME cells (Clontech) were cultivated in DMEM/Ham's F-12 (Biochrom) containing insulin (3.5 μg/ml), EGF (0.1 ng/ml), hydrocortison (0.5 μg/ml), and 10% FBS (Biochrom). Huh7- and Hep3B-derived isogenic clones were obtained by either G-418 selection after transfection with neomycin-resistance pcDNA3.1 (Invitrogen) or pEGFP-N2 (Clontech) plasmids, or by low-density cloning. Huh7-derived isogenic clones C1 and C3 were obtained with pCDNA3.1, and G12 with pEGFP-N2. Huh7-derived C11, and Hep3B-derived 3B-C6, 3B-C11 and 3B-C13 were obtained by low-density cloning. Cells transfected with calcium phosphate/DNA-precipitation method were cultivated in the presence of geneticin G-418 sulfate (500 μg/ml; GIBCO), and isolated single cell-derived colonies were picked up by using cloning cylinders and expanded in the presence of 200 μg/ml geneticin G-418 sulfate. For low-density cloning, cells were plated at 30 cells per cm^2 and single-cell derived colonies were expanded. Initial cell stocks were prepared when total number of cells became 1–3 $\times$ 10^7, and the number of accumulated population doubling (PD) at this stage was estimated to be 24, assuming that the progeny of the initial colony-forming cells performed at least 24 successive cell divisions until that step. Subsequent passages were performed every 4–7 days, and the number of additional PD was determined by using a described protocol (34).

Low-Density Clonogenic Assay. Cells (30–50 per cm^2) were plated in six-well plates and grown 1–3 weeks to obtain isolated colonies formed with 100–1,000 cells. The medium was changed every 4 days, and colonies were subjected to SABG staining (see below).

***In Vivo* Studies.** Cells were injected s.c. into CD-1 *nude* mice (Charles River Breeding Laboratory). Tumors and nontumorigenic cells at the injection sites were collected at day 35 and analyzed directly or after *in vitro* culture by SABG assay (see below). These experiments have been approved by the Bilkent University Animal Ethics Committee.

SABG Assay. SABG activity was detected by using a described protocol (15). After DAPI or eosin counterstaining, SABG-positive and negative cells were identified and counted.

BrdUrd Incorporation Assay. Subconfluent cells were labeled with BrdUrd for 24 h in freshly added culture medium and tested as described (33), using anti-BrdUrd antibody (Dako) followed by tetramethylrhodamine B isothiocyanate-labeled secondary antibody (Sigma). DAPI (Sigma) was used for counterstaining.

Immunoblotting. Antibodies against cyclin D1, CDK4, CDK2, $p21^{Cip1}$, pRb (all from Santa Cruz Biotechnology), cyclin E (Transduction), cyclin A (Abcam), $p16^{INK4a}$ (Abcam), p53 (clone 6B10; ref. 35), and calnexin (Sigma) were used for immunoblotting as described (33).

RT-PCR. RT-PCR expression analysis was performed as described (33), using primers listed in Table 1, which is published as supporting information on the PNAS web site.

TRAP and Telomere Length Assays. Telomerase activity and telomere length assays were performed by using Telo*TAGGG* Telomerase PCR $ELISA^{PLUS}$ and Telo*TAGGG* Telomere Length Assay (Roche Diagnostics), following kit instructions.

shRNA. SIP1-directed shRNA was designed according to a previously described effective siRNA sequence (14) using the pSUPER RNAi system instructions (Oligoengine) and cloned into pSuper.retro.neo+GFP and pSUPER.puro (Oligoengine), respectively. SIP1 shRNA-encoding sequence was inserted by using 5′-GATCCCCCTGCCATCTGATCCGCTCTTTCAAGAGAAGAGCGGATCAGATGGCAGTTTTTA-3′ (sense) and 5′-AGCTTAAAAACTGCCATCTGATCCGCTCTTCTCTTGAAAG AGCGGATCAG ATGGCAGGGG-3′ (antisense) oligonucleotides.

The integrity of the inserted shRNA-coding sequence has been confirmed by nucleic acid sequencing of recombinant plasmids. Clone C3 cells were transfected with calcium phosphate precipitation method, using either pSuper.retro.neo+GFP-based or pSUPER.puro-based SIP1 shRNA expression plasmid, and cells were maintained in the presence of 500 μg/ml geneticin G-418 sulfate and 2 μg/ml puromycin (Sigma), respectively. Empty vectors were used as control. Media changed every 3 days, and cells were tested at days 5 and 30.

We thank E. Galun, G. Hotamisligil, F. Saatcioglu, and A. Sancar for reading the manuscript and helpful suggestions. This work was supported by Grant SBAG-2774/104S045 from the Scientific and Technological Research Council of Turkey (TUBITAK) and funds from Bilkent University and Turkish Academy of Sciences (TUBA).

1. Nowell, P. C. (1976) *Science* **194,** 23–28.
2. Vogelstein, B. & Kinzler, K. W. (1993) *Trends. Genet.* **9,** 138–141.
3. Shay, J. W. & Wright, W. E. (2005) *Carcinogenesis* **26,** 867–874.
4. Campisi, J. (2005) *Cell* **120,** 513–522.
5. Dimri, G. P. (2005) *Cancer Cell* **7,** 505–512.
6. Ben-Porath, I. & Weinberg, R. A. (2004) *J. Clin. Invest.* **113,** 8–13.
7. Shay, J. W. & Bacchetti, S. (1997) *Eur. J. Cancer* **33,** 787–791.
8. Sherr, C. J. & McCormick, F. (2002) *Cancer Cell* **2,** 103–112.
9. Boehm, J. S. & Hahn, W. C. (2005) *Curr. Opin. Genet. Dev.* **15,** 13–17.
10. Roninson, I. B. (2003) *Cancer Res.* **63,** 2705–2715.
11. Shay, J. W. & Roninson, I. B. (2004) *Oncogene* **23,** 2919–2933.
12. Verschueren, K., Remacle, J. E., Collart, C., Kraft, H., Baker, B. S., Tylzanowski, P., Nelles, L., Wuytens, G., Su, M. T., Bodmer, R., *et al.* (1999) *J. Biol. Chem.* **274,** 20489–20498.
13. Postigo, A. A., Depp, J. L., Taylor, J. J. & Kroll, K. L. (2003) *EMBO J.* **22,** 2453–2462.
14. Lin, S. Y. & Elledge, S. J. (2003) *Cell* **113,** 881–889.
15. Dimri, G. P., Lee, X., Basile, G., Acosta, M., Scott, G., Roskelley, C., Medrano, E. E., Linskens, M., Rubelj, I., Pereira-Smith, O., *et al.* (1995) *Proc. Natl. Acad. Sci. USA* **92,** 9363–9367.
16. Lasfargues, E. Y., Coutinho, W. G. & Redfield, E. S. (1978) *J. Natl. Cancer Inst.* **61,** 967–978.

17. Keydar, I., Chen, L., Karby, S., Weiss, F. R., Delarea, J., Radu, M., Chaitcik, S. & Brenner, H. J. (1979) *Eur. J. Cancer* **15,** 659–670.
18. Nakabayashi, H., Taketa, K., Miyano, K., Yamane, T. & Sato, J. (1982) *Cancer Res.* **42,** 3858–3863.
19. Wei, W. & Sedivy, J. M. (1999) *Exp. Cell Res.* **253,** 519–522.
20. Bressac, B., Galvin, K. M., Liang, T. J., Isselbacher, K. J., Wands, J. R. & Ozturk, M. (1990) *Proc. Natl. Acad. Sci. USA* **87,** 1973–1977.
21. Volkmann, M., Hofmann, W. J., Muller, M., Rath, U., Otto, G., Zentgraf, H. & Galle, P. R. (1994) *Oncogene* **9,** 195–204.
22. Kubica, S., Trauwein, C., Niehof, M. & Manns, M. (1997) *Hepatology* **25,** 867–873.
23. Roncalli, M., Bianchi, P., Bruni, B., Laghi, L., Destro, A., Di Gioia, S., Gennari, L., Tommasini, M., Malesci, A. & Coggi, G. (2002) *Hepatology* **36,** 427–432.
24. Kaneko, S., Hallenbeck, P., Kotani, T., Nakabayashi, H., McGarrity, G., Tamaoki, T., Anderson, W. F. & Chiang, Y. L. (1995) *Cancer Res.* **55,** 5283–5287.
25. Wang, J., Xie, L. Y., Allan, S., Beach, D. & Hannon, G. J. (1998) *Genes Dev.* **12,** 1769–1774.
26. Young, J. I., Sedivy, J. M. & Smith, J. R. (2003) *J. Biol. Chem.* **278,** 19904–19908.
27. Remacle, J. E., Kraft, H., Lerchner, W., Wuytens, G., Collart, C., Verschueren, K., Smith, J. C. & Huylebroeck, D. (1999) *EMBO J.* **18,** 5073–5084.
28. Cacheux, V., Dastot-Le Moal, F., Kaariainen, H., Bondurand, N., Rintala, R., Boissier, B., Wilson, M., Mowat, D. & Goossens, M. (2001) *Hum. Mol. Genet.* **10,** 1503–1510.
29. Comijn, J., Berx, G., Vermassen, P., Verschueren, K., van Grunsven, L., Bruyneel, E., Mareel, M., Huylebroeck, D. & van Roy, F. (2001) *Mol. Cell* **7,** 1267–1278.
30. Thorgeirsson, S. S. & Grisham, J. W. (2002) *Nat. Genet.* **31,** 339–346.
31. Bruix, J., Boix, L., Sala, M. & Llovet, J. M. (2004) *Cancer Cell* **5,** 215–219.
32. Satyanarayana, A., Manns, M. P. & Rudolph, K. L. (2004) *Hepatology* **40,** 276–283.
33. Erdal, E., Ozturk, N., Cagatay, T., Eksioglu-Demiralp, E. & Ozturk, M. (2005) *Int. J. Cancer* **115,** 903–910.
34. Masutomi, K., Yu, E. Y., Khurts, S., Ben-Porath, I., Currier, J. L., Metz, G. B., Brooks, M. W., Kaneko, S., Murakami, S., DeCaprio, J. A., *et al.* (2003) *Cell* **114,** 241–253.
35. Yolcu, E., Sayan, B. S., Yagci, T., Cetin-Atalay, R., Soussi, T., Yurdusev, N. & Ozturk, M. (2001) *Oncogene* **15,** 1398–1401.

Manuscript submitted to Proc. Nat. Acad. Sci. USA

A Major Role for the Senescence and Immortality Gene Network in Hepatocellular Carcinoma

Ayca Arslan-Ergul[1,*], Sevgi Bagislar[1,2,*], Ozlen Konu[1], Nuri Ozturk[1], Hilal Ozdag[3], Rasit Ozturk[1], Esra Erdal[4], Sedat Karademir[5], Ozgul Sagol[6], Dilsa Mizrak[7], Hakan Bozkaya[7], Biter Bilen[1], Gokhan Ilk[8], Ozlem Ilk[9], Rengul Cetin-Atalay[1], Mehmet Ozturk[1,2,10]

[1]BilGen Genetics and Biotechnology Center, Department of Molecular Biology and Genetics, Bilkent University, 06800 Ankara, Turkey; [2]INSERM – Université Joseph Fourrier U823, 038706 Grenoble, France; [3]Ankara University Biotechnology Institute; Departments of [4]Medical Biology, [5]Surgery and [6]Pathology, Dokuz Eylul University Medical School, Izmir; Departments of [7]Gastroenterology and [8]Electrical and Electronic Engineering, Ankara University, Ankara; [9]Department of Statistics, Middle-East Technical University, Ankara, Turkey.
*These authors contributed equally to this work.

[10]Corresponding author: Mehmet Ozturk, INSERM – Université Joseph Fourrier U823, 038706 Grenoble, France; Telephone: Fax: e-mail: ozturkm@ujf-grenoble.fr
Manuscript information: 23 text pages (including references and figure legends), 3 figures, and 2 tables.

Author contributions: AAE and HO performed microarray analyses; AAE, SB, EE and NO and carried out other laboratory studies; HB, SK, DM and OS provided tissue material and collected associated clinical data; AAE, SB, BB, RCA, GI, OI, OK and RO performed bioinformatic and statistical analyses; MO designed the study and wrote the paper.

Key words: Senescence, Liver Cancer, Gene Expression Profiling, Molecular Classification, Biological Pathways, DNA Damage Response.

Data deposition footnote: Supply all database accession numbers and/or codes.
Abbreviations: SIGN, senescence and immortality gene network; SABG, Senescence- associated-β- galactosidase; DDR, DNA damage response.

ABSTRACT

Cellular senescence is a tumor-suppression mechanism, and immortalization facilitates neoplastic transformation. Both mechanisms may be highly relevant to hepatocellular carcinoma (HCC) development and its molecular heterogeneity. We integrated gene expression data from senescence-programmed and immortal HCC cells with the data from cirrhosis and HCC tissues to generate a senescence and immortality gene network (SIGN) signature. The SIGN signature accurately classified normal liver, cirrhosis, dysplasia and HCC lesions, and indicated that senescence-to-immortality switch occurs during dysplasia-to early HCC transition. Senescence-to-immortality transition contributes also to tumor progression. The SIGN signature identified several HCC classes, including one "normal-like", and two with increased expression of immortality genes. Senescence-to-immortality transition was accompanied by hepatic dedifferentiation and increased expression of cell proliferation, chromosome modification and DNA damage response genes. Thus, HCC immortalization is closely associated with the acquisition of stem/progenitor-like features. Finally, we identified a large set of upregulated DNA damage checkpoint and DNA repair genes that showed

significant associations with tumor initiation and progression. These genes may serve as potential targets for HCC prevention and therapy.